Tumor-associated neutrophils during *Pseudomonas aeruginosa*-mediated tumor therapy

Von der Fakultät für Lebenswissenschaften

der Technischen Universität Carolo-Wilhelmina zu Braunschweig

zur Erlangung des Grades einer

Doktorin der Naturwissenschaften

(Dr. rer. nat.)

genehmigte

D i s s e r t a t i o n

von **Nadine Kasnitz**
aus Nassau

1. Referent: apl. Professor Dr. Manfred Rohde

2. Referent: Professor Dr. Stefan Dübel

eingereicht am: 18.11.2015

mündliche Prüfung (Disputation) am: 05.02.2016

Druckjahr 2016

Vorveröffentlichungen der Dissertation

Teilergebnisse aus dieser Arbeit wurden mit Genehmigung der Fakultät für Lebenswissenschaften, vertreten durch den Mentor der Arbeit, in folgenden Beiträgen vorab veröffentlicht:

Publikationen

Stern C., **Kasnitz N.**, Kocijancic D., Trittel S., Riese P., Guzman C. A., Leschner S., Weiss S. Induction of CD4(+) and CD8(+) anti-tumor effector T cell responses by bacteria mediated tumor therapy. **International Journal of Cancer**. 137 (8): 2019-28 (2015).

Pawar V.*, Komor U.*, **Kasnitz N.***, Bielecki P., Pils M. C., Gocht B., Moter A., Rohde M., Weiss S., Häussler S. *In Vivo* Efficacy of Antimicrobials against Biofilm-Producing *Pseudomonas aeruginosa*. **Antimicrobial Agents and Chemotherapy**. 59 (8): 4974-81 (2015).*Co-First Authors

Tagungsbeiträge

Kasnitz N., Pils M., Schleicher I., Rohde M., Häussler S., Weiss S.: *In vivo* interactions of *Pseudomonas aeruginosa* with the innate and adaptive immune system. **Poster IIP13**. 4. Joint Conference of the Association for General and Applied Microbiology (VAAM) and the Society of Hygiene and Microbiology (DGHM), Dresden (2014).

Kasnitz N., Weiss S.: Influence of the components of the immune system on biofilm formation by *Pseudomonas aeruginosa*. **Poster 313**. 43rd Annual Meeting German Society for Immunology, Mainz (2013).

Posterbeiträge

Kasnitz, N.: Influence of *Pseudomonas aeruginosa* on the innate and adaptive immune system of tumor bearing mice. 11th Spring School on Immunology, Ettal (2015).

Kasnitz N., Rohde M., Häussler S., Weiss S.: Interaction of *Pseudomonas aeruginosa* with the innate and adaptive immune system of tumor bearing mice. 7th International PhD Symposium, Braunschweig (2014).

Kasnitz N., Schleicher I., Rohde M., Häussler S., Weiss S.: Mutual interaction of T cells and *Pseudomonas aeruginosa*. Summer School on Infection Research, Dresden (2014).

Kasnitz N., Schleicher I., Rohde M., Häussler S., Weiss S.: Mutual interaction of T cells and *Pseudomonas aeruginosa*. 6th International PhD Symposium, Braunschweig (2013).

Kasnitz N., Schleicher I., Rohde M., Häussler S., Weiss S.: Influence of components of the immune system on biofilm formation by *Pseudomonas aeruginosa*. 5th Autumn School of German Society for Immunology (DGfI) - Current Concepts in Immunology (CCII), Merseburg (2013).

Table of content

List of figures

List of tables

List of abbreviations

Abbreviation	Name
AA	Aleuria Aurantia
ACK	Ammonium-chloride-potassium
AMP	Antimicrobial peptide
APC	Antigen-presenting cell
BM	Bone marrow
BMDC	Bone marrow-derived cell
CD	Cluster of differentiation
CTL	Cytotoxic $CD8^+$ T-lymphocyte
CTLA-4	Cytotoxic T-lymphocyte late antigen-4
DAB	3,3´-Diaminobenzidine
DAMP	Damage-associated molecular pattern
DC	Dendritic cell
DNA	Deoxyribonucleic acid
EDTA	Ethylenediaminetetraacetic acid
FACS	Fluorescence-activated cell sorting
FCS	Fetal calf serum
GCP	Granulocyte chemotactic peptide
G-CSF	Granulocyte colony-stimulation factor
GM-CSF	Granulocyte-macrophage colony-stimulation factor
G-MDSC	Granulocytic myeloid-derived suppressor cell
H&E	Hematoxylin and eosin
HIF-1α	Hypoxia-inducible factor-1 alpha
HLA	Human leukocyte antigen
i.e.	*id est* (that is)
i.v.	intravenous
Icam	Intercellular adhesion molecule
IDO	Indoleamine-2,3-dioxygenase
IFN	Interferon
IL	Interleukin
IMDM	Iscove's modified Dulbecco's medium
IP-10	Interferon-gamma-inducible protein 10
KC	Keratinocyte chemoattractant

LPS	Lipopolysaccharide
mAb	Monoclonal antibody
MCP	Monocyte chemoattractant protein
MDC	Macrophage derived cytokine
MDSC	Myeloid-derived suppressor cell
MHC	Major histocompatibility complex
MIP	Macrophage inflammatory protein
M-MDSC	Monocytic myeloid-derived suppressor cell
MMP-9	Matrix metallopeptidase 9
MPO	Myeloperoxidase
NCD	Noncommunicable disease
NO	Nitric oxide
NOS	Nitric oxide synthase
PAMP	Pathogen-associated molecular pattern
PBS	Phosphate-buffered saline
PDGF-bb	Platelet-derived growth factor with two B-chains
PD-L1	Programmed cell-death ligand 1
pH	*potentia hydrogenii* (potential of hydrogen)
-R	Receptor
ROS	Reactive oxygen species
RT	Room temperature
s.c.	subcutaneous
T reg	Regulatory T cell
TAA	Tumor-associated antigen
TAM	Tumor-associated macrophage
TAN	Tumor-associated neutrophil
TC	T cell
TCR	T cell receptor
TGF-β	Transforming growth factor-beta
Th	T helper cell
TIL	Tumor-infiltrating lymphocyte
TLR	Toll-like receptor
TNF-α	Tumor necrosis factor-alpha
VEGF	Vascular endothelial growth factor
WT	Wild-type

Unit	Name
°C	Degree Celsius
µg	Microgram
µl	Microliter
µm	Micrometer
µmol	Micromole
d	Day
g	Gram
G	Gauge
h	Hour
kg	Kilogram
kV	Kilovolt
l	Liter
M	Molar
mg	Milligram
min	Minute
ml	Milliliter
mm^3	Cubic millimeter
OD	Optical density
p	Probability
rmp	Rounds per minute
v	Volume
V	Volume
w	Weight

Symbol	Meaning
%	Percent
+	Positive
-	Gene knock-out
α	Alpha
β	Beta
γ	Gamma
π	Pi

1 Introduction

1.1 Frequency and development of cancer

Cancer is one of the four main types of chronic, so called noncommunicable diseases (NCD). Altogether 38 million people worldwide die from such diseases, summing up to 68% of all death in 2012. The mortality from cancer was 8.2 million people worldwide in that year. Only cardiovascular diseases accounted for more NCD death. In the upper-middle to high-income countries, cancer is still amongst the top ten killers (Figure 1) [1, 2].

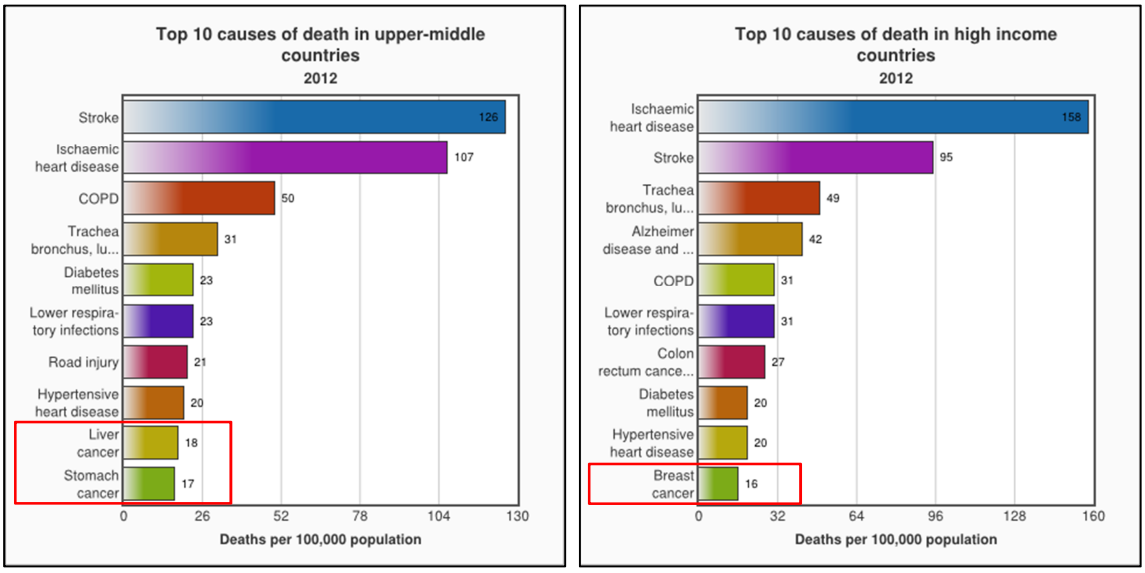

Figure 1: Top10 causes of death in upper-income countries worldwide
The ten leading causes of death by the globally two highest income groups [2]. Liver-, stomach-, and breast cancer highlighted in red boxes belong to this Top10.

The reason for the high incidence of cancer becomes clear when differences between high- and low-income countries (Figure 2, p.9) are compared. Apparently, the cause of death is mainly related to hygiene and life expectancy. In high-income countries like Germany or the United States, individuals above 70 years account for seven of ten deaths, while only one in hundred children under the age of fifteen years dies. In contrast, in low-income countries like Somalia or Tanzania, only two of ten deaths concern individuals above seventy years, while four of ten deaths occur among children below fifteen years. Such children mostly die of infectious diseases or complications during childbirth [2]. With an average age of 69 years every second person in Germany will have been diagnosed for cancer (“cancer incidence”), involved are 51 % of the male and 43 % of the female population. Half of these cancer patients will die due to the disease (“cancer mortality”). This sums up to every fourth man and fifth woman of the entire German population [3].

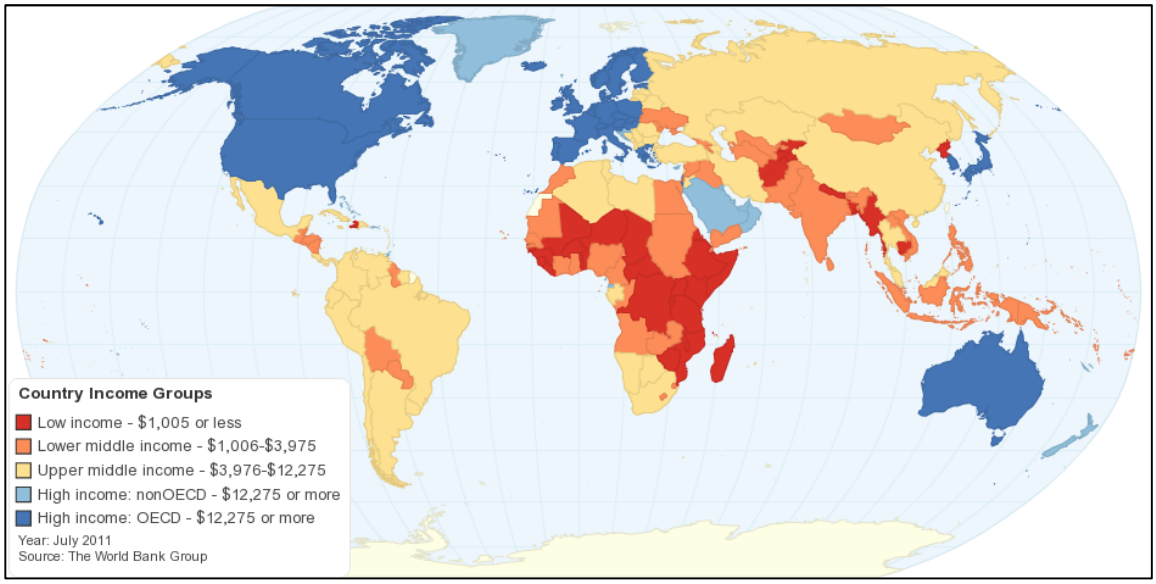

Figure 2: Country income groups
Economies with populations of more than 30,000 were used for operational and analytical purposes. They are divided among income groups according to 2010 gross national income per capita [4].

The most prominent cancers in Germany are prostate or lung cancer for men, and breast- or intestinal cancer for women (Figure 3) [5].

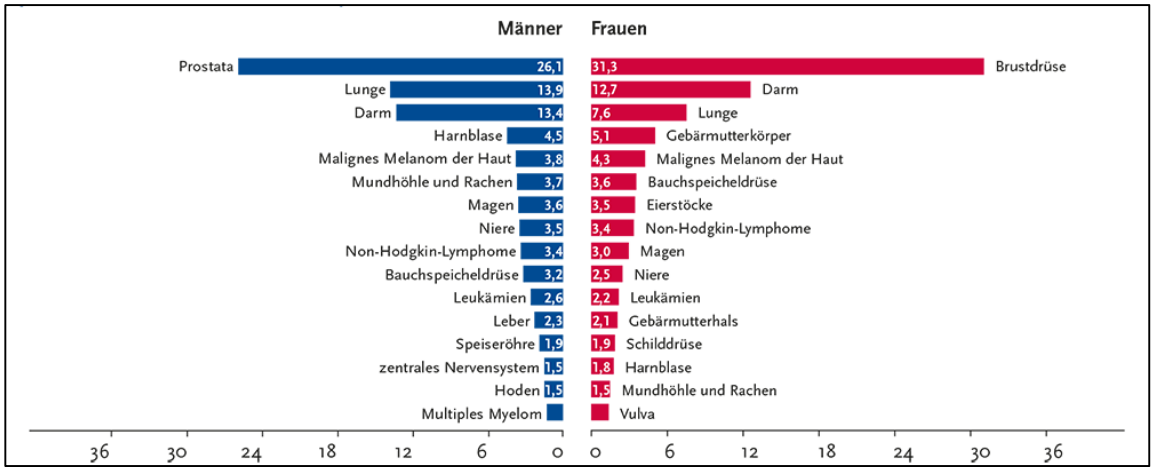

Figure 3: Cancer incidences in Germany
The most frequent tumor sites as a percentage of all new cases of cancer in Germany 2010 [5].

Importantly, the number of new cases of cancer increased up to 21 % for males and 14 % for females between the years 2000 and 2011 in Germany. Here, the demographic change is considered to be the main factor for such augmented cancer incidences [6]. Individuals of higher age i.e. with a longer life span exhibit a higher chance to acquire mutational changes within their cells that finally lead to cancer.

In order to systemize knowledge on cancer development and cancer death, ten so-called hallmarks were formulated by Hanahan and Weinberg [7] to explain the mutational switch from normal cells to a neoplastic phenotype, resulting in malignant tumor cells (Figure 4):

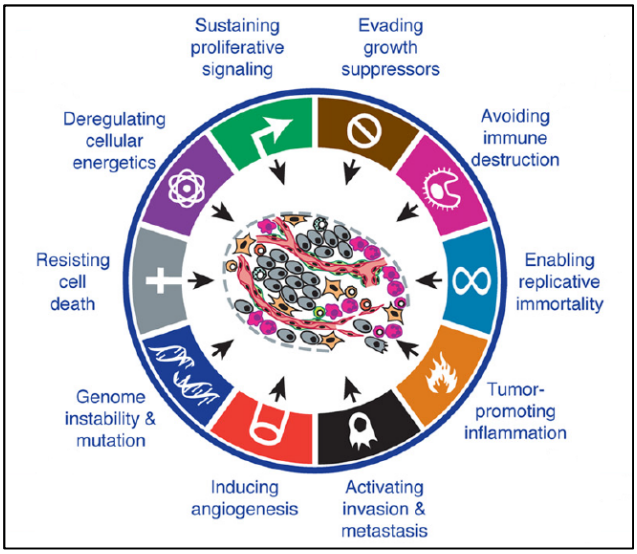

Figure 4: Hallmarks of cancer
Normal cells can be transformed into malignant variants by acquisition of the presented capabilities and enabling characteristics [7].

In the following paragraph, the ten hallmarks of cancer are described in short detail:

The most obvious property of cancer cells is their ability of unrestricted growth and proliferation.

Under normal circumstances tumor suppressor genes inhibit abnormal cell growth, but cancer cells are not susceptible to the released anti-growth signals.

To continually grow, tumor cells are furthermore resistant to the induction of programmed cell death, called “apoptosis”.

Cancer cells are able to exceed the intrinsically predefined number of cell cycles that normally results in growth termination of viable cells by maintaining the length of telomeres at the end of the chromosomal DNA.

To ensure a sufficient supply with nutrients and oxygen once they surpass a certain size, tumors develop their own neovasculature system, a process which is called “angiogenesis”.

 By the “metabolic switch” cancer cells gain energy by aerobic glycolysis to ensure the unrestricted availability of glycolytic intermediates for the biosynthesis of new cellular components.

 Immunogenic cancer cells are able to evade “immune surveillance”, the ubiquitous function of the host´s immune system to detect and eradicate neoplastic and pathogenic cells.

 Tumor cells are able to migrate from their primary localization to new niches in the body. There they can establish further cell assemblies called “metastases”, which are responsible for the majority of human cancer deaths [8].

The acquisition of the described functional capabilities of cancer cells to enable growth, survival and dissemination are based on two fundamental cell characteristics:

 The genome integrity of cancer cells is altered compared to normal cells. Mutations occur especially in such genes that favor the onset of neoplasia [7] and thereby the possibility to selectively outgrow the cellular colony.

 The tumor microenvironment, which contains innate and adaptive immune cells, releases growth-, survival-, and pro-angiogenic factors that support tumor growth and facilitate cancer cell mutations.

1.2 The tumor microenvironment

The development of a tumor is not only dependent on the malignant cells themselves, they also need a supportive microenvironment. This consists of different cell types of the immune system, as well as of mesenchymal cells forming the tumor-associated stroma. When they start to develop, tumors take up nutrients from their close environment. During the exponential growth phase of the tumor, the need for oxygen is especially high and amounts to 3 - 7 % of oxygen concentration [9]. However, during growth progression the tumor diameter increases (Figure 5, p.12) and cells of the inner part of the tumor receive insufficient amounts of nutrients and oxygen by the diffusion processes. In this avascular phase of growth, the tumor proliferation is therefore counterbalanced by cell death and chronic hypoxia [10]. Hypoxic tumors have 1 % or less of oxygen available, which promotes cell death by apoptosis or necrosis [9].

Over the developmental process, the occurrence of such hypoxic regions inside solid tumors is transient and locally instable. Under hypoxic conditions, tumor cells react by activating the transcription factor hypoxia-inducible factor-1α (HIF-1α) [11, 12]. As consequence, cancer cells start to transcribe and secrete angiogenic factors like vascular endothelial growth factor (VEGF) or basic fibroblast growth factor [13, 14]. These cytokines activate the proliferation and mobilization of endothelial cells from already existing normal blood vessels to from a tumor neovasculatur, a process called "tumor angiogenesis" (Figure 5) [15]. This results in an appropriate supply of energy and oxygen in all malignant cell layers.

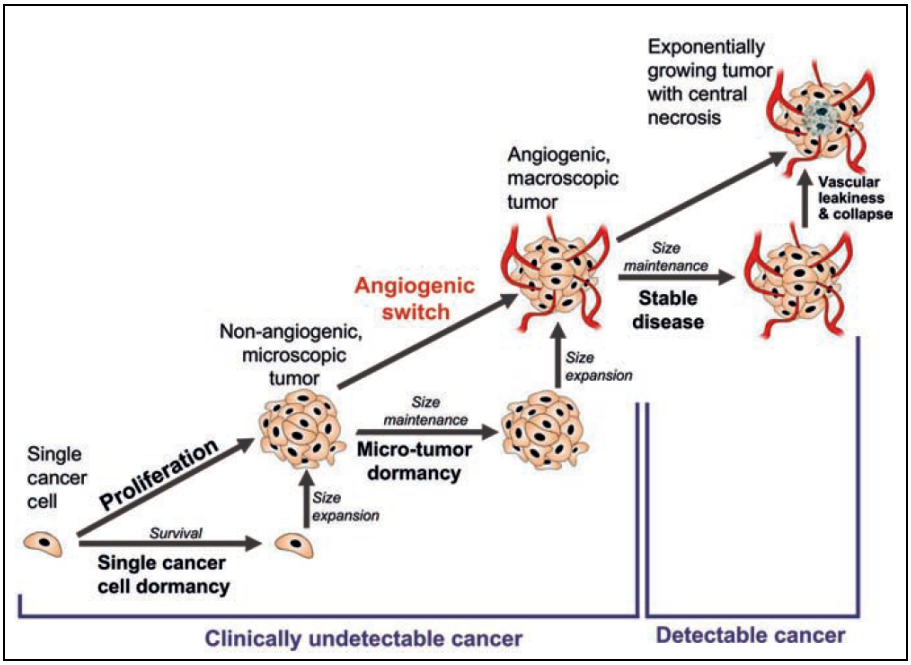

Figure 5: Developmental steps during tumor progression
The developmental processes from a single mutated cancer cell to an exponentially growing tumor require certain metabolic switches of the tumor cells. To ensure appropriate supply of energy and oxygen, tumor-associated blood vessels are formed by the tumor itself through the secretion of pro-angiogenic cytokines. An event defined as "angiogenic switch" [16].

However, the novel tumor-associated blood vessels have an abnormal structure due to a loose attachment of pericytes [17]. This leads to leakiness of the vessels and might cause irregular, temporally obstructed, or dysfunctional blood flow [10]. To counteract the resultant development of huge hypoxic areas within the tumor, the secretion of pro-angiogenic proteins is further upregulated within the whole tumor microenvironment to enhance neovascularization [16].

Not only the tumor cells, but for instance also neutrophils as part of the tumor microenvironment (Figure 6, p.13) can stimulate angiogenesis via secretion of matrix metallopeptidase 9 (MMP-9 / gelatinase-B) function and activation of VEGF [18]. Such inflammatory reactions by immune cells are considered to favor tumor growth progression and dissemination [10, 19].

In the last decade it became obvious, that the ongoing attraction of immune cells like neutrophils, macrophages, myeloid-derived suppressor cells (MDSCs) or regulatory T cells (T regs) by cancer cells facilitates tumor growth progression by the establishment of an immunosuppressive environment [20, 21]. Preceding such findings, the immune system was believed to exclusively exert immune surveillance, i.e. the prevention or rescue from cancer. Now a more complex situation starts to appear. A recent review of Joyce and Pollard [20] illustrated the main effector cells of the innate and adaptive immune system for tumor development (Figure 6):

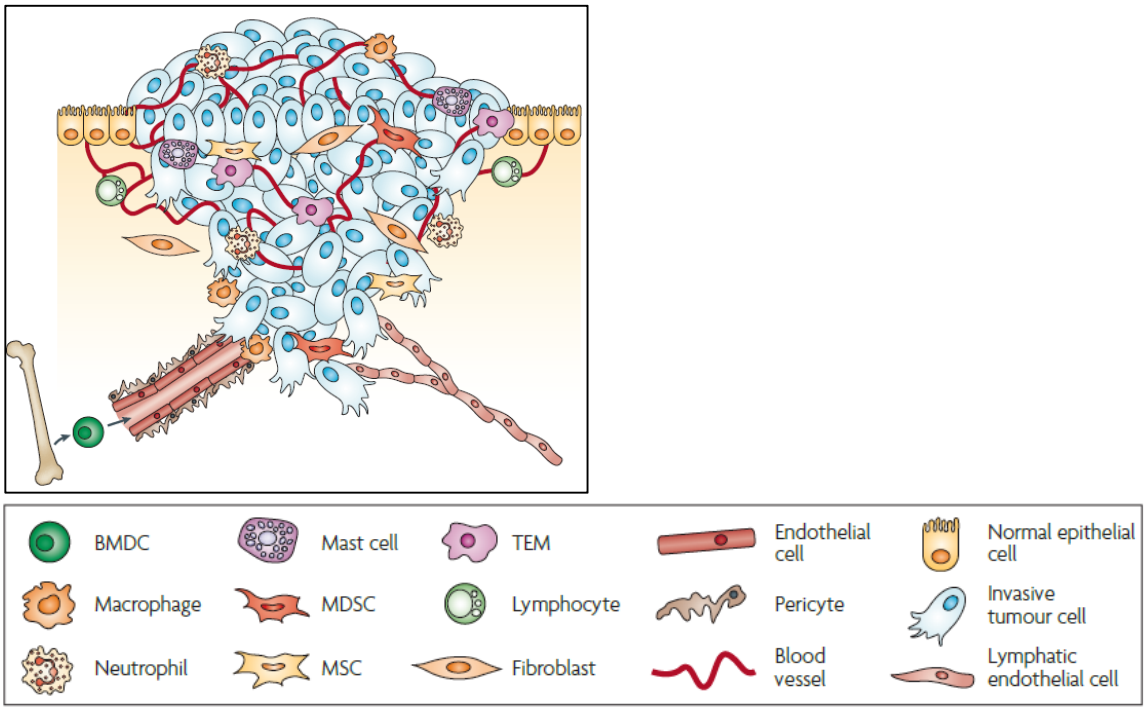

Figure 6: The tumor microenvironment
Primary tumors consist of cancer cells surrounded by a network of different cell types. This tumor microenvironment includes cells of the innate and adaptive immune system, endothelial cells, and stromal fibroblasts. Cells originating from the bone marrow (BMDC) include myeloid-derived suppressor cells (MDSC), TIE2-expressing monocytes (TEM), and mesenchymal stem cells (MSC) [20].

In the following paragraph, tumor-infiltrating cells that are important for the present study are described in short details:

 Neutrophils are $CD11b^+$ $Ly6G^+$ cells and defined as tumor-associated neutrophils (TANs) once they infiltrate cancerous tissues. Fridlender *et al.* [22] described different activation states of TANs. They characterized the distinct end-staged phenotypes as "N1" for neutrophils with anti-tumorigenic properties and "N2" for neutrophils with pro-tumorigenic functions. N1 TANs release e.g. increased amounts of pro-inflammatory cytokines to activate additional cells in the microenvironment. Furthermore, they have a higher capacity to directly kill tumor cells via superoxide or H_2O_2 secretion, and can activate cytotoxic T cells (CTLs) to destroy tumor cells [22]. N2 neutrophils on the other hand are for instance able to support tumor development [23] via an increased production of arginase that inhibits immune cells, and pro-angiogenic factors like VEGF. Besides, they exhibit downregulated cellular cytotoxicity [22]. Further information on TANs is highlighted in the chapter below.

 Myeloid-derived suppressor cells (MDSCs) are a heterogeneous population of immature cells, progenitor cells, and mature myeloid cells [23, 24]. They are generally defined as a $CD11b^+$ and $Gr1^+$ (this antibody binds to LyG^+ and $Ly6C^+$) cell population consisting of two main, functionally similar cell types: monocytic MDSCs (M-MDSCs) defined as $CD11b^+$ $Ly6C^{high}$ $Ly6G^-$ and granulocytic MDSCs (G-MDSCs) classified as $CD11b^+$ $Ly6C^{low}$ $Ly6G^+$ [25, 26]. M-MDSCs resemble G-MDSCs also in their phenotype [27]. Depending on the tumor-derived factors, MDSCs inside the tumor microenvironment can develop into several myeloid cell subsets with the general task to suppress immune functions [25, 28]. This mainly concerns the suppression of proliferation of effector T cells by the secretion of the cytokines transforming growth factor-β (TGF-β) or interleukin-10 (IL-10) [23, 25]. MDSC subsets with an identical purpose occur also in bone marrow (BM), blood, spleen and liver [29].Immature MDSCs can mature into $CD11b^+$ $Gr1^-$ $F4/80^+$ tumor-associated macrophages (TAMs) or $CD11b^+$ $Gr1^-$ $CD11c^+$ dendritic cells (DCs) [30]. A clear characterization of such at least seven $CD11b^+$ tumor-infiltrating subsets is not possible until today due to a lack of unique markers [28, 31].

MDSCs and N2 TANs do not only share cell surface molecules. They also show identical phenotypes according to cell morphology or biomarker expression. They additionally perform similar functions with respect to angiogenesis, tumor-supporting activities and cell recruitment [27]. Both belong to a low-density neutrophil subpopulation [32], which is present in mice and humans [33, 34]. The discussions about a distinction of G-MDSCs and N2 neutrophils into two separate cell populations most likely arose because of the fact, that MDSC and neutrophil research was performed in separated research communities [35]. No specific marker reliably distinguishes immunosuppressive N2 neutrophils from G-MDSCs [20, 35].

Therefore, these two cell phenotypes represent morphologically distinct neutrophil subsets within a continuum of differential phenotypes in tumor-bearing mice [32, 35]. Sine MDSCs are immature precursors of neutrophils [36], G-MDSCs can [30, 35] and will in the following be considered as an immune-suppressive status of neutrophils.

 Tumor associated macrophages (TAMs) are $CD11b^+$ $F4/80^+$ myeloid cells, which can also be separated into two functionally distinct phenotypes. Classically activated "M1" TAMs are able to directly kill tumor cells or stimulate anti-tumor functions in T cells. Alternatively activated "M2" TAMs suppress the anti-tumor immunity of the tumor microenvironment [25]. Like reported for TANs, the TAM-population also contains cells of the MDSC pool [29].

 $CD4^+$ and $CD8^+$ T cells infiltrate tumors as well during the developmental process. Within the $CD4^+$ lineage, T helper (Th) 1 cells function as helpers for tumor rejection by stimulating cytotoxic $CD8^+$ T cells. T regs on the other hand suppress activities of the immune system, especially $CD8^+$ T cells and natural killer cells functions [37, 38]. Cytotoxic $CD8^+$ T cells are very important for the anti-tumor activity of the immune system, because these effector cells can destroy cancer cells through granzyme B- and perforin facilitated apoptosis [39].

For the present study, the function of neutrophils and T cells within the tumor microenvironment was of main interest. Therefore, these cell types will be described in more detail in the following chapters.

1.2.1 Neutrophilic Granulocytes

1.2.1.1 Activation and function

Neutrophils belong to the cellular part of the innate immune system and represent one kind of phagocytic cell. Originating from hematopoietic stem cells in the BM, they mature under the influence of the hematopoietic growth factors granulocyte colony-stimulation factor (G-CSF), and granulocyte-macrophage colony-stimulation factor (GM-CSF) which also stimulates monocyte development [40]. Neutrophils are the first cells of the innate immune system that migrate to sides of infection or inflammation to perform their pro-inflammatory functions [35, 41]. These include (i) phagocytosis, (ii) the release of cytotoxic granular contents including proteases, anti-microbial peptides (AMPs), or proteins like myeloperoxidase (MPO), and (iii) the destruction of cells in their environment [42].

The latter is performed by the release of reactive oxygen species (ROS) like O_2^-, H_2O_2, HOCl, and OH, or nuclear contents as the major component of neutrophil extracellular traps with attached proteases and AMPs [35, 43-45]. Neutrophils are able to recognize invading pathogens e.g. via pathogen recognition receptors. These receptors, that include Toll-like receptor (TLR) 4 or TLR5, bind to pathogen-associated molecular patterns (PAMPs), like lipopolysaccharide (LPS) or flagellin [39], respectively. Additionally they recognize damage-associated molecular patterns (DAMPs), which are uncontrollably released by tumors, as well. Therewith, neutrophils are recruited into the tumor microenvironment [46].

Further neutrophil receptors which are important for the immigration into tumors are the chemokine receptors CCR1, CCR2, CXCR2 and CXCR4 [47-49]. The chemotactic migration of neutrophils is activated after binding of a receptor´s agonist. Such chemokines can be secreted by various immune and epithelial cells, but also tumor cells themselves can mediate recruitment of neutrophils via an increased expression of neutrophil attracting chemokines [40, 50]. Murine tumors secrete for example CCL-3 / MIP-1α (macrophage inflammatory protein 1 alpha), CXCL-1 / KC (keratinocyte chemoattractant), and CXCL-2 / MIP-2 (macrophage inflammatory protein 2) [22, 51]. All chemokines have besides their systematic names (CCL/CXCL) also names which were derived from the original discovered function. These give most of the times a more detailed understanding of the chemokine´s functions. Hence, both names will be used in the present study for optimal notations of the tumor microenvironment.

Due to their receptor repertoire, neutrophils have a high chance to migrate into tumors and perform their pro-inflammatory functions in this tissue. However, because of the already mentioned abnormal structures of the tumor-associated blood vessels, the tumor microenvironment exhibits gradients of oxygen [52]. Nevertheless, such TANs are able to fulfill their function under low oxygen conditions. They carry out a metabolic switch that results in a metabolism primarily based on glycolysis [53, 54]. Since their cytotoxic functions are unaffected by that, neutrophils rapidly die via apoptosis in the tumor, as they are well known as short-lived cells [35, 55]. However, recently it was shown that TANs have multiple phenotypes [35]. One characteristic is a prolonged survival time, extended from the familiar half-life of 7 hours up to 5.4 days [56, 57]. A prolonged life span enhances the possibility for such cells to change their phenotype in accordance to their environment and the required functions [35]. Together, due to the phenotypic specialization, neutrophils acquire the possibility to fulfill either pro- or anti-inflammatory immune functions, based on the type, combination and concentration of released cytokines in their environment [58].

1.2.1.2 Characterization of tumor-associated neutrophils

Out of the pool of hematopoietic cells, neutrophils are identified by a high expression of the markers CD11b and Ly6G [22]. When approaching an inflammatory site, neutrophils start to roll via interactions of the selectin CD62L with appropriate ligands on endothelial cells [59]. They then migrate to the site of function using the integrin CD11b [60, 61]. In accordance, upon maturation and activation CD62L is downregulated, whereas the expression of CD11b is upregulated [59].

The protein Ly6G, whose functions still needs to be characterized [62], is expressed from low to high levels by neutrophils, and is reported to be present also at a low level on eosinophils as well [62]. But the identification of tumor infiltrated cells by Ly6G is exclusively limited to neutrophils [36] and routinely used in research [22, 63-65]. However, the actual literature displays a controversy about the expression and intensity of a third protein "Ly6C" by neutrophils, with definitions ranging from $Ly6C^-$ [66] over $Ly6C^{-/int}$ [67], LyC^{int} [28] or $Ly6C^{low}$ [68], to $Ly6C^+$ [23]. Ly6C is also expressed by DCs and some cells of the $CD4^+$ and $CD8^+$ lineages. Currently it is used to distinguish inflammatory monocytes from residential monocytes [62]. In the present work, neutrophils are reliably characterized on the basis of their $CD11b^+$ and $Ly6G^+$ expression.

In addition to these two surface molecules, the literature uses plenty of further markers and genes to describe the phenotypical specialization of neutrophils (Table 1, p.18). The transient phenotype of tumor-associated neutrophils is influenced by the neighboring cells and soluble molecules within the tumor microenvironment. These parameters change during the process of tumor development. In the early and pre-clinical stage (Figure 5, p.12), the immune system is able to control the growth of cancer cells. In this phase of cancer control, many inflammatory processes are activated within the tumor microenvironment, which favor the induction of pro-inflammatory neutrophil functions and a consequent specialization into N1 TANs. Cytokines which support such tumor-suppressing activities in TANs are for example interferon-β (IFN-β), interferon-γ (IFN-γ), and GM-CSF [69, 70]. Whereby the type I interferon IFN-β is probably the trigger responsible for the induction of the tumor-suppressing N1 phenotype (Figure 7, p.19) [48, 51, 71]. Such N1-specialized cells show an increased capacity to migrate into tumors by an upregulation of cell adhesion molecules like CD11b [60]. Furthermore, specific cytokines or chemokines like tumor necrosis factor-α (TNF-α) or IFN-γ guide the extravasation of the cells out of the blood vessels into the tumor tissue [60]. Also the protein FasL, which can be expressed on epithelial cells as well as on tumor cells, supports neutrophil infiltration into cancerous tissues [72]. In addition, the interaction of FasL and its receptor Fas on neutrophils regulates the cells´ lifespan via the induction of apoptosis [73].

This process is induced after FasL-Fas interaction and the resulting activation of the Fas receptor. Thereby the death receptor-induced apoptosis pathway is stimulated. This leads to the activation of caspase 8, which then further activates the effector caspases 3 and - 7. Cell death is the final outcome [74]. Since N1 TANs have a shorter life time as N2 TANs, they can be identified by an upregulation of Fas and active caspase 3 [22, 75]. Extrinsic receptor-induced pathways triggering apoptosis can also be induced in other cells within the tumor microenvironment. Therefore, neutrophils release large amounts of pro-inflammatory cytokines like TNF-α or IL-1 [40]. The secreted TNF-α has cytotoxic functions on for example the tumor neovasculature which exhibits increased numbers of the TNF-α receptor-1. The activation of the receptors for TNF-α results in hyperpermeability of the already leaky tumor-associated blood vessels and huge amounts of erythrocytes and other circulating cells are able to extravasate into the tumor tissue, resulting in a massive hemorrhagic necrosis of the tumor [76, 77].

Table 1: Overview of neutrophil phenotyping markers
The following cell surface molecules, cytokines, chemokines, enzymes and substances are used to distinguish functional phenotypes of tumor-associated neutrophils.

Type of biomarker	Biomarker	Characterization of neutrophil polarization as	
		N1 tumor-suppressive	N2 tumor-supportive
Cell surface molecule	Icam (CD54)	X [22]	
	Fas (CD95)	X [22]	
	CD62L (L-selectin)		X [78]
	CXCR2		X [48]
	CXCR4		X [51]
Chemokine	CCL-2 / MCP-1		X [22]
	CCL-3 / MIP-1α	X [22]	
	CCL-5 / RANTES		X [22]
	CCL-17 / TARC		X [47]
	CXCL-1 / KC		X [48]
	CXCL-2 / MIP-2		X [48]
	CXCL-5 / ENA-78	X [48]	
Cytokine	Active caspase 3	X [75]	
	G-CSF		X [79]
	GM-CSF	X [22]	
	TNF-α	X [22]	
	VEGF		X [51]
Enzyme	Arginase		X [22]
	MMP-9/ gelatinase-B		X [22]
Substance	iNOS	X [47]	
	ROS	X [22]	

Besides killing of tumor cells within the tumor microenvironment, N1 TANs can also interact with further immune cells. Neutrophils of N1 phenotype are for example characterized by an increased presentation of intercellular adhesion molecule-1 (Icam-1 or Icam) on their surface [51]. By that, TANs can receive immunoregulatory signals from T cells. Their lymphocyte function associated antigen-1 binds to Icam [80]. At the same time, the T cell can receive stimulatory signals from the antigen-presenting neutrophil possibly via the T cell receptor (TCR), and co-stimulatory molecules like cluster of differentiation (CD) 80 and CD86 which bind to CD28 on the T cell surface.

Since some antigen-presenting cells (APCs) lack the expression of appropriate CD28 co-stimulators, alternative co-stimulatory ligands like Icam can perform important roles during cognate interaction [81]. Especially when antigen is limited like in tumors with low immunogenicity, Icam leads to an accumulation of major histocompatibility complex (MCH) molecules, which increases the chance for antigen presentation and T cell activation [81]. By that, N1 TANs can contribute to tumor-inhibitory processes within the tumor microenvironment.

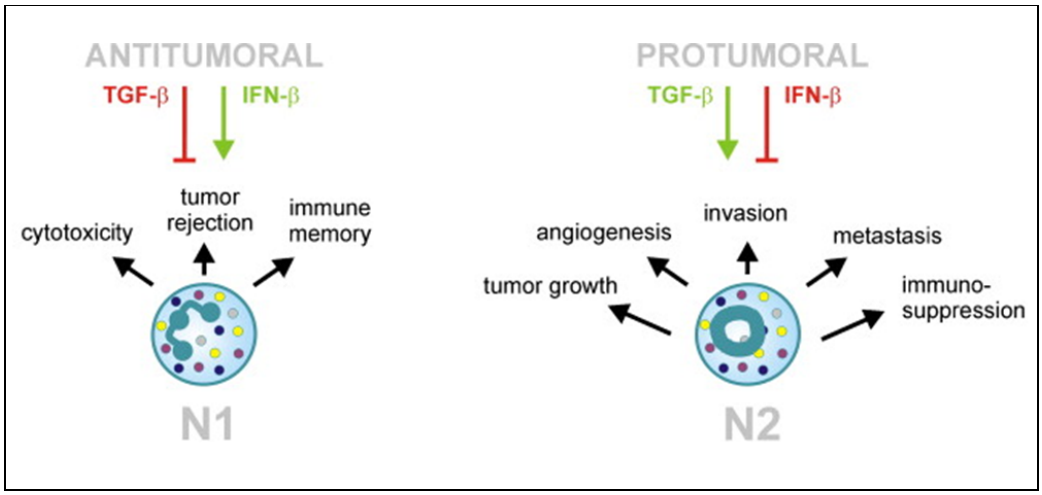

Figure 7: Cytokines causing neutrophil polarization in tumors
The switch of neutrophils between the two end-stage functional phenotypes “N1” and “N2” are guided by the cytokines TNG-β and IFN-β [51].

On the other hand, aged and clinical detectable tumors (Figure 5, p.12) consist of cancer cell-accumulates that were able to escape the immune system and started to establish an immunosuppressive microenvironment favoring tumor growth progression. Such cancer cells secrete VEGF, TGF-β, galectin, or indoleamine-2,3-dioxygenase (IDO) [82]. TGF-β activates tumor-supporting functions in TANs and induces a phenotypic switch from tumor-suppressing N1 TANs to pro-tumorigenic N2 TANs (Figure 7) [32, 47, 51]. By that, tumors exploit the plasticity of TANs and manipulates them to support tumor growth [19].

Further environmental conditions which favor the activation of tumor-supportive functions in TANs are the hypoxic conditions inside the tumor and the cytokines G-CSF, IL-4, IL-10, IL-17 and CCL-2 [70, 83]. Neutrophils with an N2 phenotype can (i) produce various cytokines which positively influence hematopoiesis, angiogenesis, and fibrogenesis, thereby promoting further tumor escape mechanisms [58], (ii) release elastase which supports cancer cell proliferation when taken up by tumor cells [84], or (iii) secrete the hepatocyte growth factor, upon stimulation with tumor derived cytokines like GM-CSF, to directly favor migration of cancer cells and thereby promoting tumor growth and dissemination [85]. In addition, activated N2 TANs are able to (iv) downregulate their own apoptotic and cytotoxic functions [78], (v) suppress the activities of effector T cells by the secretion of nitric oxide synthase type 2 [86, 87], or (vi) inhibit cytotoxic $CD8^+$ T cells responses via arginase secretion.

The impact that different functional phenotypes of TANs might have on tumor development is presently in research focus and is still emerging [51]. Nevertheless, it is quite accepted that at least the two cytokines TGF-β and IFN-β trigger phenotypic switches of neutrophils within tumor microenvironments (Figure 7, p.19).

1.2.2 Functions of tumor-infiltrating T-lymphocytes

Most solid tumors contain also T cells within their microenvironment, which are defined as tumor-infiltrating lymphocytes (TILs). Like for TANs, the cytokine milieu inside the tumor is responsible for the attraction of TILs. The general differentiation of $CD4^+$ T cells into different subsets is mainly influenced by the cytokine milieu present at the initiation site of T cell activation i.e. in immune inductive sites like lymph node or spleen. Whereas IFN-γ and IL-12 induce the development of Th 1 cells, IL-4 favors the proliferation of Th 2 cells [39]. A combination of the cytokines IL-2 and TGF-β polarizes $CD4^+$ T cells into T regs, IL-6 and TGF-β induce Th17 cells, and IL-6 together with IL-21 favors the development of T follicular helper cells [88]. Th 1 cells are important for the priming of $CD8^+$ T cells and enable their proliferation by the release of IL-2 and IFN-γ [39]. The CTLs are able to kill cancer cells by the release of lytic proteins and expression of FasL. The three secreted cytotoxic effector molecules perforin, granzyme, and granulysin are stored in lytic granules that are discharged upon recognition of the cognate antigen on the tumor cell [39]. In the pre-clinical stage of tumor development, APCs can present tumor-derived antigens of immunogenic cancer cells via their MHC class I - or MHC class II - molecules to naïve T cells in peripheral lymphoid organs [39]. This results in the activation and differentiation of such T cells.

After maturation within the lymph node, the effector $CD4^+$ and $CD8^+$ T cells migrate to their antigen-target via the circulation, guided for example by upregulation of CXCR-3. By that, they can be triggered by CXCL-9 / Mig (monokine induced by gamma-interferon) and CXCL-10 / IP-10 (IFN-γ-inducible protein 10) which are produced inside tumors [89]. Via the functions of such activated effector T cells, tumors can be cleared completely. The existence of cancer cell antigens, which distinguish the neoplastic cells from their normal counterparts, is therefore very important for a successful anti-tumor immunity executed by T cells. However, tumors are able to use such T cell properties for their own purposes, a process called cancer immunoediting. For example, tumor antigens which are often either products of mutated genes like p53 or over-expressed normal antigens like human epidermal growth factor receptor 2, can lead to immunological T cell tolerance or anergy, when presented to the T cell without a co-stimulatory signal in addition [82, 90].

Another possibility of cancer immunoediting is the development of cancer cell variants. Such cells arise due to immunological pressures, and use their neoplastic properties of genetic instability and unrestricted proliferation to evade activities of the immune system by for example a loss of tumor-specific antigens [19, 91]. A further way of tumor cells to block functions of tumor-inhibitory T cells is to increase (i) the number of immunosuppressive cells in the tumor microenvironment like T regs, or (ii) the presence of immune inhibitory cytokines like TGF-β or (iii) immunosuppressive cancer cell ligands like programmed cell-death ligand 1 (PD-L1) [92, 93]. But also the co-stimulatory ligands CD80 and CD86 on APCs can contribute to an inactivation of CTLs by binding to the cytotoxic T-lymphocyte late antigen (CTLA)-4 on activated $CD8^+$ T cells [92]. All these escape mechanisms of cancer contribute to the progressive development from a small cancer cell accumulate to a clinically detectable tumor.

1.3 Cancer therapies

1.3.1 Immunotherapy

Besides the well-established therapies against cancer (surgery, chemo-, and radiation-therapy), new targeted cancer immunotherapies were developed recently. One promising immunotherapy that is forwarded very strongly is the adoptive $CD8^+$ T cell therapy. Here, TILs e.g. already specific against tumor-associated antigens (TAA) are isolated, expanded in number, and re-injected into the patient [91]. Because such tumor-reactive TILs are originally very low in number and difficult to isolate [94], further strategies for cancer therapy by T cells were designed (Figure 8, p.22).

Therapeutic targets for that are molecules and cytokines which are used by solid tumors to suppress immune responses. For instance, CTLs which are reactive to IDO, a molecule expressed by cancer cells to induce immunosuppression and neutrophil apoptosis [95, 96], or T cells resistant to the immunosuppressive cytokine TGF-β are propagated [97]. Another possibility is to block the accumulation of immunosuppressive T regs by the use of anti-CD25 monoclonal antibodies [91]. A further strategy of molecular targeting is the administration of monoclonal antibodies that directly block CTL-inhibitory signals, like the commercially available drugs ipilimumab or nivolumab. Ipilimumab is a human monoclonal anti-CTLA-4 antibody that blocks the upregulated inhibitory molecule able to bind to CD28 on T cells [98]. It is used to treat melanoma, prostate-, lung-, and kidney cancer [91, 99-103]. Nivolumab is an anti-PD-1 antibody which prevents the inactivation of T cells via binding of PD-L1 expressed by tumor cells [104] (Figure 8, p. 22), and showed in up to 28 % of patients responses against melanoma, renal-cell carcinoma, and non-small-cell lung carcinoma [91, 105].

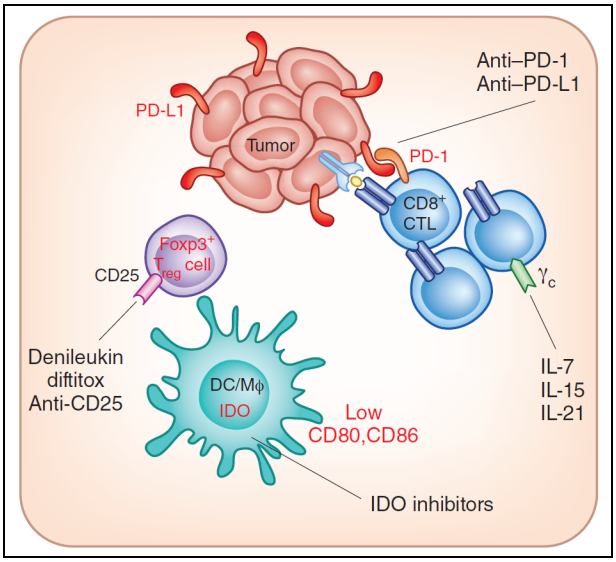

Figure 8: Molecular targeting via monoclonal antibodies increases CTL activity in tumors
The monoclonal antibodies PD-1, anti-IDO, and anti-CD25 are able to block the inhibition of tumor-infiltrated CTLs and the recruitment of immunosuppressive T regs into the tumor tissue [92].

Monoclonal antibodies (mAbs) are also used to link neutrophils to cancer cells (Figure 9). This can occur by chance via the free Fc domain of a designed cancer cell-specific mAb that can be targeted by the IgG Fcγ-receptors of neutrophils. By that, the cells are able to recognize and most likely to phagocytose the mAb-opsonized tumor cells, as TAMs do [106]. The induction of tumor cell death by autophagy or necrosis are additional mechanisms supposed to be induced by neutrophils, but the exact killing mechanism is still unknown [106, 107]. Alternatively, bi-specific mAbs can be used, which directly link neutrophils to the target tumor cells.

The cytotoxic functions of the neutrophils will subsequently be activated, resulting in tumor destruction. For example the bi-specific mAb against CD89 and human leukocyte antigen (HLA) -class II enables the lysis of HLA-class II expressing malignant B-lymphoid cells by activated neutrophils [108].

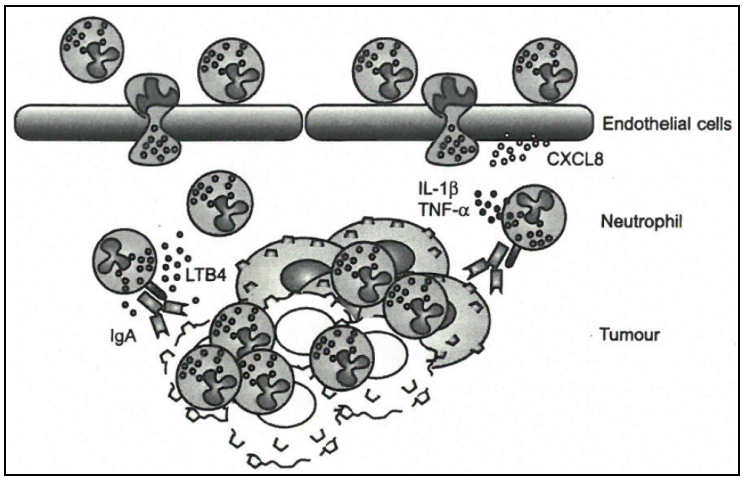

Figure 9: Monoclonal antibody-induced activation of TANs
The designed IgA mAb specifically binds to tumor cells. Its free Fc domain links TANs to the target cancer cell. Thereby the cell gets activated and secretes pro-inflammatory cytokines (IL-1β and TNF-α) or facilitates the recruitment of further N1 TANs by Leukotriene B4 (LTB4) secretion or CXCL-8 production by endothelial cells [106].

Importantly, the ongoing investigations on immunological functions of cells within the tumor microenvironment will provide many novel molecular targets for new immunotherapeutic strategies [92]. Additional strategies to activate / stimulate the immune system against the tumor are the administration of auto-reactive effector cells [109], vaccinations against TAAs with viral-based vectors [110], or the administration of bacteria [111, 112].

1.3.2 Bacteria-mediated tumor therapy

The first attempts to use bacteria systematically for tumor therapy go back to the turn of the 19th to the 20th century [113]. The American physician William Coley started these studies based on previous episodic approaches, which demonstrated the induction of tumor regression after the application of bacteria. Therefore, he treated his patients suffering from ulcerated tumors with a mixture of inactivated *Streptococcus pyogenes* and *Serratia marcescens* [114]. The application of this so called “Coley´s toxin” led to tumor clearance in many of the treated patients [114, 115]. He explained the effect as a systemic action probably induced by toxic products of *Streptococcus pyogenes*.

Today we know that he activated the immune system of the patients by the intratumoral injection of his toxin and induced an anti-tumor immune effect [115]. This therapy did not yield general acceptance and became ignored for almost 100 years. Recently, this concept was resurrected and many bacterial species have been shown in animal models to target solid tumors and retard their growth [111, 116, 117].

Nowadays, for safety reasons many bacteria were attenuated or inactivated to be applicable for tumor therapy. The *Mycobacterium bovis* strain Bacillus Calmette-Guerin is for example used today as an immunotherapeutic intravesical agent for relapse inhibition of bladder cancer [118]. Moreover, glioblastomas are successfully destructed in rats by the intravenous application of *Clostridium novyi*-NT spores [119]. Nevertheless, the mechanisms of the anti-tumor effect by *Clostridia* is restricted to the anaerobic areas of the tumor tissue and so far poorly understood [120]. A further commonly used bacterium at present is *Salmonella enteric* serovar Typhimurium (*S.* Typhimurium). By the intravenous application of the bacteria into tumor-bearing mice, a dramatic cytokine storm of pro-inflammatory mediators is induced. Among such cytokines are IL-1β, VEGF, TNF-α, and IFN-α, which have the primary function to promote further activities of the immune system [121]. Additionally, TNF-α activates the release of nitric oxide by endothelial cells, which results in vasorelaxation and a slowdown of the blood flow. As the most probable active compound elicited by "Coley´s toxin", it furthermore acts directly on the tumor neovasculature and induces a hemorrhagic necrosis of the tumor [77].

An additional subsequent increase in endothelial permeability is induced by VEGF, which is supposed to facilitate the invasion of bacteria into the tumor tissue [112]. Due to the induction of tumor-vessel hyperpermeability, the bacteria can accumulate inside the neoplastic tissue and colonize tumor zones according to their oxygen need. The secretion of several pro-inflammatory cytokines and chemokines inside the circulation and tumor microenvironment subsequently activates the adaptive immune system. By this adjuvant effect of *S.* Typhimurium, tumor-specific immune responses of T cells are induced [120, 122].

In addition to *S.* Typhimurium*, Pseudomonas aeruginosa* is a further opportunistic pathogen which is used for the induction of anti-tumor immune responses in tumor-bearing mice. For example, the subcutaneous application of *P. aeruginosa* into C57BL/6 mice induced the rejection of B16-ova tumors [123]. Moreover, Komor *et al.* [124] showed recently that *P. aeruginosa* successfully colonizes the viable part of solid tumors on BALB/c wild-type animals after intravenous injection and induces tumor clearance. Besides that, they furthermore observed that the bacteria formed *in vivo* biofilms inside the tumor tissue. Biofilms are defined by Bjarnsholt *et al.* [125] as "coherent clusters of bacterial cells embedded in a biopolymer matrix, which compared to planktonic cells, shows increased tolerance to antimicrobials and resists the antimicrobial properties of the host defence". The ability of *P. aeruginosa* to form biofilms in the host is most likely one ecological survival strategy [125]. Due to the biofilm matrix, that mainly consists of exopolysaccharides, polypeptides, biomolecules, and extracellular DNA, the bacterium is able to overcome immune surveillance and antibiotic treatment *in vivo* [126, 127].

1.4 Aim of the study

The knowledge about the host immune system´s impact on tumor development and patient survival has strongly increased within the last years. The use of engineered T cells and innate immune cells for cancer immunotherapies are new approaches, which directly influence the host´s immune system. They are able to convert cell functions within the tumor microenvironment from tumor-promoting into tumor-suppressing. One strategy to trigger the re-establishment of a pro-inflammatory tumor microenvironment is the application of bacteria. For example the injection of *S.* Typhimurium or *Escherichia coli* induced the rejection of tumors by the activation of CTLs in mice [111, 128]. In the present study, the bacterium *Pseudomonas aeruginosa* was used in a recently described murine solid tumor model [129]. The first aim was to confirm that the final anti-tumor effect induced by the bacterium is based on the activation of CTLs, and whether this quality is tumor specific.

Tumor cells are able to downregulate or alter their antigen expression pattern. Thereby they can evade the antigen-guided responses of immunotherapy. Therefore, further cells of the tumor microenvironment should be analyzed for their therapeutic anti-tumor features. Neutrophils represent a significant portion of the tumor-infiltrating immune cells in murine models as well as in human cancers [130]. Neutrophil numbers are already used as prognostic markers for the clinical outcome. For patients suffering from melanoma, glioma, or lung-carcinoma, increased numbers of neutrophils are interpreted as negative indicators. In contrast, increased numbers of neutrophils stand for a good prognosis for gastric carcinoma patients [131-134]. Thus, the use of neutrophils as prognostic markers for tumor progression is very much dependent on the tumor type, the applied methodology, and the phenotype of the tumor-associated neutrophils [27, 51]. A new concept of cancer immunotherapy is therefore to convert pro-tumor N2 neutrophils back into tumor-suppressing N1 neutrophils [135, 136]. Using our murine solid tumor model for C57BL/6-WT and -IFN-β knock-out mice, the dependency of TANs´ phenotypes on the pro-inflammatory cytokine IFN-β was recently demonstrated [75]. Since the application of *P. aeruginosa* was supposed to activate the innate and adaptive immune system of tumor-bearing BALB/c wild-type mice [124], the present study aimed (i) to characterize functional phenotypes of TANs in colonized tumor tissues of BALB/c WT mice, (ii) to compare the functional specializations of TANs from distinct tumor microenvironments, and (iii) to identify pro- or anti-inflammatory triggers influencing such TAN phenotypes *in vivo*. By that, further application possibilities for bacteria-mediated tumor therapy may be identified.

2 Materials and Methods

2.1 Materials

2.1.1 Animals

All experiments were performed with 7 - 12 week old female mice under the approval of LAVES (Niedersächsisches Landesamt für Verbraucherschutz und Lebensmittelsicherheit), Permission 33.9-42502-04-12/0173. BALB/c WT mice were purchased from Janvier (France). BALB/c -Rag1 knock-out and -IFN-$\beta^{+/\Delta\beta\text{-luc}}$ transgenic mice were bread in the animal facility of the HZI. All mice were kept under elaborate hygiene and specific pathogen free conditions with a light-dark cycle of 12 h.

2.1.2 Tumor cell lines and preparation

CT26 murine colon carcinoma cells (ATCC CRL-2638) or F1A11 murine fibrosarcoma cells (kindly provided by Dr. Pablo Becker, HZI, Braunschweig) were cultivated in Iscove's modified Dulbecco's medium (IMDM) (Invitrogen, USA) supplemented with 10 % (v/v) heat-inactivated fetal calf serum (FCS), 250 µmol/l β-mercaptoethanol, and 1 % (v/v) penicillin/streptomycin at 37°C and 5 % CO_2 in a humidified atmosphere. The inoculum for subcutaneous (s.c.) injection into the mice was prepared using the following protocol: cancer cells were first shortly washed with Trypsin/Ethylenediaminetetraacetic acid (EDTA) to remove dead cells on the cell layer, before they were incubated for 5 min at 37°C in Trypsin/EDTA till the cancer cells detached from the culture flask. 15 ml pre-warmed IMDM was added to stop the reaction and carefully dissolve cancer cell clots. The cell suspension was transferred into a 50 ml falcon and filled up to 40 ml with IMDM, and centrifuged (5 min, 120 rmp, RT). The cell pellet was washed in 25 ml pyrogen-free phosphate-buffered saline (PBS) (Biochrom, Germany) by centrifugation (5 min, 120 rmp, RT), before the cancer cells were resolved in PBS and a 10 µl aliquot was used to determine the cell number. Therefore the cells were 1:10 diluted in 0.5 % w/v Trypan blue/PBS and counted within a Neubauer chamber using a light microscope. The inoculum was adjusted to get $5x10^5$ cancer cells per 100 µl PBS per mouse.

2.1.3 Bacterial culture and preparation

The *Pseudomonas aeruginosa* wild-type strain PA14 (UCBPP-PA14, kindly provided by Prof. Dr. Susanne Häußler) is a burn wound isolate and was used for infections exclusively. Bacteria were cultivated out from frozen samples kept at -80°C on LB-plates supplemented with 100 µg/ml ampicillin for 1 day at 37°C, before they were prepared for injection. To this end, several colonies were dissolved in 1 ml pyrogen-free PBS and spun down (5 min, 6.000 rmp, RT). The pellet was washed again in 1 ml PBS (5 min, 6000 rmp, RT) and afterwards resolved in 1 ml PBS. A 1:10 dilution in PBS was used to determine the OD_{600} of the cell solution within the linear range (OD_{600} 0.1 – 1) of the photometer. The inoculum was adjusted to OD_{600} of 0.065 which was equivalent to approximately $5x10^6$ bacteria per 100 µl injected per mouse. Alternative OD_{600}-values of 0.0009, 0.009, or 0.525 were justified to obtain $5x10^4$, $5x10^5$, or $5x10^7$ bacteria. The exact infection dose was always determined by subsequent plating of the final inoculum.

2.1.4 Antibodies

Table 2: Utilized antibodies for flow cytometric and histological analyses

Specificity	Clone	Fluorochrome	Dilution	Company
CD3	145-2C11	FITC	1:200	eBioscience
CD4	RM4-5	APC	1:200	eBioscience
CD8	53-6.7	PE	1:400	eBioscience
CD19	1D3	APC-Cy7	1:150	BD
CD45	30-F11	APC-Cy7	1:400	BioLegend
CD11c	N418	PE-Cy7	1:200	eBioscience
CD11b	M1/70	APC	1:500	eBioscience
CD11b	M1/70	PE-Cy5	1:300	eBioscience
Ly6G	1A8	PE-Cy7	1:500	BioLegend
Icam	YN1/1.7	FITC	1:200	eBioscience
Fas	15A7	PE	1:200	eBioscience
CD62L	MEL-14	Biotin	1:200	eBioscience
Ki-67 (rabbit)	SP6	x	1:800	NeoMarkers
TNF-α	MP6-XT22	FITC	1:100	eBioscience
Active caspase 3	C92-605	PE	1:10	BD
MPO (rabbit)	polyclonal	x	1:200	Medac
P. aeruginosa	polyclonal	x	1:150	BIOTREND
AA-Lectin	x	Biotin	1:200	Vector Laboratories
Streptavidin	x	APC	1:400	BD
Streptavidin	x	PerCP-Cy5.5	1:1500	eBioscience
Goat-anti-rabbit	polyclonal	Alexa488	1:200	Invitrogen
Goat-anti-rabbit	TR-060-BN	Biotin		Thermo Fisher
Rabbit-anti-pimonidazole	PAb2627AP	x	1:1600	Hypoxyprobe™-1
Succinimidyl ester	x	Alexa350	1:1000	Thermo Fisher

2.2 Methods

2.2.1 Tumor model

Mice were immobilized, their abdomen was shaved, and 100 µl with $5x10^5$ CT26 cells solved in pyrogen-free PBS were injected s.c.. Tumors established for 10 days to have an optimal size of 100-150 mm³. Next, the mice were intravenously (i.v.) injected with $5x10^6$ bacteria or 1 µg recombinant TNF-α in 100 µl PBS, or solely pyrogen-free PBS as control. Tumor development was monitored by size measurement with a caliper and calculation of the tumor volume by the formula: $V = 4/3 \cdot \pi (h \cdot w^2) / 8$, h = tumor height and w = tumor width. At defined time points after bacterial infection, PBS- or TNF-α treatment, the mice were sacrificed and organs, as well as tumors were analyzed by the several methods. Mice, which had been infected with *P. aeruginosa* before they cleared the tumors, were treated twice with 10 mg/kg Ciprofloxacin (CiproHEXAL, Hexal AG, Germany) 1 day before they were re-challenged with cancer cells.

2.2.2 Adoptive T cell transfers

Spleens of BALB/c WT mice were flushed with 5 ml IMDM on ice, filtered through a 50 µm filter (Cell Trics, Partec), and spun down (8 min, 1200 rpm, 4°C). The erythrocytes in the cell pellets were lysed in ammonium-chloride-potassium (ACK) buffer (8.29 g NH_4Cl, 1.0 g $KHCO_3$, 200 µl 0.5 M EDTA per liter H_2O, pH 7.3, sterile) for 2 min, before the reaction was stopped by 10 ml IMDM, and the solution was centrifuged (8 min, 1200 rpm, 4°C); this procedure was repeated once. The isolated splenocyte pellets were used to isolate total-, $CD4^+$-, or $CD8^+$ T cells by use of negative isolation kids (Dynabeads Untouched Mouse T cells, or CD4 / CD8 T Cells (Invitrogen, USA)). For adoptive transfer, $2x10^7$-$3.5x10^7$ T cells were injected i.v.. To determine the exact number of transferred cells, an aliquot was diluted 1:1000 in PBS and Trypan blue, and counted in a Neubauer chamber using a light microscope. The purity was controlled by flow cytometry and incubation of the cells with first an anti-mouse CD16/CD32 antibody to block Fc receptors on the cells surface to avoid unspecific binding of the afterwards applied antibodies against (i) CD3, CD4, CD8 to detect the respective T cell subset, (ii) CD19 to exclude B cells, and (iii) CD11b as well as CD11c to exclude myeloid cells.

2.2.3 Flow cytometry of tumor-infiltrated neutrophils

Tumor tissues were digested (45 min, 37°C, moved) using a dispase (0.2 mg/ml)/collagenase A (0.2 mg/ml)/DNase (100 mg/ml) solution. The cell homogenates were meshed through 50 µm filters (Sysmex Partec GmbH, Germany), spun down (5 min, 1000 rmp, 4°C), and erythrocytes were removed by 2 min ACK-lysis. The cell suspension was washed in 4 ml fluorescence-activated cell sorting (FACS)-Buffer (PBS, 2 % FCS, 0.5 M EDTA) (5 min, 1000 rmp, 4°C), and single cell suspensions were prepared. These were each firstly incubated in 200 µl brefeldin-A (2 h, 37°C) to block the golgi-apparatus and, if an intracellular staining was applied, additionally stained with an Alexa Fluor 350 succinimidyl ester to visualize dead cells. Afterwards, all samples were firstly labeled with an anti-mouse CD16/CD32 antibody to block Fc receptors and secondly with the appropriate antibodies against CD45, CD11b, Ly6G, Icam, Fas, TNF-α, active caspase 3, and CD62L. For intracellular staining, samples were next fixed and permeabilized using the Cytofix-Cytoperm buffer (BD Bioscience, USA), before antibodies for intracellular targets were applied. Samples for extracellular antibody detection were mixed with Dapi directly before measurement to discriminate live and dead cells. Flow cytometry was performed using the LSRII system (BD Bioscience, USA) and the corresponding data were analyzed using the BD FACSDiva software (BD Bioscience, USA).

2.2.4 Luminex analyses of serum and tumor lysate

Heartblood was taken with a 26 G needle, filled into serum tubes (Sarstedt, Germany), incubated for 10 min at RT to enable agglutination, and centrifuged (5 min, 10,000 rmp, RT). The serum was 1:2 diluted in Sample Diluent buffer (BioRad laboratories Inc., USA) for analyses. Tumors were cut off from the mouse skin, incubated in lysis buffer (9.9 ml Bioplex Cell Lysis Buffer, 40 µl Bioplex Cell Lysis Buffer Factor 1 (250x), 20 µl Bioplex Cell Lysis Buffer Factor 2 (500x) (all from BioRad laboratories Inc., USA), 40 µl 500 mM phenylmethylsulfonyl fluoride (Sigma-Aldrich, USA)) and dissected into homogeneous 1 mm pieces on ice. Afterwards, the samples were vortexed, incubated for 20 min at -80°C, thawed for 20 min at RT, placed for 10 min into an ultrasonic bath at 4°C, stored again for at least 20 min at -80°C, and also thawed again for 20 min at RT. After vortexing, the samples were spun down (20 min, 13,000 rmp, 4°C), and the supernatant was taken for determination of the protein concentration by the use of Pierce™ BCA protein assay kit (Thermo Fisher Scientific Inc., USA). Tumor lysates were diluted to 1 mg/ml with Sample Diluent buffer (BioRad laboratories Inc., USA) for the subsequent analyses. Cytokine concentrations in serum and tumor lysates were quantified by the Luminex-based multiplex technique according to the manufacturer's instructions (BioRad, USA).

Standard curves and concentrations were calculated with Bio-Plex Manager 6.1 software. Analyses and evaluations were kindly performed by Kerstin Daemen and Prof. Dr. Christine Falk at the Institute of Transplantation Immunology, Hannover Medical School.

2.2.5 Histology

2.2.5.1 Light microscopy of paraffin sections

Tumors were cut out and fixed for 24 - 48 h in 4 % (v/v) formalin, before they were embedded in paraffin. Consecutive 3 µm sections were cut and stained with antibodies against Ki67, MPO, pimonidazole, and *P. aeruginosa* according to standardized protocols. Streptavidin conjugated with horseradish peroxidase was used as a secondary reagent (Thermo Fisher Scientific, USA) and incubated with 3,3´-diaminobenzidine (DAB) (Zytomed Systems, Germany) as peroxidase-compatible chromogen. Hematoxylin was used as counterstain. For the immunohistochemical detection of hypoxia inside tumors, 1.5 mg solid pimonidazole HCl (Hypoxyprobe^{TM}-1, USA) were solved in 100 µl saline per mouse and applied i.v. 1 h prior to sacrifice and sample preparation. Sections were additionally stained with hematoxylin and eosin to visualize tumor tissue structures including blood vessels and infiltrated cells. Preparations of samples were kindly performed by Anna Rinkel, Rebecka Wünsche, and Dr. Marina Pils at the mouse-pathology platform of the HZI.

2.2.5.2 Confocal laser scanning microscopy of cryosections

Tumors were cut out, embedded in Tissue Tek O.C.T (Sakura, USA) and snap frozen for 10 min in liquid nitrogen before they were put to -21 C or stored at -80°C. Sections of 10 µm were cut using a microtome-cryostat (HYRAX C50 Zeiss, Germany) and dried overnight (RT). Sections were rehydrated in PBS (15 min, RT), labeled with an anti-mouse CD16/CD32 antibody to block Fc receptors on the cells surface to avoid unspecific binding, and stained with the appropriate antibodies against *P. aeruginosa*, Aleuria Aurantia (AA)-Lectin, CD11b, and Gr-1. Afterwards the sections were dried for 15 min under the chemical hood and mounted with NeoMount and a coverslip. Analyses were performed at a laser scanning confocal microscope (LSM 5 META, Zeiss, Germany) and the images were processed by the LSM 5 Image Browser software (Zeiss, Germany).

2.2.5.3 Electron microscopy of ultra-thin resin sections

Tumors were cut out and fixed at least for 24 h in a solution of 5 % formaldehyde and 2 % glutaraldehyde in cacodylate buffer (0.1 M cacodylate, 0.01 M CaCl2, 0.01 M MgCl2, 0.09 M sucrose, pH 6.9). Out of one tumor, several cubes of 4 mm diameter were prepared and osmificated for 1 h in 1 % aqueous osmium tetroxide, before they were washed for 1 h in cacodylate buffer. Several steps of dehydration with graded series of acetone (10 %, 30 %, 50 %, 70 %, 90 %, 100 %) were performed for 30 min each, out of which the 70 % step was done overnight with 2 % uranyl acetate. The cubes were than infiltrated with an epoxy resin according to Spurr´s formula. A diamond knife was used to cut ultrathin sections of the cubes. These were picked up with formvar-coated grids, counterstained with uranyl acetate and lead citrate, and analysed by a TEM910 transmission electron microscope (Zeiss, Germany) at an acceleration voltage of 80 kV. The depicted images were taken at calibrated magnifications and processed with an ITEM-software (Olympus Soft Imaging Solutions, Germany). Preparations and evaluations of the samples were kindly performed by Ina Schleicher and Prof. Dr. Manfred Rohde at the electron microscopy platform of the HZI.

2.2.6 Detection of luciferase activity *in vivo*

Tumor-bearing IFN-$\beta^{+/\Delta\beta\text{-luc}}$ mice were treated with the respective inoculum, i.v. injected with 150 mg/kg D-luciferin (Perkin Elmer, USA) prior to each imaging, anesthetized using 2 % Isofluran (Abbott, USA), and monitored with an IVIS 200 imaging system (Xenogen, USA) [137]. The resulting photon flux, reflecting the enzymatic activity of luciferase which corresponds to the amount of expressed IFN-β, was quantified using the Live Imaging 3.0 software (Perkin Elmer, USA).

2.2.7 Statistical analyses

All statistical analyses were performed on *ex vivo* data of small groups with less than 10 mice. Therefore the data were always presented as median and the error bars represented the range of the median. Significances were calculated by the Mann-Whitney Test for comparison of two groups using the software GraphPad Prism 5 (GraphPad Software Inc., USA).

3 Results

In the present study the well-established tumor colonization properties of *Pseudomonas. aeruginosa* should be used to better understand the biology of bacteria-mediated tumor therapy. Especially parameters of the anti-tumor response of the innate as well as the adaptive immune system should be studied. For this purpose, first optimal parameters for the colonization of tumors by *P. aeruginosa* had to be established.

3.1 Optimal parameters for tumor colonization

To be able to reliably receive a maximal colonization of infected tumors, some parameters of the model system needed to be calibrated. First, the influence of the tumor size on a sufficient colonization with *P. aeruginosa* was investigated. Syngeneic CT26 tumor cells were s.c. injected on different days into the respective hosts to receive a broad spectrum of tumor sizes at the day of infection, such that the same bacterial inoculum could be used for all tumor-bearing mice.

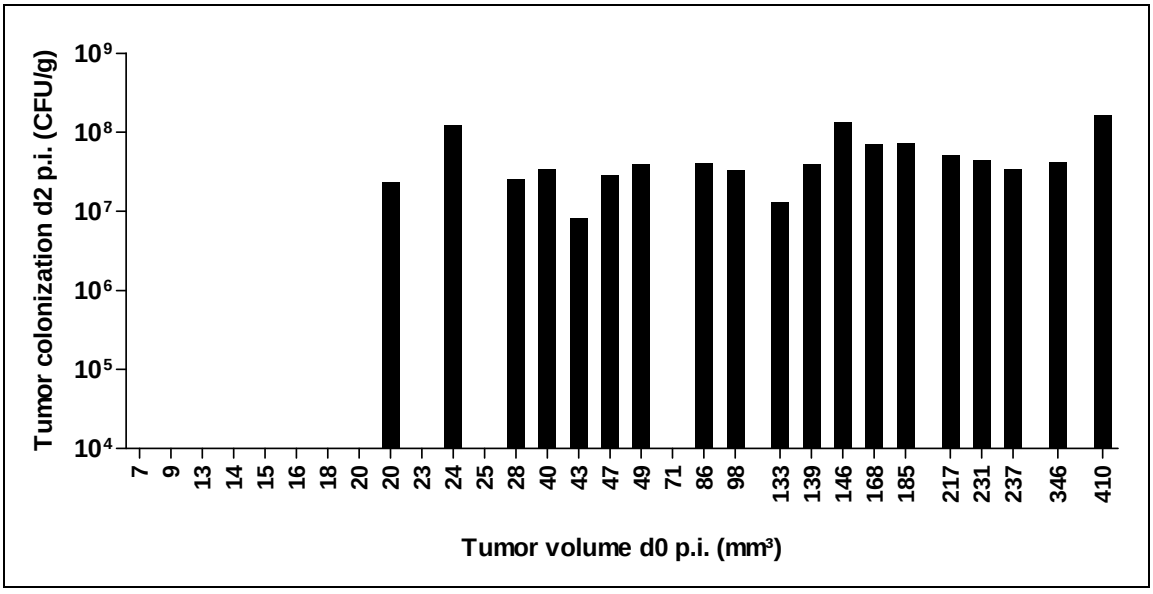

Figure 10: Efficiency of tumor colonization is tumor size-dependent
To get various tumor sizes, cancer cells were injected on several days. Tumors of 7-23 mm³ were 2 to 5 days old, 24-43 mm³ tumors were 7 days old, 47-237 mm³ tumors developed for 9 days, and 146-410 mm³ tumors developed for 13 days. Mice were infected with 2.33 or 4.4×10^6 *P. aeruginosa** and tumors were analyzed 2 days later for bacterial colonization by plating. Bars represent individual mice, *combined from two experiments, and depicted in 100 mm³-stages. Data published in Pawar V., Komor U., Kasnitz N. *et al.* [138].

As shown in (Figure 10, p.32), tumors with a smaller size than approximately 100 mm³ carried the risk of not being colonized by bacteria whereas tumors in the range between 100 to 400 mm³ were all well colonized. Normally, after around 10 days of development tumors reached a size of 100-150 mm³. At that size they were obviously sufficiently vascularized to guarantee a robust bacterial colonization. Therefore, the optimal time point to infect tumor-bearing BALB/c WT mice was 10 days after CT26 cell inoculation with $5x10^5$ cells.

Besides the tumor volume, the infection dose could also be very important for stable tumor colonization. The inoculum represents furthermore the most critical parameter for the health of the mice. It should therefore be as low as possible to limit the burden for the animals. On the other hand, it should be high enough to ensure a robust colonization of the tumor tissue. Based on the above established optimal tumor volume, different infection doses of *P. aeruginosa* PA14 were tested (Figure 11).

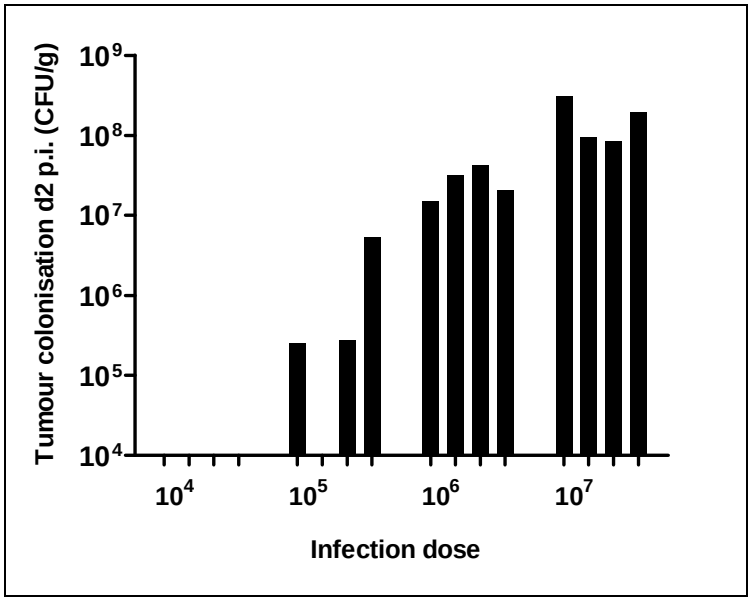

Figure 11: Efficiency of tumor colonization is infection dose-dependent
When tumors had optimal sizes of about 100-150 mm³, mice were i.v. infected with $4.7x10^4$ (10^4), $6.3x10^5$ (10^5), $4.0x10^6$ (10^6), and $3.8x10^7$ (10^7) *P. aeruginosa* PA14 in 100 µl PBS. Tumors were plated 2 d p.i. to analyze bacterial colonization. Bars represent individual mice of one experiment. Data published in Pawar V., Komor U., Kasnitz N. *et al.* [138].

An injection dose of less than $5x10^6$ *P. aeruginosa* per tumor-bearing WT mouse did not result in a sufficient colonization (Figure 11): with $5x10^4$ injected bacteria the tumors were not colonized at all, and when $5x10^5$ bacteria were applied only some tumors were colonized, but to a lower degree. In contrast, with an injection of $5x10^7$ *P. aeruginosa* per mouse, all tumors were in fact highly colonized. However, the health burden for the mice was too high. They showed rough fur and agglutinated eyes.

A systemic infection with $5x10^6$ *P. aeruginosa* PA14 appeared to be optimal. All tumors were colonized to a high degree. The health burden was acceptable thus allowing observations over several days.

3.2 Tumor development after bacterial infection

Within the first day after intravenous administration of the bacteria, the visible phenotype of the transplanted subcutaneous tumors changed. The clinically detectable, well vascularized, and reddish-looking tumors turned into a red-dark to black color (Figure 12). The mice behaved normal and did not show any kind of health burden. This tumor phenotype was independent from the genotype of the mice used during the studies and appeared always within 1 day post i.v. infection.

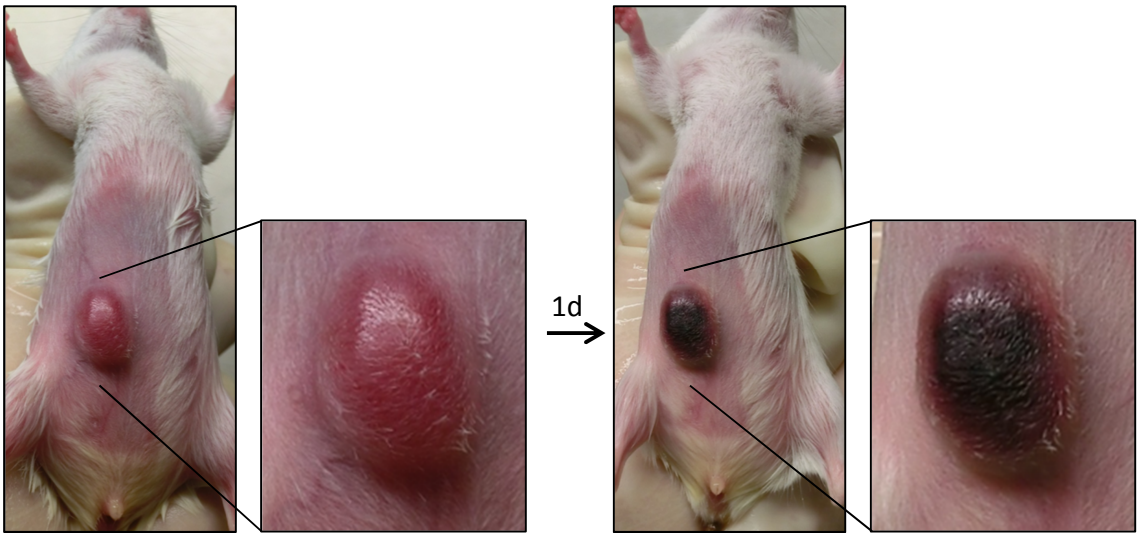

Figure 12: Development of necrotic tumors after infection
Tumor-bearing mice were i.v. infected with $6.3x10^6$ *P.aeruginosa* PA14 in 100 µl PBS after 10 days of tumor growth. After the first 24 h after infection, the visible phenotype of the s.c. tumor appeared to be dark. The depicted tumor illustrates a general effect observed in all infection experiments.

To see the long term consequences of tumor colonization on tumor growth, tumor-bearing BALB/c WT mice were infected i.v. with *P. aeruginosa* and the ongoing development of tumor size was followed. Tumors started to decrease in size already within the first 24 h after infection (Figure 13, p.35). This trend was significant with $p<0.05$ on day 3 p.i. and with $p<0.01$ from day 5 p.i. onwards. On day 13 p.i. all tumors were rejected completely and the mice stayed tumor free without any further treatment.

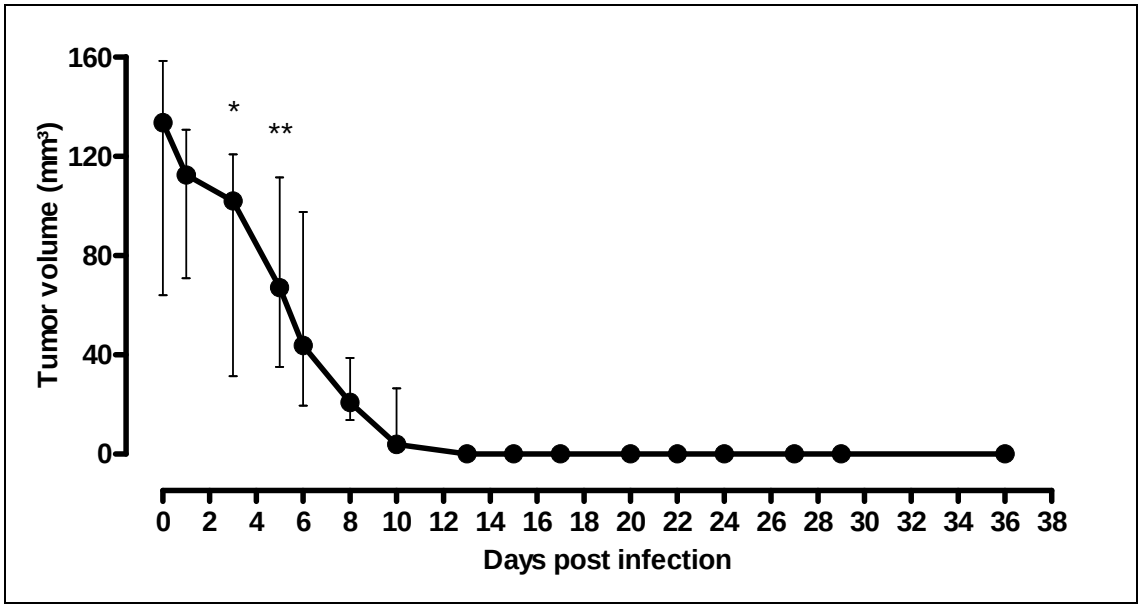

Figure 13: Tumor rejection after intravenous infection of WT mice
Tumor-bearing BALB/c WT mice were i.v. infected with $3.6x10^6$ *P. aeruginosa* PA14 when tumors had reached an optimal size of about 100-150 mm³. Data are represented as median and range from n=6 of one experiment. For statistical analyses the Mann-Whitney test, one-tailed, *p<0.05, ** p<0.01 were used to compare respective tumor sizes with the tumor size on the day of infection (d0).

To investigate whether bacterial induced rejection of the CT26 tumors was due to a reaction of the adaptive immune system, mice that had cleared the tumor were re-challenged with CT26 colon carcinoma cells after 43 days of tumor clearance. Two treatments with 10 mg/kg CiproHEXAL (Hexal AG, Germany) were made 1 day before tumor setting to exclude any residual bacterial influence on tumor development. For this re-challenge, the CT26 cells were injected into the right side of the abdomen to exclude any inflammatory local influences, since the rejected CT26 tumors had been implanted on the backs of the animals. At the same time the mice received a second cancer cell line, F1A11 fibrosarcoma cells, injected s.c. into the left side of the abdomen as specificity control. Because the F1A11 cancer cells are unrelated to CT26 cells and were applied for the first time, the immune system of the host, if involved in the rejection process, should not be able to counteract F1A11 development, while it should strongly react against the original CT26. Both tumor cell lines started to develop and became palpable within the first 5 days after injection (Figure 14, p.36). Whereas the CT26 tumors eventually started to decrease in size and were finally completely rejected, the F1A11 tumors grew continually. Starting on day 5 p.t., the two distinct tumors on the abdomen of individual mice showed significant size differences with p<0.01 from day 7 p.t. onwards. Importantly, only the CT26 cancer cells were rejected for which the mice should have developed an immune memory. Thus, the reaction was specific.

These two criteria, memory and specificity, are characteristic for the adaptive immune system and indicated that a specific immune reaction was involved in the process of tumor rejection.

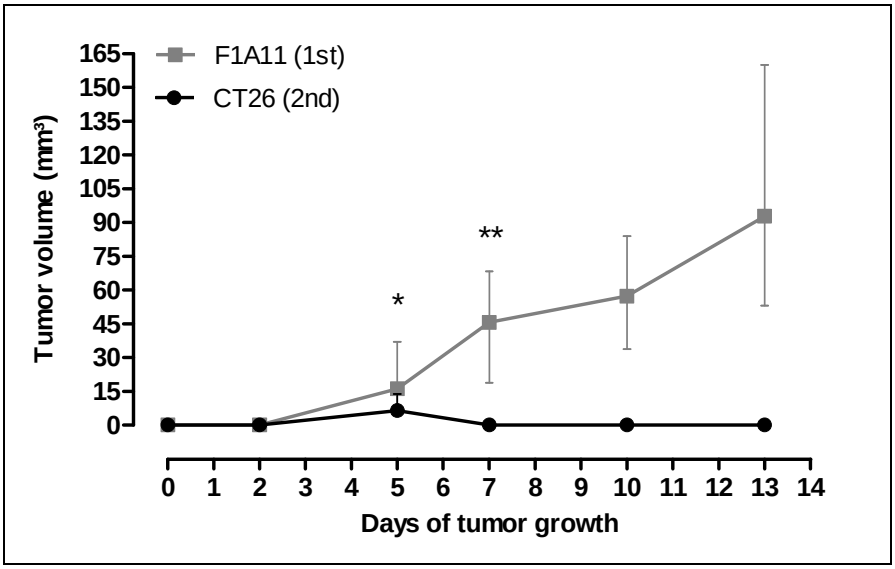

Figure 14: Tumor development after first- or repetitive cancer cell challenge in WT mice
Tumor-free BALB/c WT mice were s.c. treated with two different cancer cell lines at a time. They received CT26 colon carcinoma cells for a second time (2nd) and F1A11 fibrosarcoma cells for the first time (1st). Both were injected into the abdomen, since the previous CT26 tumor was implanted into the back. Data are represented as median and range from n=6 of one experiment. For statistical analyses the Mann-Whitney test, one-tailed, *p<0.05, ** p<0.01 was used to compare tumor sizes of CT26 and F1A11 tumors at the same time point.

To confirm the importance of the adaptive immune system for tumor rejection in our infection model, BALB/c Rag1$^{-/-}$ mice which lack the adaptive arm of the immune system were employed. The progress of CT26 tumor development was compared between infected BALB/c WT and Rag1$^{-/-}$ mice (Figure 15, p.37). Already before infection, tumors on Rag1$^{-/-}$ mice grew faster than on WT mice. The difference in tumor size between the two mice genotypes diverged from day 7 of tumor growth (reflected as day -3 in Figure 15, p.37) onwards. This indicates that already under undisturbed conditions the adaptive immune system exerts a certain cancer control. As expected, after infection with *P. aeruginosa* only tumors on WT mice started to shrink, whereas the same tumor cell line continued to grow on Rag1$^{-/-}$ animals (Figure 13, p.35). This confirms that tumor rejection of bacterial infection is elicited by a tumor specific immune reaction.

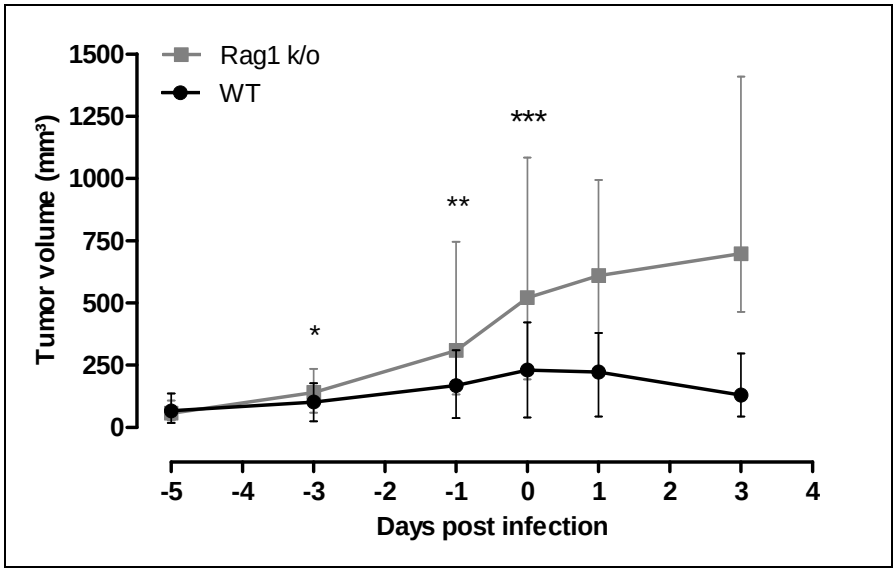

Figure 15: Distinct tumor development in syngeneic mice
Tumor development was investigated in BALB/c WT and Rag1$^{-/-}$ mice, infected on day 10 with 6.2x10^{6} *P. aeruginosa* PA14. Data are represented as median and range from n=12 of one experiment. For statistical analyses the Mann Whitney test, one-tailed, *p<0.05, ** p<0.01, *** p<0.001 were used to compare tumor sizes on WT and Rag1$^{-/-}$ on the same day.

3.3 Contribution of T-lymphocytes on tumor development and therapy

The tumor-suppressive impact of especially effector T cells is well established. Therefore, Rag1$^{-/-}$ mice were reconstituted with different T cells and the subsequent tumor development was compared to unmodified Rag1$^{-/-}$ mice. No additional infection was applied to the mice. Splenic total T cells (CD4^{+} and CD8^{+}) from differentially treated or untreated BALB/c WT animals were used for the experiment. These included T cells of naïve BALB/c mice, T cells of WT mice which were each bearing a 12 day old tumor, and T cells from WT mice which have been infected with *P. aeruginosa* after 10 days of tumor growth and were at that time tumor free since 40 days. The growth of tumors on naïve Rag1$^{-/-}$ mice and on Rag1$^{-/-}$ mice adoptively modified with naïve T cells was similar (Figure 16, p.38). In contrast, the transfer of T cells from tumor-bearing mice retarded the growth of tumors from day 9 p.t. onwards. However, only the transfer of T cells isolated from mice, which have been able to clear tumors after *P. aeruginosa* infection enabled the rejection of tumors in uninfected Rag1 mice. From day 11 onwards, the median tumor size of that group was significantly smaller than that of naïve Rag1$^{-/-}$animals.

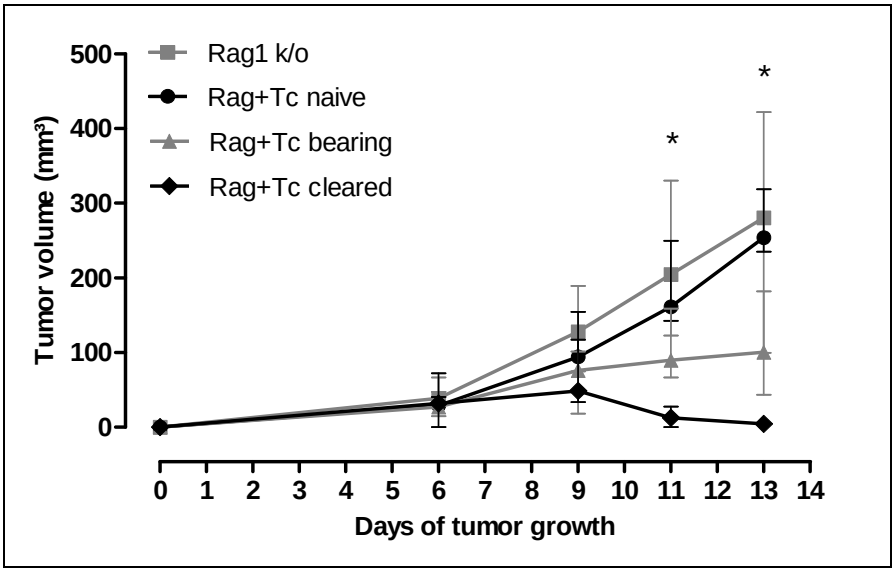

Figure 16: Total T cells-priming-dependent tumor development after adoptive transfer
Tumor development in Rag1$^{-/-}$ mice and reconstituted Rag1 mice was compared. For the adoptive transfer, mice received differentially stimulated splenic CD4^{+}+CD8^{+} T cells of BALB/c WT mice: (i) 2x10^{7} naïve T cells (Tc naïve), (ii) 3x10^{7} T cells of tumor-bearing mice (Tc bearing) with tumor growth since 12 days, and (iii) 3x10^{7} T cells from previously infected mice which had cleared tumors since 40 days (Tc cleared). Data are represented as median and range from n=3-4 of one experiment. For statistical analyses the Mann-Whitney test, one-tailed, *p<0.05 was used to compare tumor sizes of Rag1$^{-/-}$ and modified Rag1 mice (i-iii) on the same time point. Statistical data represent comparison for (iii). Data published in Stern C., Kasnitz N. *et al.* [111].

To test if isolated splenic CD4^{+} or CD8^{+} T cells are sufficient to decrease tumor growth or even to reject tumors completely, the individual cells were independently isolated and transferred into Rag1$^{-/-}$ animals together with CT26 tumor cells. Again, the tumors on unmodified Rag1$^{-/-}$ animals and on those Rag1$^{-/-}$ mice transferred with naïve total T cells from BALB/c mice grew very similar (Figure 17, p.39). A weak retardation in tumor growth did occur after transfer of CD4^{+} T cells from tumor-bearing mice. This was significantly different with p<0.05 to the tumor growth on Rag1 animals that received naïve T cells from day 11 onwards (Figure 18B, p.40). The transfer of equal numbers of CD8^{+} T cells of tumor-bearing mice exhibited significantly stronger growth retardation. Even though such T cells were not sufficient to suppress tumor development, they did show a stronger tumor-suppressive effect than the CD4^{+} T cells of tumor-bearing WT mice with p<0.01 (Figure 18B, p.40). However, by applying a mixture of both kinds of such T cells at the same time, tumors were already significantly smaller on day 6 p.t. compared to Rag1 mice treated with naïve total T cells. Most of these mice were even able to reject CT26 tumors completely. Only one out of four tumors started to re-grow between day 11 and 14 after cancer cell injection. This explains the increasing range of the median in Figure 18A+B, p.40.

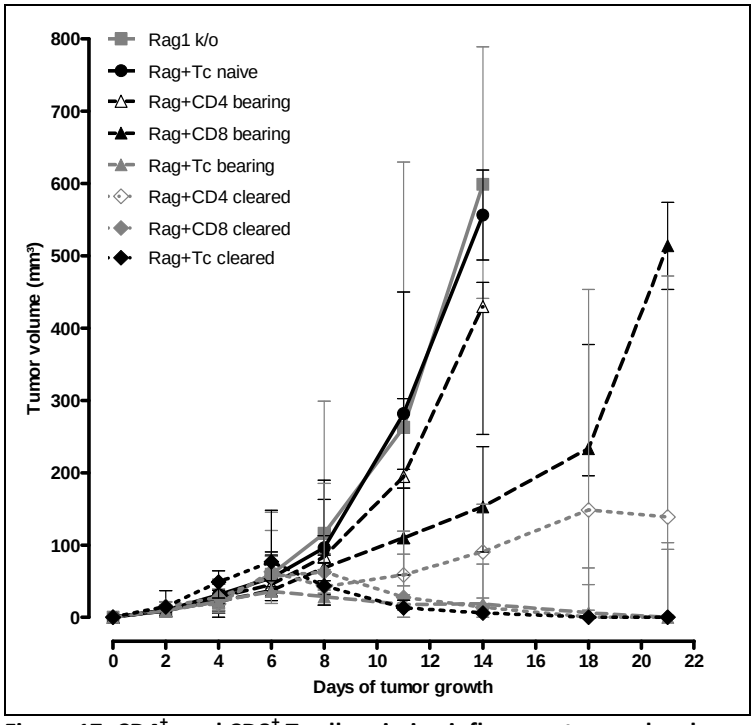

Figure 17: CD4$^+$- and CD8$^+$ T cells-priming influences tumor development after adoptive transfer
Tumor development in naïve and reconstituted Rag1$^{-/-}$ mice stimulated with splenic CD4$^+$, CD8$^+$, or total (Tc) T cells out of BALB/c WT mice: (i) 3.5x10^7 naïve total T cells (Tc naïve), (ii) 3x10^7 T cells (CD4$^+$, CD8$^+$, Tc bearing) of tumor-bearing mice with tumor growth since 12 days, (iii) 3x10^7 T cells from previously infected mice which had cleared tumors since 4 month (CD4$^+$, CD8$^+$, Tc cleared). Data are represented as median and range from n=4-7 of one experiment and are separated per treatment in Figure 18 , p.40 and Figure 19, p.41.

The strongest anti-tumor reaction of all eight analyzed groups in Figure 17 showed Rag1$^{-/-}$ mice, which had received T cells from mice that had been infected and consequently cleared the tumors. After injection of isolated CD4$^+$ T cells from such mice, the tumor development was admittedly decreased with a significance of $p<0.01$ from day 8 onwards (Figure 19B, p.41). But this group of seven mice reacted heterogeneous, which was reflected by the increased range of the tumor size median. Three mice showed tumor rejection, whereas tumors continued to grow on four mice. The transfer of equivalent CD8$^+$ T cells showed a more prominent effect. From day 11 of tumor growth onwards, tumors of such Rag1 mice were significantly smaller with $p<0.01$ than tumors on mice treated with naïve total T cells. A complete tumor rejection did occur in three of five mice, therefore in Figure 19B (p.41) only the range of the median at day 18 and 21 p.t. is shown. An even stronger trend was observed by the injection of total T cells from mice that had cleared the tumors. In that case, tumors were already significantly smaller with $p<0.01$ from day 8 after transfer of tumor and T cells onwards, and all the mice were tumor free from day 18 on. The impact of purified CD8$^+$ T cells and total T cells from tumor-immune mice on the development of new CT26 tumors was similar. No significant difference between the median tumor sizes of the respective groups was detected (Figure 19, p.41).

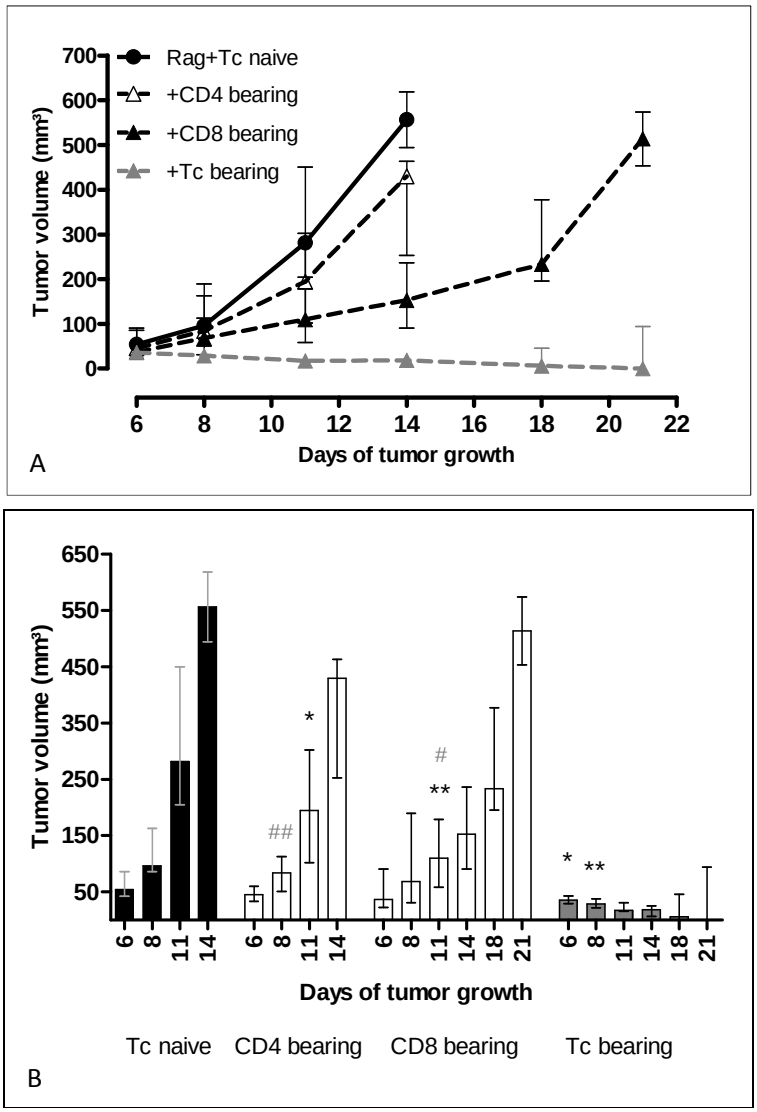

Figure 18: T cells out of tumor-bearing mice retard tumor growth after adoptive transfer
Figure 17, p.39 in detail. A: tumor growth on reconstituted Rag1 mice which received splenic $CD4^+$, $CD8^+$,or total (Tc) T cells out of BALB/c WT mice: (i) $3.5x10^7$ naïve total T cells (Tc naïve) or (ii) $3x10^7$ T cells of tumor-bearing mice ($CD4^+$, $CD8^+$, Tc bearing) with tumor growth since 12 days. B: Comparison of tumor growth. Data are represented as median and range from n=4-7 of one experiment. The Mann-Whitney test, one-tailed was used to compare tumor sizes at the same time point: *p<0.05, **p<0.01 to compare Tc naïve with $CD4^+$/$CD8^+$/Tc bearing. #p<0.05, ##p<0.01 to compare $CD4^+$/$CD8^+$ Tc bearing with total T cells bearing. Groups were analyzed in 3 independent experiments.

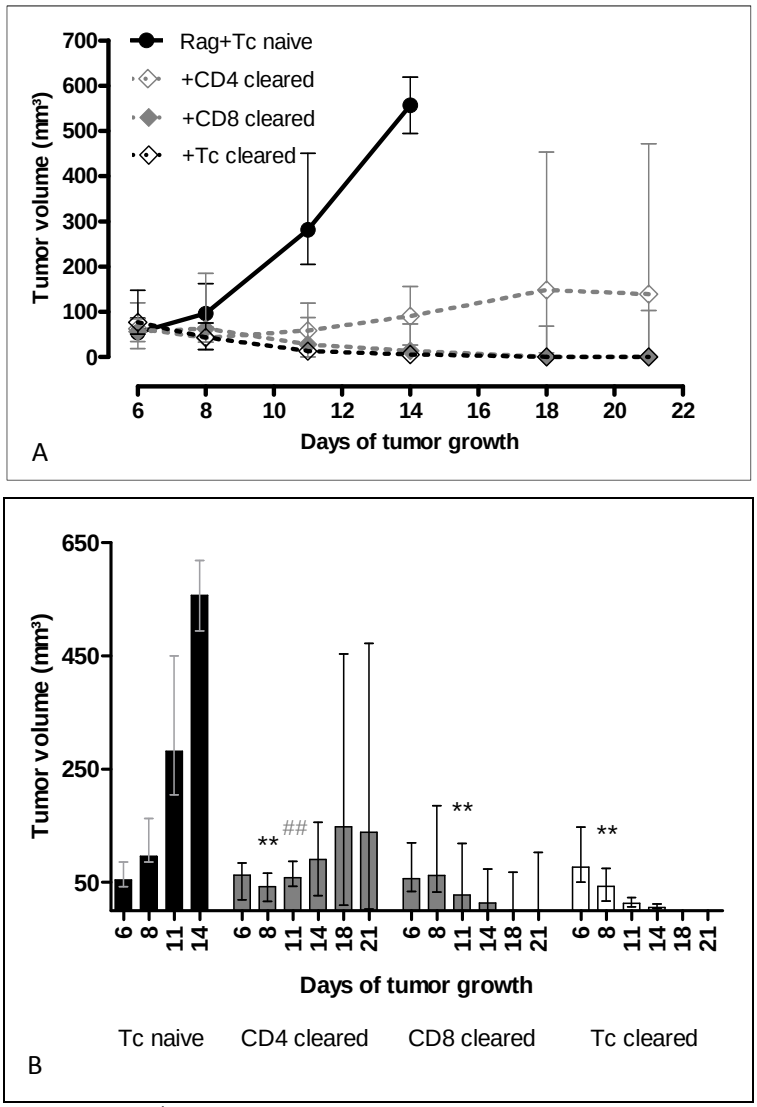

Figure 19: CD8$^+$ T cells out of treated tumor-free mice reject tumors after adoptive transfer
Figure 17, p.39 in detail. A: tumor growth on reconstituted Rag1 mice which received splenic CD4$^+$, CD8$^+$,or total (Tc) T cells out of BALB/c WT mice: (i) 3.5x10^7 naïve total T cells (Tc naïve) or (ii) 3x10^7 T cells from previously infected mice which had cleared tumors since 4 month (CD4$^+$, CD8$^+$, Tc cleared). B: Comparison of tumor growth. Data are represented as median and range from n=4-7 of one experiment. The Mann-Whitney test, one tailed was used to compare tumor sizes at the same time point. **p<0.01 to compare Tc naïve with CD4$^+$/CD8$^+$/Tc cleared. ##p<0.01 to compare CD4$^+$/CD8$^+$ Tc cleared with total T cells cleared. Groups were analyzed in 2 independent experiments.

3.4 Tumor-associated neutrophils and -cytokines

When tumor-bearing BALB/c or Rag1$^{-/-}$mice were infected with *P. aeruginosa*, CT26 tumors changed their macroscopic appearance from reddish to a dark color within 24 h p.i. (Figure 12, p.34). In the following, such tumors started to shrink in WT mice and were cleared within 13 days (Figure 13, p35). To investigate how the tumor microenvironment of CT26 solid tumors looks like after infection and onset of tumor-suppressive processes, immune histology was deployed. Consecutive sections of tumors were stained with different antibodies or reagents.

First, the formation of different tumor zones 3 days p.i. was detected by hematoxylin-and-eosin (H&E) staining (Figure 20A, p.43): the outer layer of the tumor was surrounded by the skin (S) of the mouse with hairs and sebaceous glands, subcutaneous tissue, and musculature (M) close to the connective area of the abdomen. The tumor underneath started with a circular zone of viable tumor cells (V). A second ring of viable, highly nucleated cells (G) was formed between the outer tumor zone and the inner necrotic tumor area (N). The classification of tumor infiltrated cells as tumor-associated neutrophilic granulocytes (G) was possible by using a higher magnification of the H&E image and thereby identifying the typical neutrophil nuclear shape (magnification image is depicted in Pawar V., Komor U., Kasnitz N. *et al.*[138]). This visual analysis serves as the gold standard for a correct identification of neutrophils [35]. In addition, anti-myeloperoxidase staining was performed which specifically revealed such granulocytes (Figure 20B, p.43). The purple circle in Figure 20A was identical to the brown circle in Figure 20B.

Plating experiments had demonstrated a strong colonization of tumors by *P. aeruginosa* (Figure 11, p.33). Hence, the side of bacterial localization was highlighted by an anti-*P. aeruginosa* staining (Figure 20C, p.43). These microscopical analyses revealed several small areas of bacterial colonization. They were located between the viable and the necrotic tumor zones, and in close proximity or even co-localized with neutrophilic granulocytes.

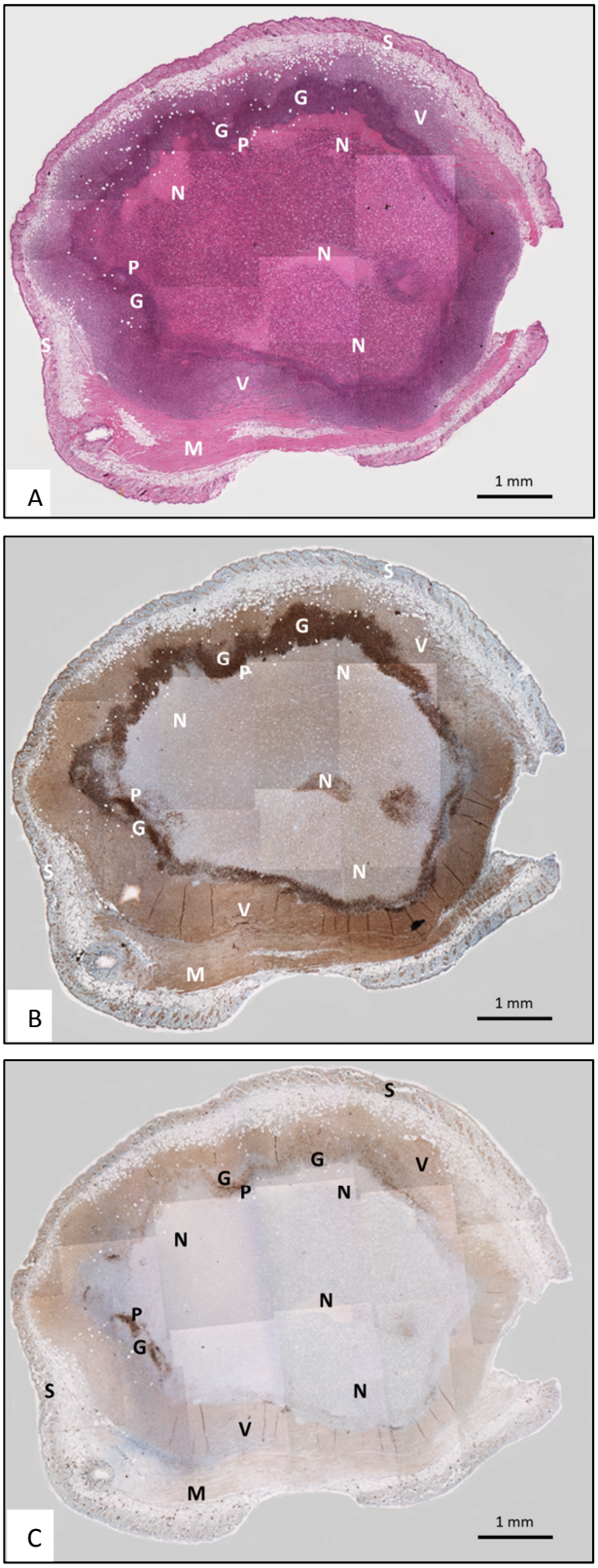

Figure 20: TANs reside close to the necrotic area and *P. aeruginosa* inside tumors.
The CT26 tumor on a BALB/c mouse was collected 3 days p.i. with $1x10^6$ *P. aeruginosa* and several consecutive sections were prepared. Sections were stained with: A: Hematoxylin-and-eosin to highlight viable (V) and necrotic (N) regions within the tumor. Around the tumor were the mouse skin (S) and musculature (M). The dark purple and circular area representing infiltrated cells with intact nuclei was further characterized in B: Staining with diaminobenzidine-myeloperioxidase to highlight neutrophilic granulocytes (G). C: *P. aeruginosa* highlighted by a diaminobenzidine-*P. aeruginosa* antibody (P). For the analyses, pictures of the sections were made transparently and put on top of each other to label exactly the same areas in all images and to demonstrate relative proximity. Image A is published in in Pawar V., Komor U., Kasnitz N. *et al.* [138].

Since neutrophils are mobilized to the tumor by cytokines and chemokines, which also induce their polarization, luminex analyses were performed on tumor lysates. Among the cytokines detected were molecules that influence the migration of neutrophils, and support their functional polarization, but also molecules which act on endothelial cells and might therefore influence the permeability of the tumor neovasculatur and neutrophil infiltration (Figure 21A+B).

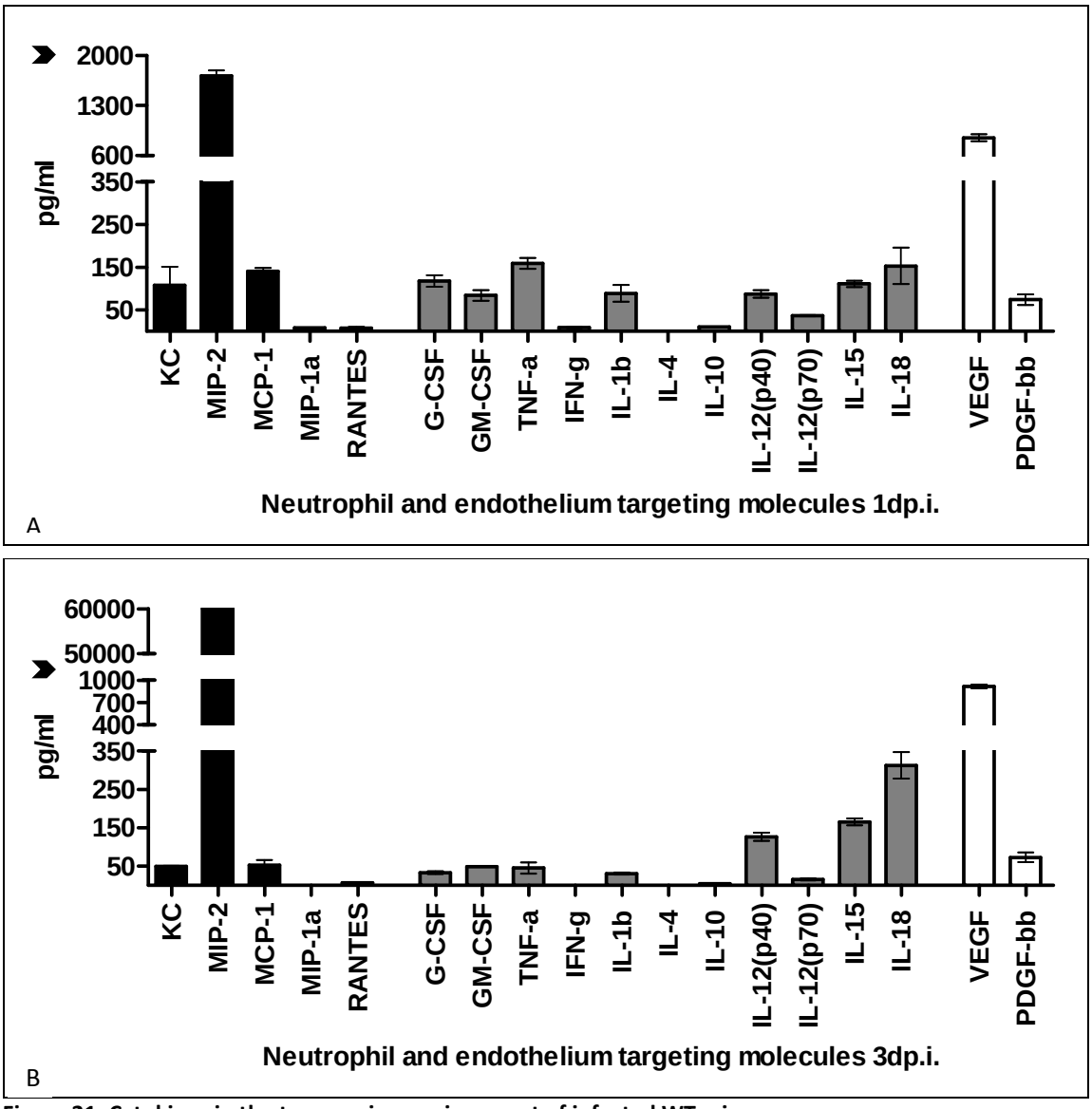

Figure 21: Cytokines in the tumor microenvironment of infected WT mice

Luminex analyses were performed on tumor lysates 1 d (A) and 3 d p.i. (B) of WT mice with $5x10^6$ *P. aeruginosa*. Black bars represent neutrophil chemoattractants, whereas gray bars indicate molecules responsible for the activation and polarization of neutrophils. White bars show molecules which act on endothelial cells. Arrows on the y-axis indicate an increased concentration of molecules 3 d p.i.. Data are represented as median and range from n=2 of one experiment.

The chemokines KC / CXCL-1, MIP-2 / CXCL-2, and MCP-1 (monocyte chemoattractant protein) / CCL-2 mainly attract neutrophil migration. The concentration of MIP-2 increased tremendously between day 1 and day 3 p.i. (Figure 21A+B, p.44). This might indicate an essential role of MIP-2 for the permanent attraction of neutrophils into the tumor. The chemokines KC and MCP-1 appeared to be less involved in the migration process. The cytokines G-CSF, GM-CSF, TNF-α, IL-1β, and IL-12 (p70) were present to low amounts in tumors on day 1 p.i. and showed even decreased concentrations on day 3 p.i. whereas the concentrations of IL-12 (p40), IL-15, and IL-18 were slightly increased two days later (Figure 21A+B, p.44). They all belong to a group of molecules in the tumor microenvironment that can influence the general polarization of neutrophils and induce the release of cytokines and chemokines by the cells. Furthermore, they can inhibit neutrophil apoptosis and thereby prolong the cells survival. The concentrations of VEGF and PDGF-bb (platelet-derived growth factor with two B-chains) stayed constant between day 1 p.i. and day 3 p.i.. Since VEGF was detected in high concentrations, it might have played a more important role for the infiltration of cells and bacteria into the tumor.

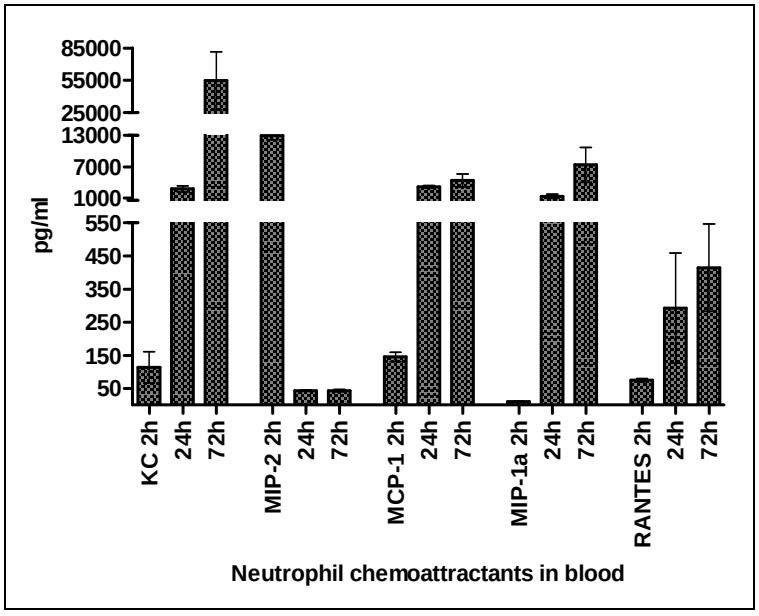

Figure 22:Neutrophil chemoattractants in the circulation of infected WT mice
Luminex analyses were performed on heart blood 2 h, 24 h, and 72 h p.i. of WT mice with $5x10^6$ *P. aeruginosa*. The illustrated molecules can influence the migration of neutrophils. Data are represented as median and range from n=2 of one experiment.

To investigate whether the five analyzed chemoattractants that neutrophils respond to are only available inside the tumor or also present in the circulation, blood samples from the same mice were also analyzed at different time points to see whether a chemokine gradient between the circulation and the tumor tissue existed.

All of such neutrophil chemoattracting molecules were available within the circulation of the host (Figure 22, p.45), whereas only three of them (KC, MIP-2, and MCP-1) were detectable in the corresponding tumor lysates (Figure 21A+B, p.44). The concentration of the four chemokines KC / CXCL-1, MCP-1 / CCL-2, MIP-1α / CCL-3, and Rantes / CCL-5 in blood increased over time, and reached different final levels with KC > MCP-1 > MIP-1α > Rantes. The only chemokine which was already upregulated at 2 h p.i. was MIP-2 / CXCL-2.

Since chemoattracting gradients should became apparent, the concentrations of such molecules in circulation and the tumor lysates were directly compared to discover the direction of chemokine gradients decisive for neutrophil migration. The chemokine MIP-2 was highly present in the circulation at 2 h p.i., but available in prominent concentrations only within the tumor microenvironment later on (Figure 23). Thus, it seemed to be initially responsible for neutrophil mobilization from the BM into the blood once bacteria are applied. While MIP-2 seemed to be responsible for the early extravasation of neutrophils into the tumor as a side of infection, alternative chemokines seemed to be responsible for that at later time points.

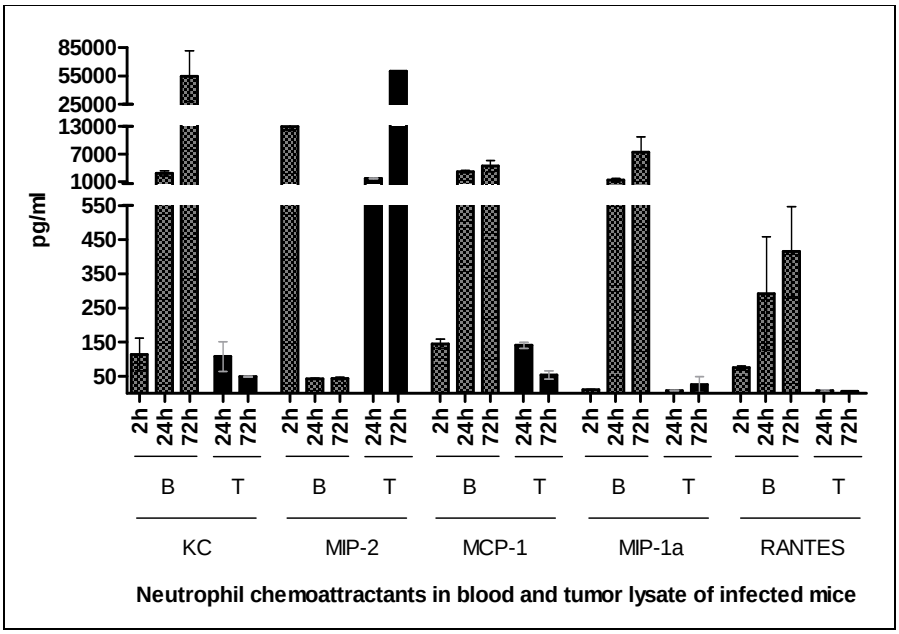

Figure 23: Neutrophil chemoattractants in blood and tumor of infected WT mice
Luminex analyses of neutrophil chemoattractants performed on heartblood (B, gray bars) and tumor lysates (T, black bars) of the same mice after 2 h, 24 h, and 72 h p.i. with $5x10^6$ *P. aeruginosa*. Data are represented as median and range from n=2 of one experiment.

Since neutrophils are also part of uninfected, growing tumors (see also later in Figure 26A+C, p.50), the concentrations of the same cytokines were also compared in blood and tumor lysates of uninfected WT mice. Under these circumstances all cytokines were found in blood and tumor lysate, especially at later time points (Figure 24).

Therefore they might all be important for the mobilization and chemoattraction of neutrophils, their intra- and extravasation, and the development of TAN populations under undisturbed conditions of tumor growth.

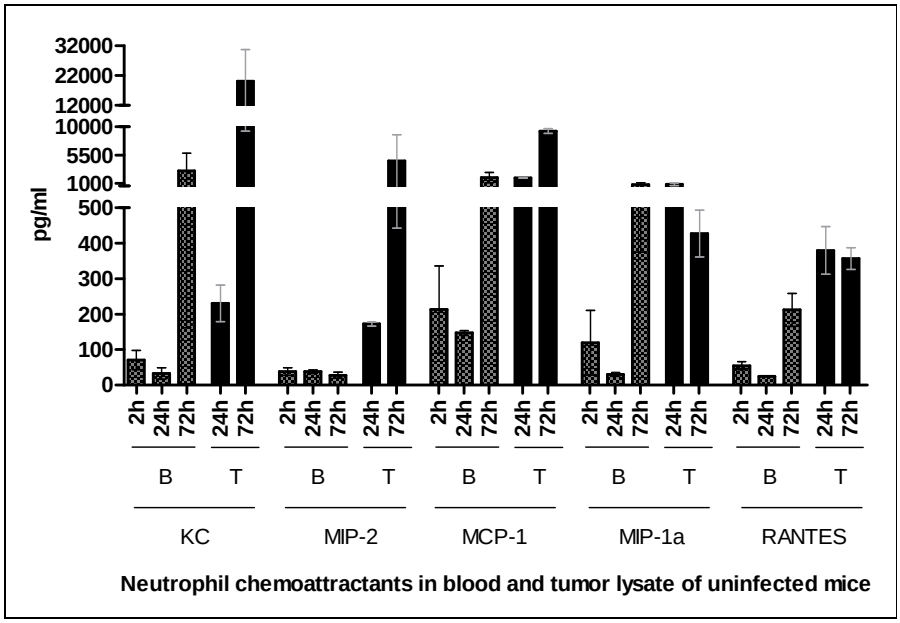

Figure 24: Neutrophil chemoattractants in blood and tumor of uninfected WT mice
Luminex analyses performed on heartblood (B, gray bars) and tumor lysates (T, black bars) of the same mice after 11 d (=2 h), 12 d (=24 h), and 14 d (=72 h) of tumor development. The time points in hours represent the time points after i.v. injection of 100 µl PBS as infection control. Data are represented as median and range from n=2.

Altogether, between tumors of uninfected and with *P. aeruginosa* infected mice, two main differences according to the detected chemokine concentrations existed. Firstly, tumors of uninfected mice contained detectable concentrations of all five chemokines tested (Figure 24). Secondly, in such tumors existed five chemokine gradients with increasing concentrations from the circulation into the tumor, at the individual time points. Whereas in infected mice, only the MIP-2 / CXCL-2 gradient was detected with the potential to attract neutrophils into the tumor (Figure 23, p.46).

3.4.1 Phenotypical characterization of TAN populations

Neutrophils in tumors are often polarized into the direction of anti-inflammatory N2 cells. However, in the present situation the normal tumor development is disturbed by the presence of an enlarged necrotic region as well as bacteria which might influence the polarization of neutrophils. Therefore, tumors were investigated by digestion of tumor tissues and subsequent flow cytometry. To standardize the analysis, always the same gating strategy was used (Figure 25A-J, p.49). As a second control group besides untreated tumors and to mimic extrinsic inflammatory effects, tumor-bearing mice were i.v. treated with 1 µg / 100 µl of recombinant TNF-α.

First of all, the total number of TANs which infiltrated the tumors of differentially treated WT mice was investigated. Within untreated (PBS) tumors, the total number of TANs amounted to 10^6 neutrophils / gram tumor and was uniform on day 11 and day 13 of tumor growth (Figure 26A+C, p.50). The neutrophil influx on day 1 p.t. with PA14 or TNF-α was comparable to that (Figure 26B, p.50), whereas at day 3 p.t. the total number of TANs per tumor was significantly higher in the two treated groups (Figure 26D, p.50).

However, not only the number of TANs, but rather their functional specialization is supposed to be influenced by the various conditions within the tumor microenvironment. While CT26 tumors continually grew on untreated BALB/c mice, they started to shrink immediately after infection with *P. aeruginosa* PA14 (Figure 13, p.35) or TNF-α-treatment [122]. Therefore, TANs inside the different tumor microenvironments were analyzed for the distinct expression of diagnostic markers of polarization, like surface molecules and cytokines, on day 11 and 13 of tumor growth. Although the number of TANs in tumors of untreated (PBS) and treated (PA14, TNF-α) animals at day 1 p.t. was similar (Figure 26A+B, p.50), the expression of phenotyping markers was different after treatment (Figure 27A, B, D, p.51). The bacterial infection or TNF-α-injection induced both the following phenotypic changes (Figure 27B-E, p.51): significant more TANs expressed Icam and Fas, but less cells produced TNF-α at the same time. Only after infection the number of TANs with active caspase 3 was additionally increased. These changes represented obvious phenotypic switches of the TAN population after treatment.

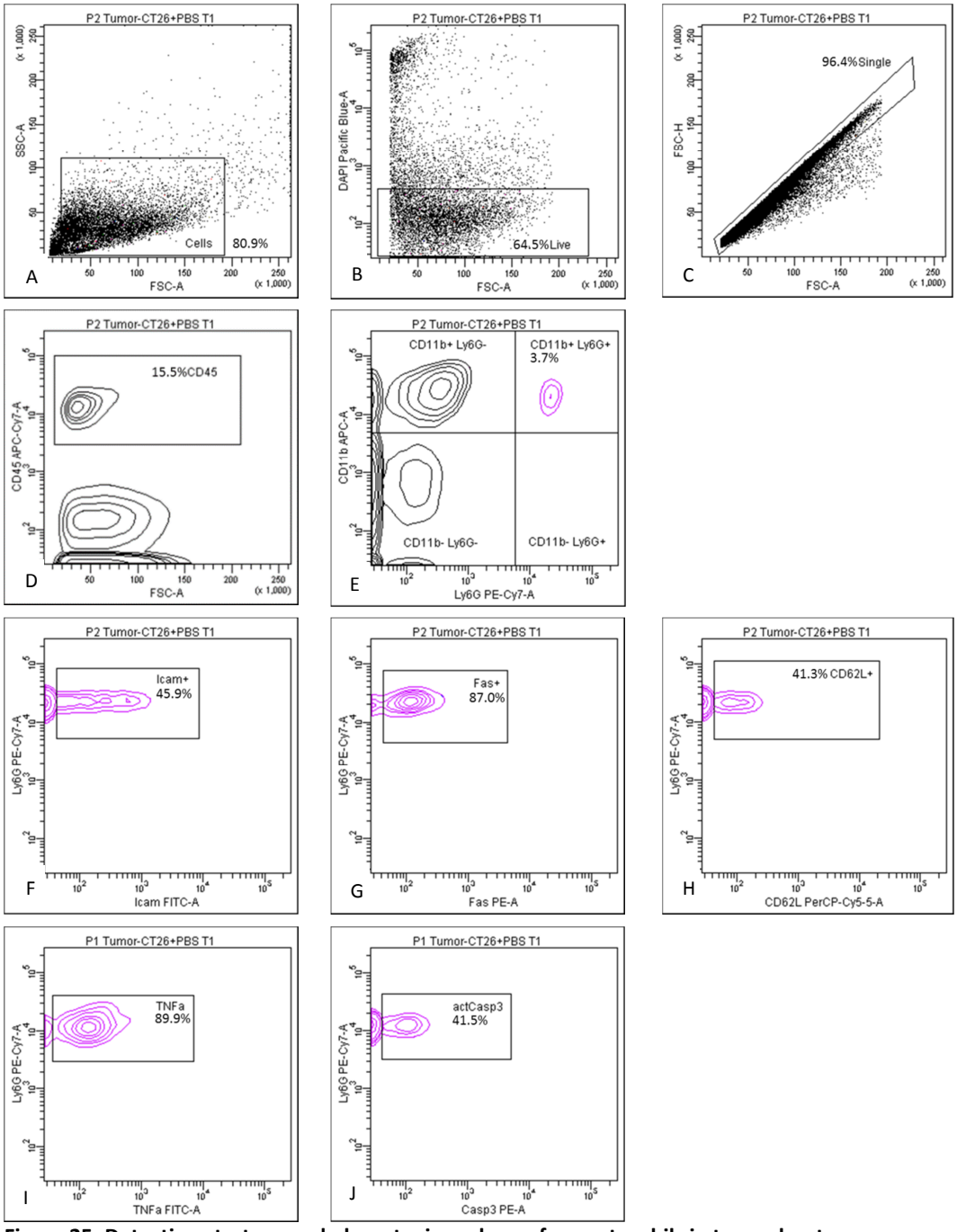

Figure 25: Detection strategy and phenotyping scheme for neutrophils in tumor lysates

The depicted gating strategy was used in BD FACSDiva to identify live Pacific Blue$^-$ CD45$^+$ CD11b$^+$ Ly6G$^+$ neutrophils (A-E) out of tumor lysates, exemplified here by a PBS-treated tumor from WT mice 1 d p.t.. In general, after 10 d of tumor growth the mice were i.v. treated with PBS / *P. aeruginosa* WT PA14 / 1 µg recombinant TNF-α and neutrophils (pink contours) were analyzed 1 d or 3 d p.t. for their phenotypic specialization by measurement of the percentage of marker positive neutrophils within the TAN population (F-J). The numbers of positive cells were indicated as percentage from the parental population which was selected one gating step before.

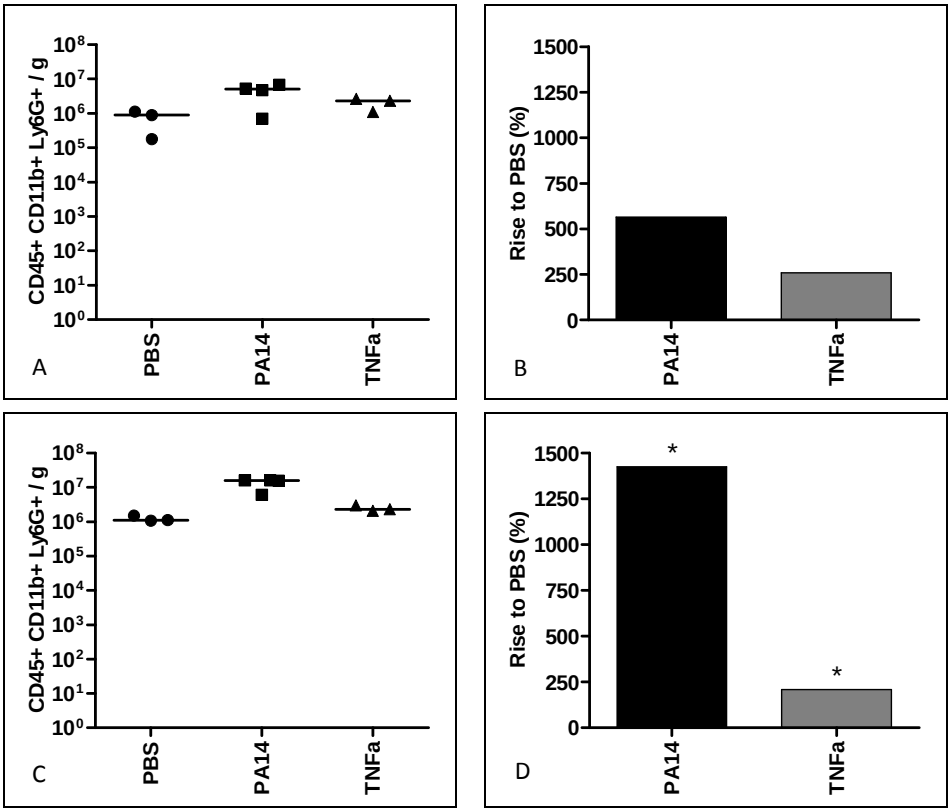

Figure 26: Total number of TANs / tumor (g) in WT mice 1 d and 3 d p.t.
The total number of TANs was investigated after 11 d (A+B) and 13 d (C+D) of tumor growth. After 10 d, tumor-bearing BALB/c mice were i.v. treated with PBS / $5.7x10^6$ *P. aeruginosa* WT PA14 / 1 µg recombinant TNF-α. Total cell numbers were achieved in three steps: (i) cell counting in a Neubauer chamber using a light microscope, (ii) correlation of this number with the percentage of live (Pacific $Blue^-$) cells in the corresponding FACS analysis, and (iii) calculation of the respective number of neutrophils (Pacific $Blue^-$ $CD45^+$ $CD11b^+Ly6G^+$) out of the percentage within the FACS analysis. To consider variations in *in vivo* tumor sizes, neutrophil numbers are depicted per gram tumor. Data are represented as median from n=3-4. For statistical analyses the Mann Whitney test, one-tailed, *p<0.05 was used to compare total TAN numbers of treated mice with the PBS group. Groups were analyzed in 2 independent experiments.

On day 3 p.t., the number of active caspase 3^+ and $CD62L^+$ TANs within tumors of untreated mice was reduced (Figure 28A, p.52) compared to day 1 p.t. (Figure 27A, p.51). Furthermore, the number of markers which were differentially expressed in treated mice compared to untreated animals decreased from 3-4 markers (Figure 27C+E, p.51) to 1-2 markers (Figure 28C+E, p.52). The percentage of $Icam^+$ and active caspase 3^+ TANs was significantly higher in infected tumors (Figure 28C), whereby TNF-α treatment activated more TANs to produce active caspase 3 (Figure 28E).

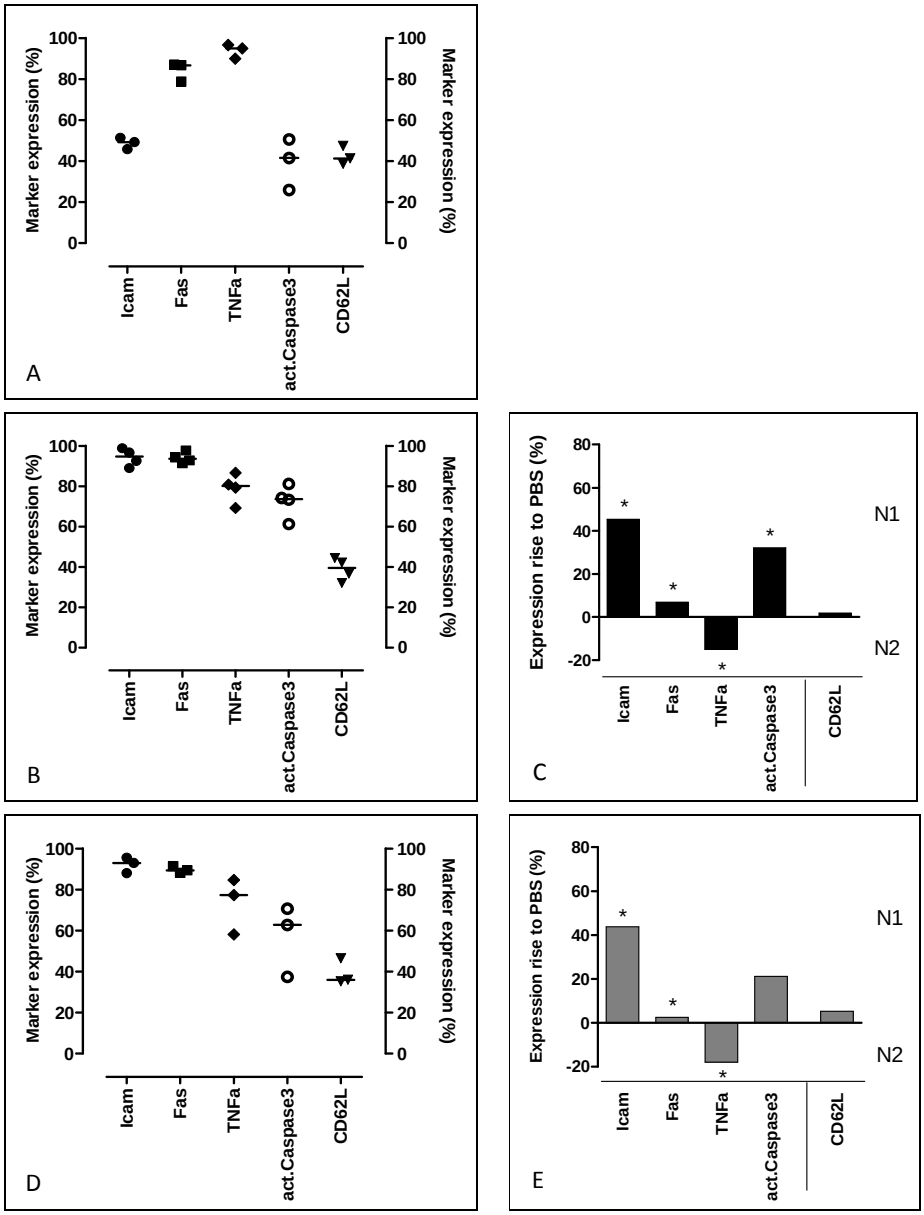

Figure 27: TAN phenotype 1 day p.t. of WT mice

The phenotype of TANs in tumors was investigated 1 d p.t. of WT mice with PBS (A) / 5.7x10^6 *P. aeruginosa* WT PA14 (B+C) / 1 µg recombinant TNF-α (D+E). The percentage of Dapi$^-$ CD45$^+$ CD11b$^+$ Ly6G$^+$ cells (TANs) expressing the extracellular proteins Icam, Fas, CD62L and the intracellular cytokines TNF-α and active caspase 3 was investigated by FACS analyses of tumor lysates. Data are represented as median from n=3-4. For statistical analyses the Mann-Whitney test, one-tailed, *p<0.05 was used to compare the percentage of marker positive TANs in tumors of treated mice with the PBS group (C, E). For CD62L the values on the y-axis have to be read with the algebraic sign vice versa (C, E). Groups were analyzed in 2 independent experiments.

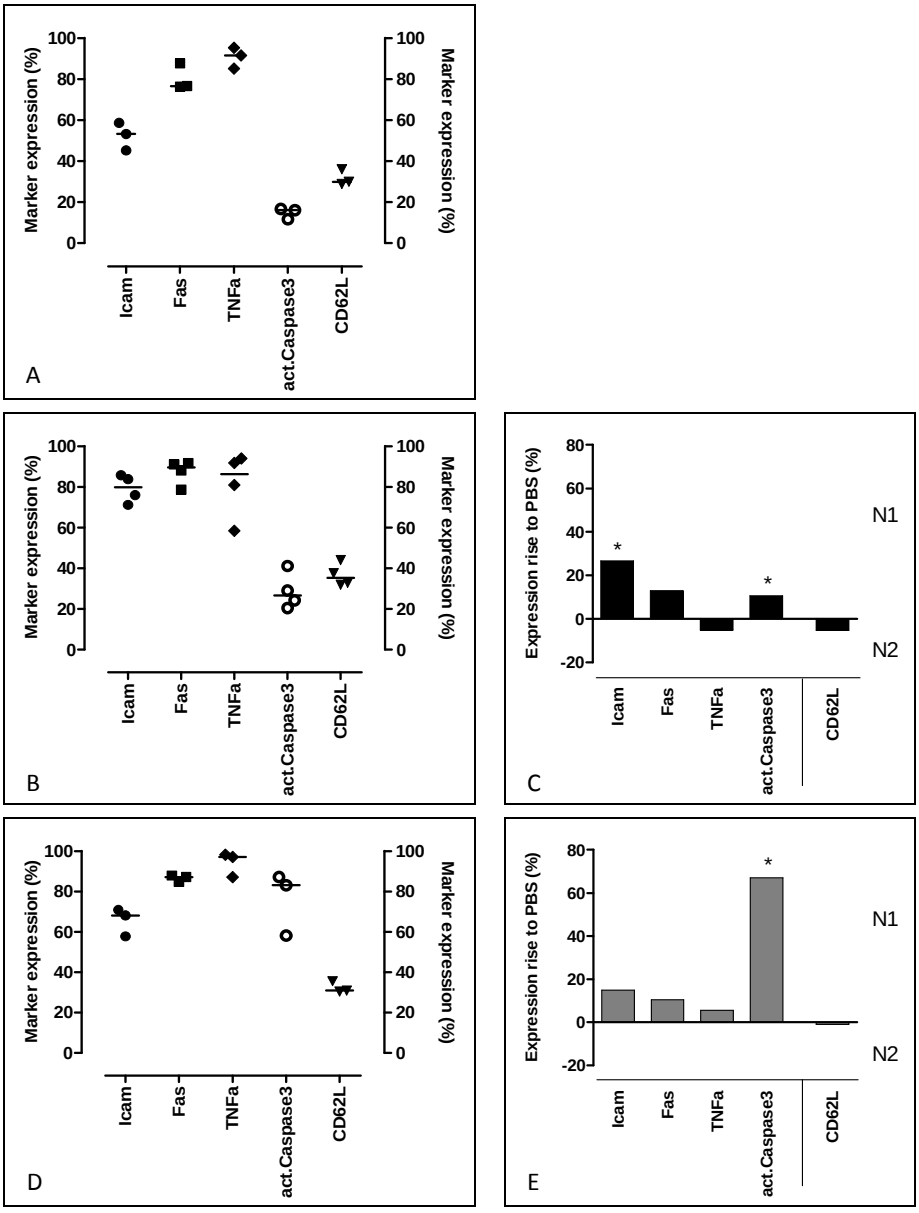

Figure 28:TAN phenotype 3 days p.t. of WT mice

The phenotype of TANs in tumors was investigated 3 d p.t. of WT mice with PBS (A) / 5.7x10^6 *P. aeruginosa* WT PA14 (B+C) / 1 µg recombinant TNF-α (D+E). The percentage of Dapi$^-$ CD45$^+$ CD11b$^+$ Ly6G$^+$ cells (TANs) expressing the extracellular proteins Icam, Fas, CD62L and the intracellular cytokines TNF-α and active caspase 3 was investigated by FACS analyses of tumor lysates. Data are represented as median from n=3-4. For statistical analyses the Mann-Whitney test, one-tailed, *p<0.05 was used to compare the percentage of marker positive TANs in tumors of treated mice with the PBS group (C, E). For CD62L the values on the y-axis have to be read with the algebraic sign vice versa (C, E). Groups were analyzed in 2 independent experiments.

Altogether, compared to untreated mice several phenotypes of the TAN population shifted on day 1 and day 3 p.t. with *P. aeruginosa* or TNF-α. More TANs expressed pro-inflammatory markers, though the whole populations became more N1-like in WT mice.

Within the tumor microenvironment a lot of other immune cells exist besides TANs. Especially T-lymphocytes are able to decisively influence tumor growth. If the presence of T cells also affects the phenotypes of the TAN population or whether the TAN phenotypes are independent of T cell signals was examined in Rag1$^{-/-}$ mice. First, the general influx of neutrophils into such tumors was investigated. The total number of TANs in untreated tumors was about 10^5 TANs / gram tumor and about 10^6 TANs / gram in treated tumors (Figure 29A+C). This was 10-fold lower than in WT animals (Figure 26A+C, p.50) under the respective conditions. However, in contrast to WT mice, the number of TANs in tumors was significantly increased 1 d p.t. with TNF-α (Figure 29B) compared to PBS. The number of TANs in PBS-treated and infected tumors was similar on day 1 and 3 p.t. (Figure 29B+D).

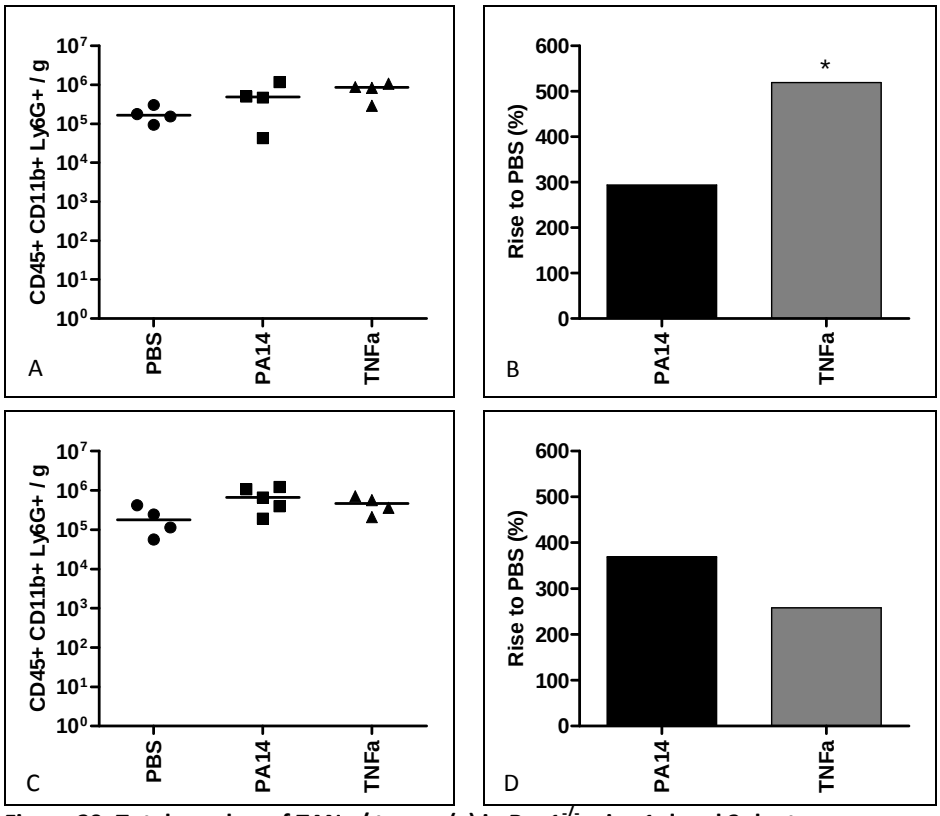

Figure 29: Total number of TANs / tumor (g) in Rag1$^{-/-}$ mice 1 d and 3 d p.t.
The total number of TANs was investigated after 11 d (A+B) and 13 d (C+D) of tumor growth. After 10 d, tumor-bearing Rag1$^{-/-}$ mice were i.v. treated with PBS / 5.3x10^6 *P. aeruginosa* WT PA14 / 1 µg recombinant TNF-α. Total cell numbers were achieved in three steps: (i) cell counting in a Neubauer chamber using a light microscope, (ii) correlation of this number with the percentage of live (Pacific Blue$^-$) cells in the corresponding FACS analysis, and (iii) calculation of the respective number of neutrophils (Pacific Blue$^-$ CD45$^+$ CD11b$^+$Ly6G$^+$) out of the percentage within the FACS analysis. To consider variations in *in vivo* tumor sizes, neutrophil numbers are depicted per gram tumor. Data are represented as median from n=4-5. For statistical analyses the Mann-Whitney test, one-tailed, *p<0.05 was used to compare total neutrophils numbers in tumors of treated mice with the PBS group. Groups were analyzed in 2 independent experiments.

To examine, whether T cells influence the phenotype of the TAN population, the percentages of marker positive TANs were also analyzed in tumor-bearing Rag1$^{-/-}$ mice treated with PBS, *P. aeruginosa* or TNF-α (Figure 30 and Figure 31, p.55).

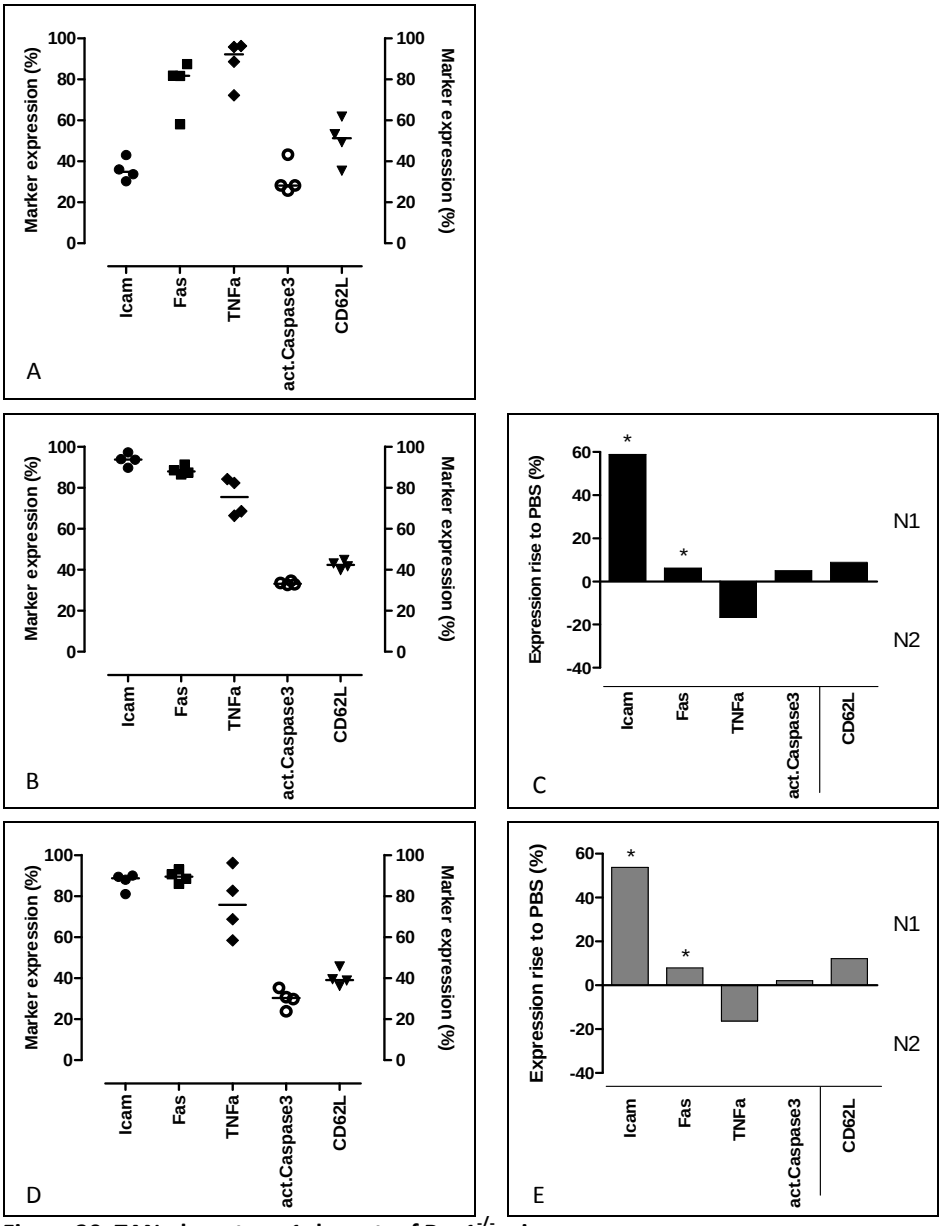

Figure 30: TAN phenotype 1 day p.t. of Rag1$^{-/-}$ mice

The phenotype of TANs in tumors was investigated 1 d p.t. of Rag1 $^{-/-}$ mice with PBS (A) / 5.3x10^6 *P. aeruginosa* WT PA14 (B+C) / 1 µg recombinant TNF-α (D+E). The percentage of live Pacific Blue$^-$ CD45$^+$ CD11b$^+$ Ly6G$^+$ TANs expressing the extracellular proteins Icam, Fas, CD62L and the intracellular cytokines TNF-α and active caspase 3 was investigated by FACS analyses of tumor lysates. Data are represented as median from n=4. For statistical analyses the Mann-Whitney test, one-tailed, *p<0.05 was used to compare the percentage of marker positive TANs in tumors of treated mice with the PBS group (C, E). For CD62L the values on the y-axis have to be read with the algebraic sign vice versa (C, E). Groups were analyzed in 2 independent experiments.

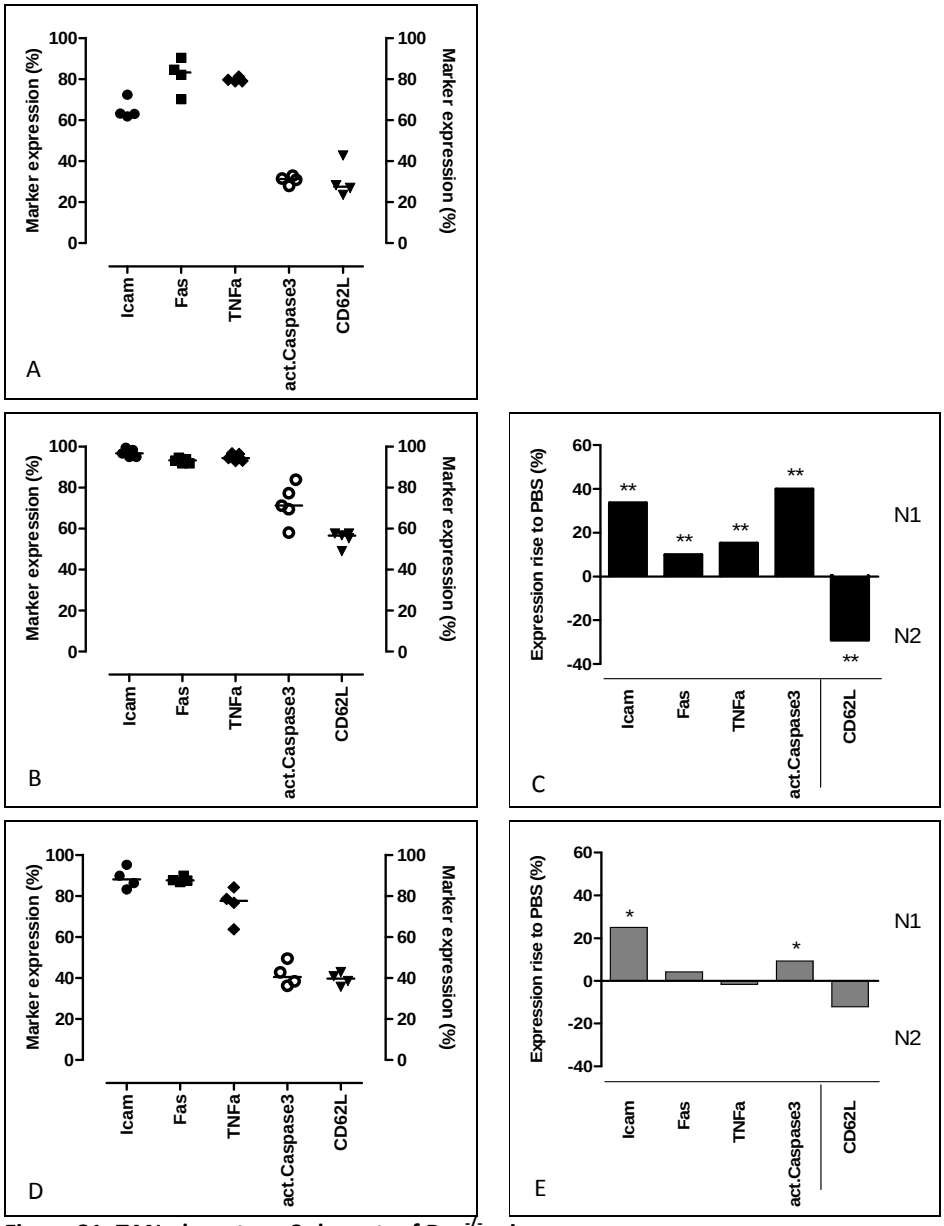

Figure 31: TAN phenotype 3 day p.t. of Rag$^{-/-}$ mice

The phenotype of TANs was analyzed 3 d p.t. of Rag1$^{-/-}$ mice with PBS (A) / 5.3x10^6 *P. aeruginosa* WT PA14 (B+C) / 1 µg recombinant TNF-α (D+E). The percentage of live Pacific Blue$^-$ CD45$^+$ CD11b$^+$ Ly6G$^+$ TANs expressing the extracellular proteins Icam, Fas, CD62L and the intracellular cytokines TNF-α and active caspase 3 was investigated by FACS analyses of tumor lysates. Data are represented as median from n=4-5. For statistical analyses the Mann-Whitney test, one-tailed, *p<0.05 and **p<0.01 were used to compare the percentage of marker positive TANs in tumors of treated mice with the PBS group (C, E). For CD62L the values on the y-axis have to be read with the algebraic sign vice versa (C, E). Groups were analyzed in 2 independent experiments.

The expression profiles of the neutrophil phenotyping markers in PBS-treated tumors in Rag1$^{-/-}$ mice were the same as in WT mice at day 1 p.t. (Figure 27A, p.51, Figure 30A, p.54): about 90% of all TANs expressed the intracellular pro-inflammatory cytokine TNF-α, 80% the apoptosis receptor Fas, 50% the leukocyte homing ligand CD62L, and approximately 30% were positive for Icam and active caspase 3. On day 3 p.t. the expression profile in Rag1$^{-/-}$ mice showed an increased number of active caspase 3^{+}, Icam^{+}, and Fas^{+} TANs, and a decreased TNF-α^{+} TAN number as in WT animals (Figure 28A, p.52, Figure 31A, p.55).

Tumor-bearing Rag1$^{-/-}$ animals which had received bacteria or recombinant TNF-α i.v. showed identical marker expression profiles at day 1 p.t. (Figure 30B+D, p.54). Consequently was the variation of marker positive TANs compared to PBS-treated animals also the same (Figure 30C+E, p.54): the number of neutrophils expressing Icam and Fas on their cellular surface increased significantly after injecting bacteria or recombinant TNF-α into Rag1$^{-/-}$ mice, whereas the drop in TNF-α^{+} as well as the rise in active caspase 3^{+} or CD62L^{+} TANs was only minor. In the respectively treated tumor-bearing WT animals, the marker expression profiles of marker positive TANs were also identical after *P. aeruginosa* or TNF-α injection (Figure 27B+D, p.51).

Three days after the treatment of Rag1$^{-/-}$ mice with *P. aeruginosa* or TNF-α the marker expression profiles were different for the two treatment groups in comparison to the PBS group (Figure 31C+E, p.55): whereas the complete profile changed highly significantly for all five markers after infection of tumor-bearing Rag1$^{-/-}$ mice, only the number of Icam^{+} and active caspase 3^{+} TANs differed after TNF-α injection. Nevertheless, in principal were the tendencies after TNF-α injection similar to the one after *P. aeruginosa* treatment, but the significances were lower. Differences between day 1 and day 3 p.t. were, that more cells of the TAN population in infected or TNF-α-treated tumors produced TNF-α, active caspase 3, and CD62L in comparison to PBS-injected Rag1$^{-/-}$ mice on day 3 p.t.. These marker profiles differed from WT mice (Figure 28, p.52), as more cells after infection and less TANs after TNF-α injection showed an upregulation of their markers in Rag1$^{-/-}$ mice.

All in all was the induced phenotypic switch of the tumor-associated neutrophil population most dramatic in Rag1$^{-/-}$ mice 3 days p.i. with *P. aeruginosa* (Figure 31C, p.55). Up to 40 % of the cells started to produce active caspase 3, or to show Icam or CD62L on their surface, 20 % more TANs generated TNF-α, and about 10 % more TANs were positive for Fas. All five variations to PBS-treated tumor-bearing Rag1$^{-/-}$ mice were highly significant with $p<0.01$. The correlating phenotypic switch in infected tumors on WT mice was less decisive (Figure 28C, p.52).

But interestingly, in WT mice was the phenotypic switch of the TAN population on 3 days p.t. with TNF-α more pivotal than in $Rag1^{-/-}$ mice (Figure 28E, p.52 and Figure 31E, p.55): the amount of active caspase 3^{+} TANs increased about 60 % in tumors on WT mice and only up to 10 % in tumors on $Rag1^{-/-}$ mice.

However, the injection of *P. aeruginosa* or TNF-α did induce phenotypic switches in the respective TAN populations in tumor-bearing WT as well as $Rag1^{-/-}$ mice. Tumors on these mice injected with PBS contained the lowest percentages of marker positive TANs and reflected therefore N2 phenotypes of the TAN populations. This was compatible with the detected continuing tumor growth on such mice (Figure 16, p.38 and later Figure 33, p.59). After infection or TNF-α treatment, the TAN populations contained more pro-inflammatory cells. Therefore their phenotypes shifted to N1. But since only tumors on WT mice started to shrink after treatment (Figure 15, p.37), the sole presence of a natural amount of anti-tumor-polarized N1 TANs seemed to be not sufficient to induce tumor rejection in our model.

3.4.2 Neutrophil polarizing cytokines and -hypoxia

It is known that the tumor microenvironment itself stimulates neutrophils to specialize towards a certain phenotype. The cytokines G-CSF, IL-4, IL-10, and MCP-1 / CCL-2 as well as hypoxic conditions inside the tumor may favor the development of pro-tumor (N2) functions in neutrophils, whereas the cytokines IFN-β, IFN-γ, and GM-CSF are known to stimulate anti-tumor (N1) functions. Anti-inflammatory N2 neutrophils represent the usual TAN phenotype in growing tumors. The emergence of for example an inflammatory tumor microenvironment can result in a phenotypic switch of TANs into pro-inflammatory N1 neutrophils.

The existence of N2- or N1-stimulating cytokines was investigated in tumor lysates of growing tumors from PBS-treated and of shrinking tumors from *P. aeruginosa* infected WT mice (Figure 32A+B, p.58). Within both kinds of treated tumors were only three of the six analyzed cytokines present at a concentration above 50 pg/ml: the N2-promoting molecules G-CSF and MCP-1 / CCL-2, and the N1-stimulating cytokine GM-CSF. In growing tumors compared to infected shrinking tumors, the concentration of (i) G-CSF was about 327-fold increased (day 3 p.t.), (ii) MCP-1 was about 13- (day 1 p.t.) to 93-fold (day 3 p.t.) increased, and (iii) GM-CSF was about 6-times higher (day 3 p.t.).

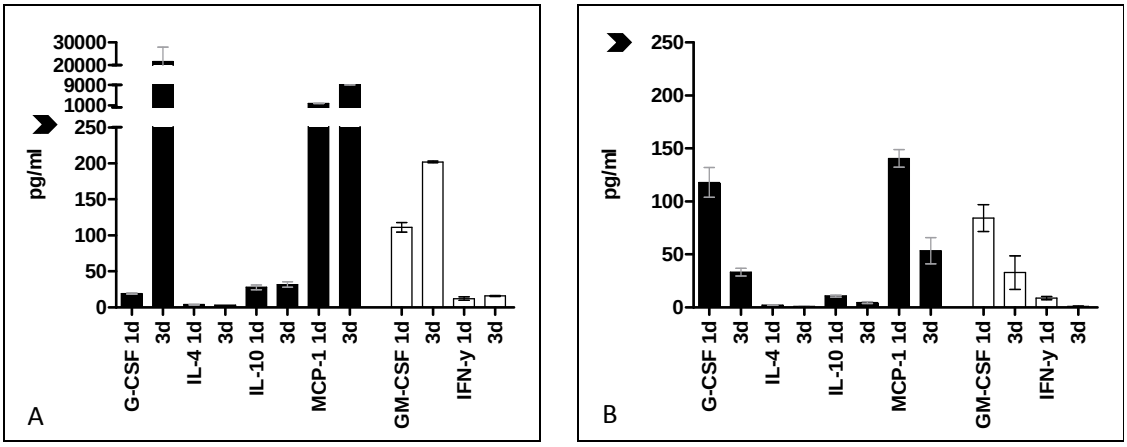

Figure 32: Neutrophil polarizing cytokines in WT tumor microenvironments
Luminex analyses were performed on tumor lysates 1 d and 3 d p.t. of BALB/c WT mice with PBS (A) or $5x10^6$ *P. aeruginosa* (B). The black bars represent cytokines which stimulate a polarization of neutrophils into tumor-supportive N2 TANs. Whereas the white bars indicate pro-inflammatory cytokines which favour tumor-suppressive N1 TAN functions. Arrows indicate a decreased concentration of N2-stimulating molecules in infected tumors (B). Data are represented as median and range from n=2.

Furthermore, the cytokine IFN-β is known to induce the polarization of N1 TANs, which were detected in shrinking tumors of infected WT mice (Figure 27C, p.51 and Figure 28C, p.52). Since the N1-supporting cytokines GM-CSF and IFN-γ were not present in shrinking tumors on day 1 and day 3 p.i. in high concentrations (Figure 32B), the intra-tumoral availability of IFN-β was investigated by *in vivo* imaging using a recently introduced reporter system [137]. The three representative IFN-$\beta^{+/\Delta\beta\text{-luc}}$ mice illustrated in Figure 33, p.59 were bearing CT26 solid tumors, which were by them not able to produce a light signal after luciferin application. The detection of light emission was therefore a clear result for the actual availability of IFN-β produced by the host cells. Mice which received PBS gave already a slight, steady and local light signal over time, which indicated the presence of IFN-β in the naïve tumor microenvironment. From these observations the IFN-β signal-intensity varied only at the first measurement after treatment of mice with recombinant TNF-α. Nevertheless, the signal at 0 h was already rather high and locally defined within the tumor center under these treated condition. Afterwards, the IFN-β intensity was the same as in PBS-treated mice.

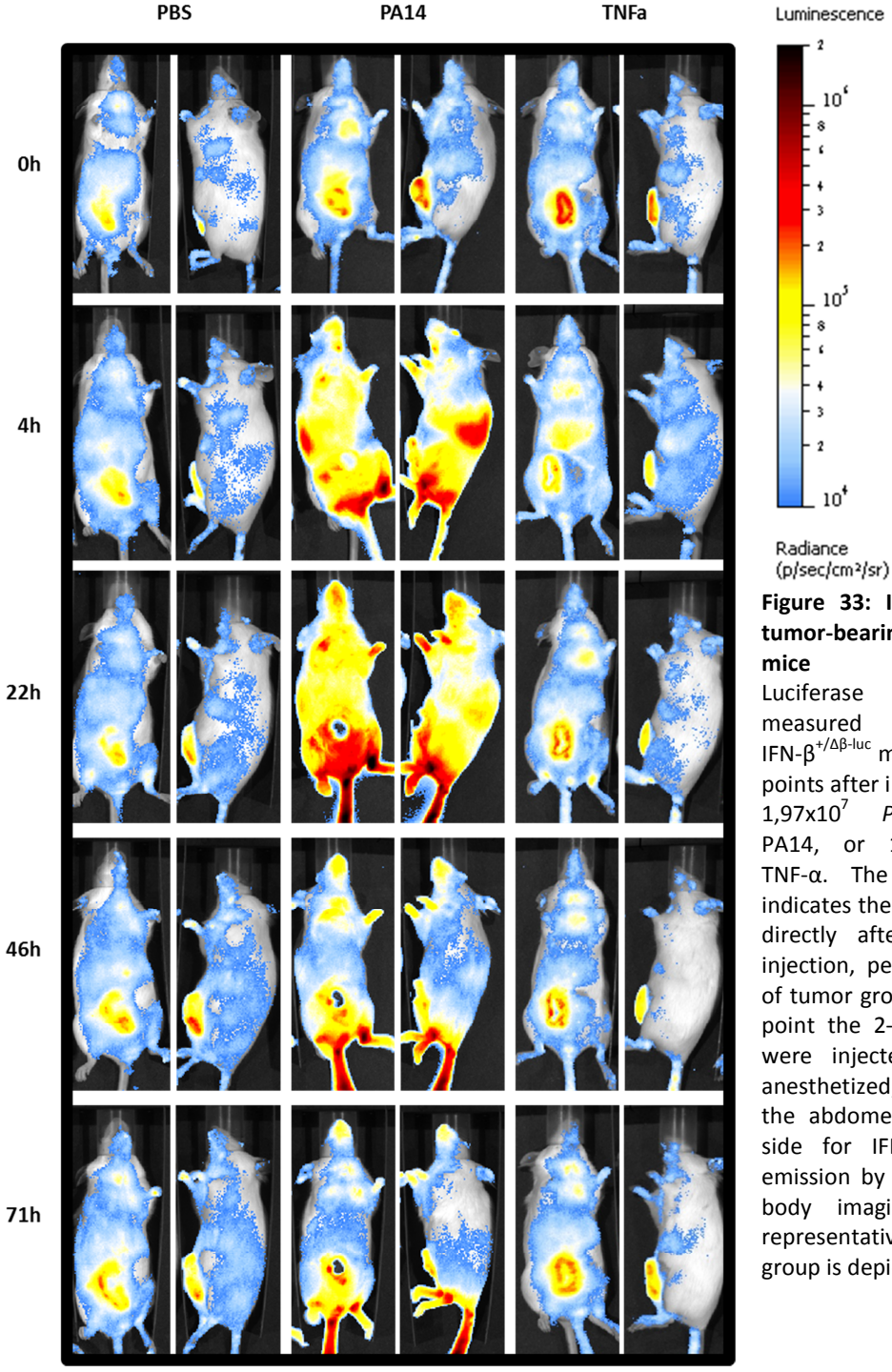

Figure 33: IFN-ß secretion in tumor-bearing IFN-ß reporter mice
Luciferase activity was measured in tumor-bearing IFN-$\beta^{+/\Delta\beta\text{-luc}}$ mice at several time points after i.v. injection of PBS, $1{,}97 \times 10^7$ *P. aeruginosa* WT PA14, or 1 µg recombinant TNF-α. The time point 0 h indicates the first measurement directly after the respective injection, performed at day 10 of tumor growth. At every time point the 2-3 mice per group were injected with luciferin, anesthetized, and monitored on the abdomen- and left body-side for IFN-β specific light emission by an IVIS 200 whole body imaging system. One representative mouse per group is depicted over time.

The infection with *P. aeruginosa* on the contrary highlighted an increase in the IFN-β expression (Figure 33). Almost the entire infected mice were emitting light, indicating a systemic production of IFN-β throughout the body. Centers of the signal were at 4 h p.i. in the lower abdomen and spleen, whereas at 22 h p.i. the signal was detected in the complete abdomen and furthermore accumulated in the tumor center.

Afterwards the intensity of IFN-β decreased slightly within the infected mice, but stayed prominent within the tumor center. The concentration of IFN-β inside infected, shrinking tumors was much higher as in PBS-treated, growing tumors. Therefore, the amount of expressed IFN-β might have been able to induce the detected phenotypic switches from N2 towards N1 TANs in infected mice.

On the other hand, a prominent factor which influences neutrophil polarization into tumor-supportive N2 cells is the occurrence of hypoxia inside tumors. Solid tumors tend to develop hypoxic regions due to their leaky vascular system and the limited distribution of oxygen in less vascularized tumor sites. When neutrophils reside in hypoxic tumor areas, the cells could be influenced by the low oxygen conditions to fulfill tumor-promoting functions. In Figure 20, p.43 it was already shown that TANs resided between the viable and necrotic tumor tissue. In follow-up experiments, infected mice were i.v. treated with pimonidazole to highlight hypoxic regions within the tumor by immunohistochemistry. The tumor in Figure 34A, p.61 was analyzed 3 days p.i. with *P. aeruginosa* and mirrored the organization of viable, granulocytic, and necrotic cells like depicted in Figure 20A, p.43, even though the sample was technically disrupted in the upper tumor part. The distribution of hypoxic areas inside the infected tumor was limited to a cellular band between viable tumor cells and live tumor-associated neutrophils (Figure 34B, p.61).

To examine the distribution of the various cell types in more detail, further consecutive tumor sections were stained with additional antibodies and a part of the tumor which includes hypoxic staining was taken for comparable analysis at a higher magnification (Figure 35, p.62). Underneath the mouse skin resided viable tumor cells which were able to divide, as indicated by Ki67 expression, and probably drive tumor growth (Figure 35A+D). The boarder for sufficient oxygen availability started underneath, even before the zone of tumor infiltrated neutrophils began (Figure 35B+C). Within the band of neutrophils were some slight signals for hypoxia (Figure 35C), but most of the area seemed to be anoxic. The density of proliferating cells decreased within the areas of hypoxia and TANs, and the subjacent necrotic tumor zone did not show any signal of cell proliferation (Figure 35D). Colonization of *P. aeruginosa* was detected mainly directly under the mouse skin between viable tumor cells, and to a low degree between the granulocytic band and necrotic tumor area (Figure 35E). Tumor-associated neutrophils obviously colonized tumor regions with very low oxygen levels, where they might also co-localize with bacteria.

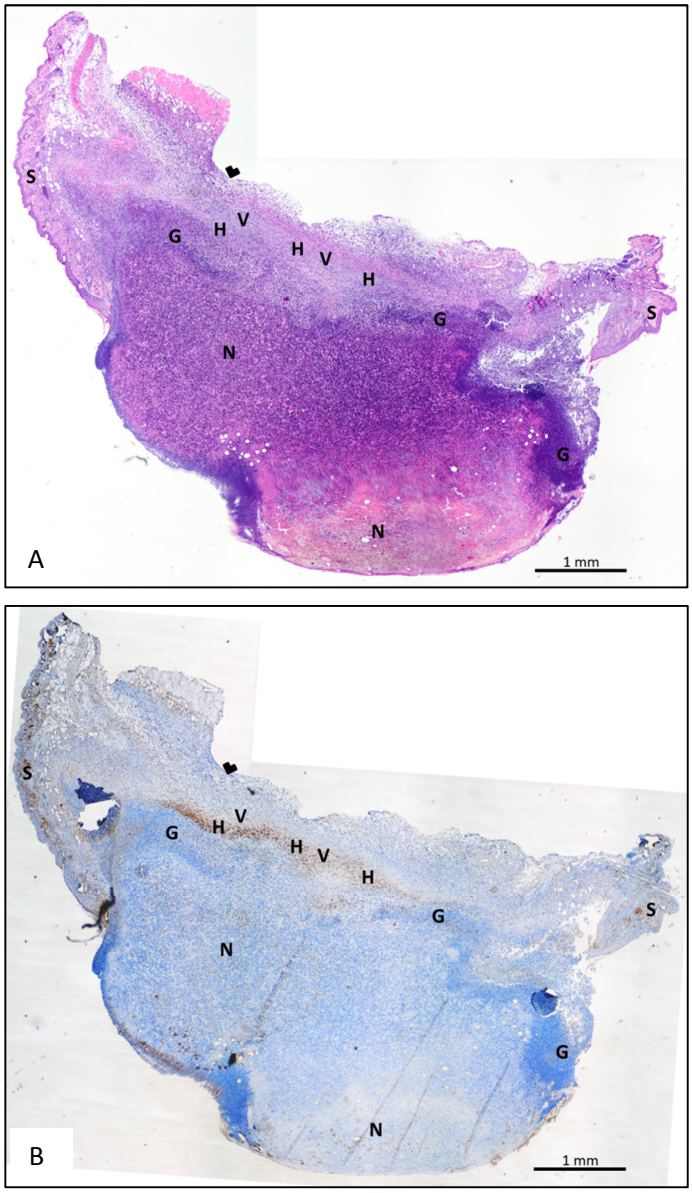

Figure 34: Hypoxic areas arise between the viable and granulocytic tumor area
The CT26 tumor on a BALB/c WT mouse was collected 3 days p.i. with $5.7x10^6$ *P. aeruginosa* and several consecutive sections were prepared. Sections were stained with A: Hematoxylin-and-eosin to highlight viable (V) and necrotic (N) tumor regions. Tumor infiltrating cells, mainly neutrophilic granulocytes (G), are indicated as dark purple cells with intact nuclei. Around the tumor is the mouse skin (S). The incrusted host skin and the subjacent loose viable tumor tissue were partially disrupted due to technical issues. B: Staining with diamino-benzidine-pimonidazole (PAb2627AP 0.5mg/ml IgG) to detect hypoxic areas with an oxygen concentration lower than 14 mM or pO_2 of 10 mm Hg at 37°C (H). The images were made transparently, and put on top of each other to label exactly the same areas and to demonstrate relative proximity. **The arrow outside the viable tumor zone highlights the point of orientation for the detailed analyses depicted in Figure 35, p.62.**

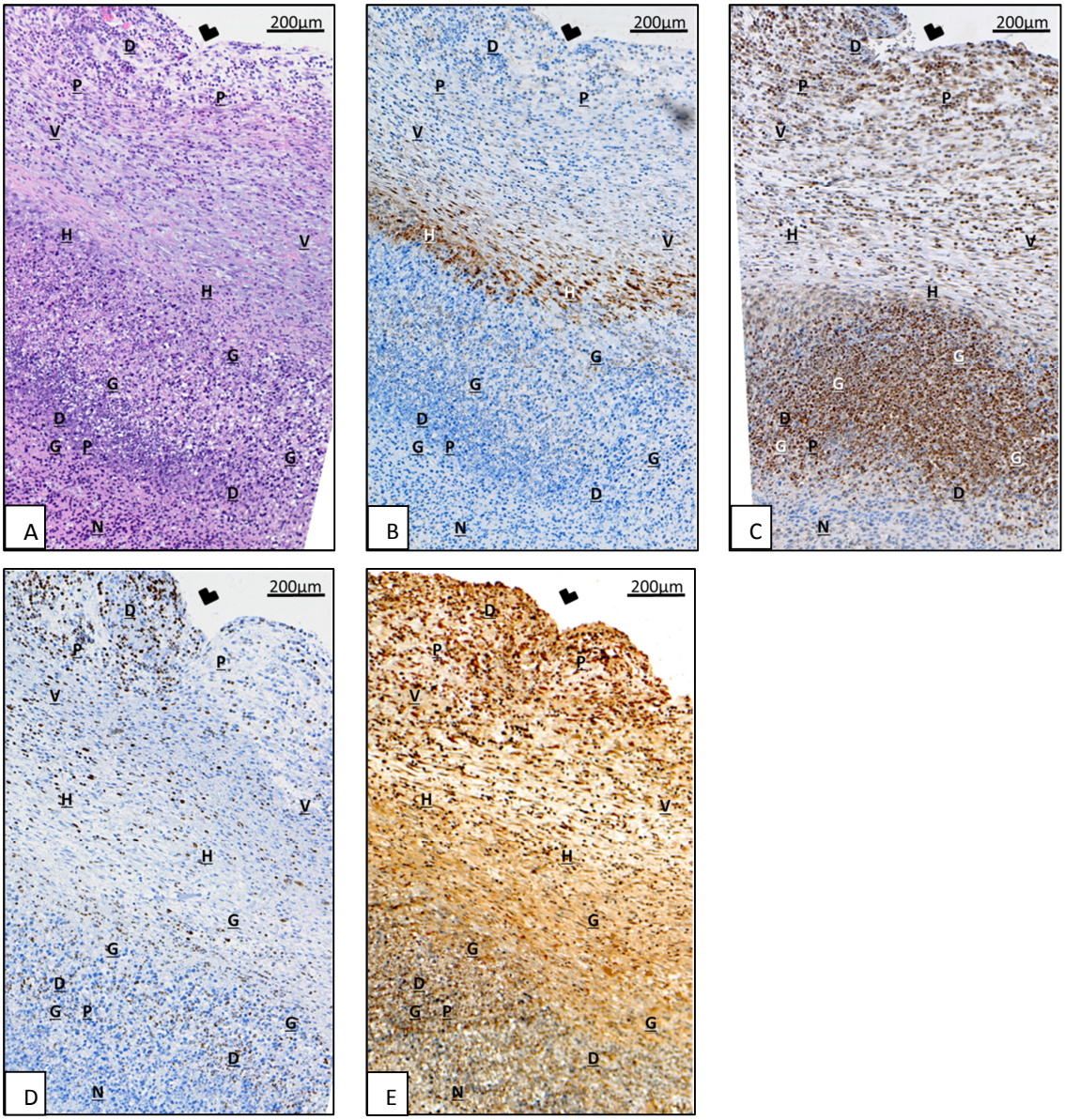

Figure 35: TANs reside between necrotic and hypoxic tumor zones

Detailed analyses of Figure 34, p.61. The arrow outside the tumor highlights the point of orientation. The CT26 tumor on a BALB/c WT mouse was collected 3 days p.i. with $5.7x10^6$ *P. aeruginosa* and several consecutive sections were made. Sections were stained with A: Hematoxylin-and-eosin to highlight viable (V) and necrotic (N) tumor regions, B: diaminobenzidine-pimonidazole (PAb2627AP 0.5mg/ml IgG) to detect hypoxic areas (H) with an oxygen concentration lower than 14 mM or pO_2 of 10 mm Hg at 37°C, C: diaminobenzidine-myeloperioxidase to highlight neutrophilic granulocytes (G), D: diaminobenzidine-Ki67 to detect proliferative and dividing cells (D), E: diaminobenzidine-*P. aeruginosa* to visualize bacterial colonization (P). The images were made transparently, and put on top of each other to label exactly the same areas in all pictures and to demonstrate relative proximity.

Previous results demonstrated the infiltration of neutrophils also into uninfected tumors (Figure 26A+C, p.50). In contrast to bacterial infected or TNF-α treated mice, tumors of PBS-treated mice showed on day 13 of tumor development (= d3 p.i./p.t.) large and distinct patterns of hypoxia throughout the huge viable tumor zone (Figure 36A+B). This hypoxic pattern was also present in 11 day old tumors of PBS-treated mice (= d1 p.i.), and surprisingly as well in tumors of mice treated with *P. aeruginosa* or TNF-α at 1 day p.i./p.t.. Besides that, the necrotic tumor zone in the PBS-treated growing tumors was much smaller than in shrinking tumors of infected or TNF-α-treated mice (Figure 34B, p.61). The tumor-associated neutrophils within untreated tumors resided within the same area as in treated tumors, between hypoxic and anoxic tumor zones (results not shown).

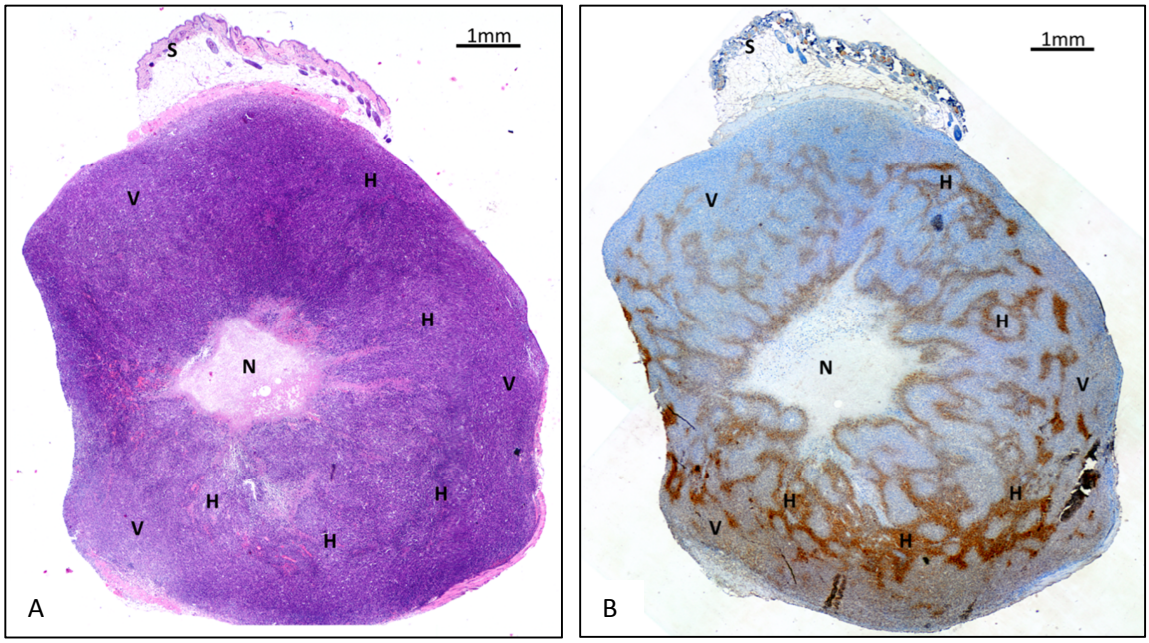

Figure 36: Uninfected tumors show extensive hypoxic patterns in the large viable tumor zone
The CT26 tumor on a BALB/c WT mouse was collected 3 days p.t. with PBS, started after 10 d of tumor growth. Several consecutive sections were cut and stained with A: Hematoxylin-and-eosin to highlight viable (V) and necrotic (N) tumor regions. Around the tumor was the mouse skin (S). This and the subjacent loose viable tumor tissue were partially disrupted due to technical issues, B: diaminobenzidine-pimonidazole (PAb2627AP 0.5mg/ml IgG) to detect hypoxic areas (H) with an oxygen concentration lower than 14 mM or pO_2 of 10 mm Hg at 37°C. The images were made transparently and put on top of each other to label exactly the same areas.

3.5 Co-localization of TANs and *P. aeruginosa* biofilms inside tumors

It was an obvious question whether such pro-inflammatory N1 neutrophils inside infected tumors on WT mice (Figure 28B+C, p.52) are able to destroy the pathogens by phagocytosis. This was investigated by transmission electron microscopy (TEM) of tumor sections. Indeed, the multinucleated TANs were able to phagocytose some bacteria (Figure 37A+B) close to the necrotic tumor zone, where most of *P. aeruginosa* reside as single bacteria (Figure 38).

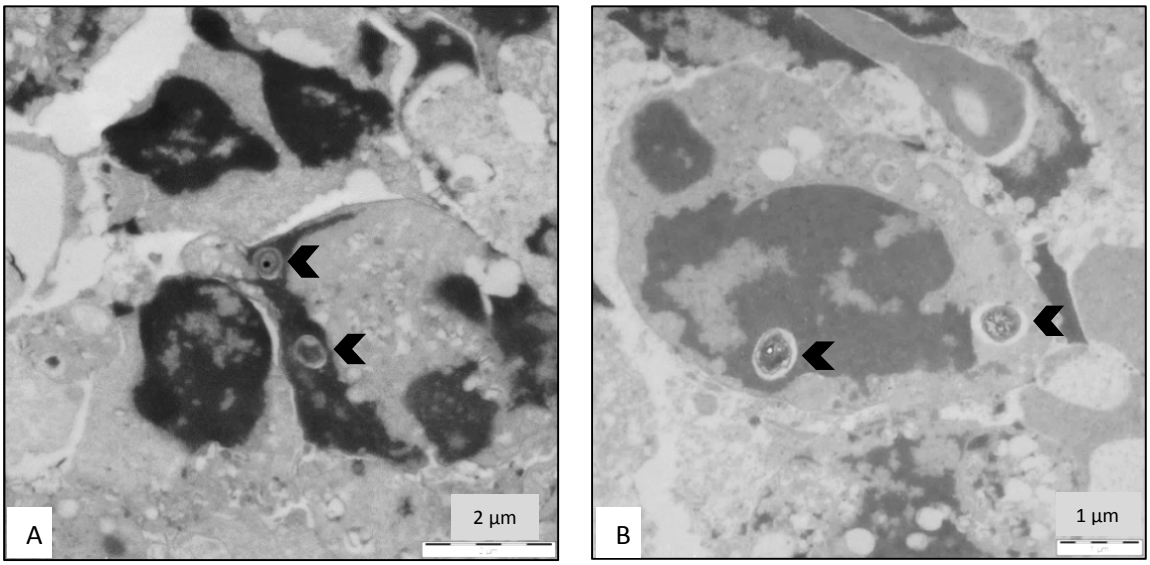

Figure 37: Phagocytosis of *P. aeruginosa* by TANs
BALB/c WT mice were s.c. injected with CT26 cells and after 10 days of tumor growth i.v. infected with $5x10^6$ *P. aeruginosa* WT PA14. Tumors were processed 3 d p.i. and prepared for transmission electron analyses. Single bacteria (black arrow) were detected inside the multinucleated tumor-associated neutrophils (A+B).

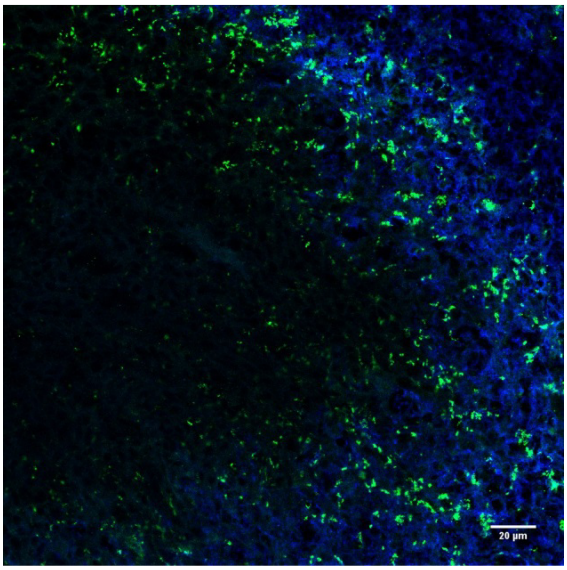

Figure 38: *P. aeruginosa* single bacteria reside close to the necrotic tumor zone
BALB/c WT mice were s.c. injected with CT26 cells and after 10 days of tumor growth i.v. infected with $9.3x10^6$ *P. aeruginosa* WT PA14. Tumors were prepped 3 d p.i.. Cryosections were fixed in -20°C acetone and stained for AA-Lectin (blue) and *P. aeruginosa* (green) depicted as merged picture.

Interestingly, no sign of bacterial stress was observed under such conditions (Figure 37, p.64). Most likely neutrophils are unable to harm the bacteria under such low oxygen conditions before phagocytosis.

Whether TANs were like bacteria also localized within the viable and proliferative part of solid tumors was furthermore analyzed by histology on cryosections.

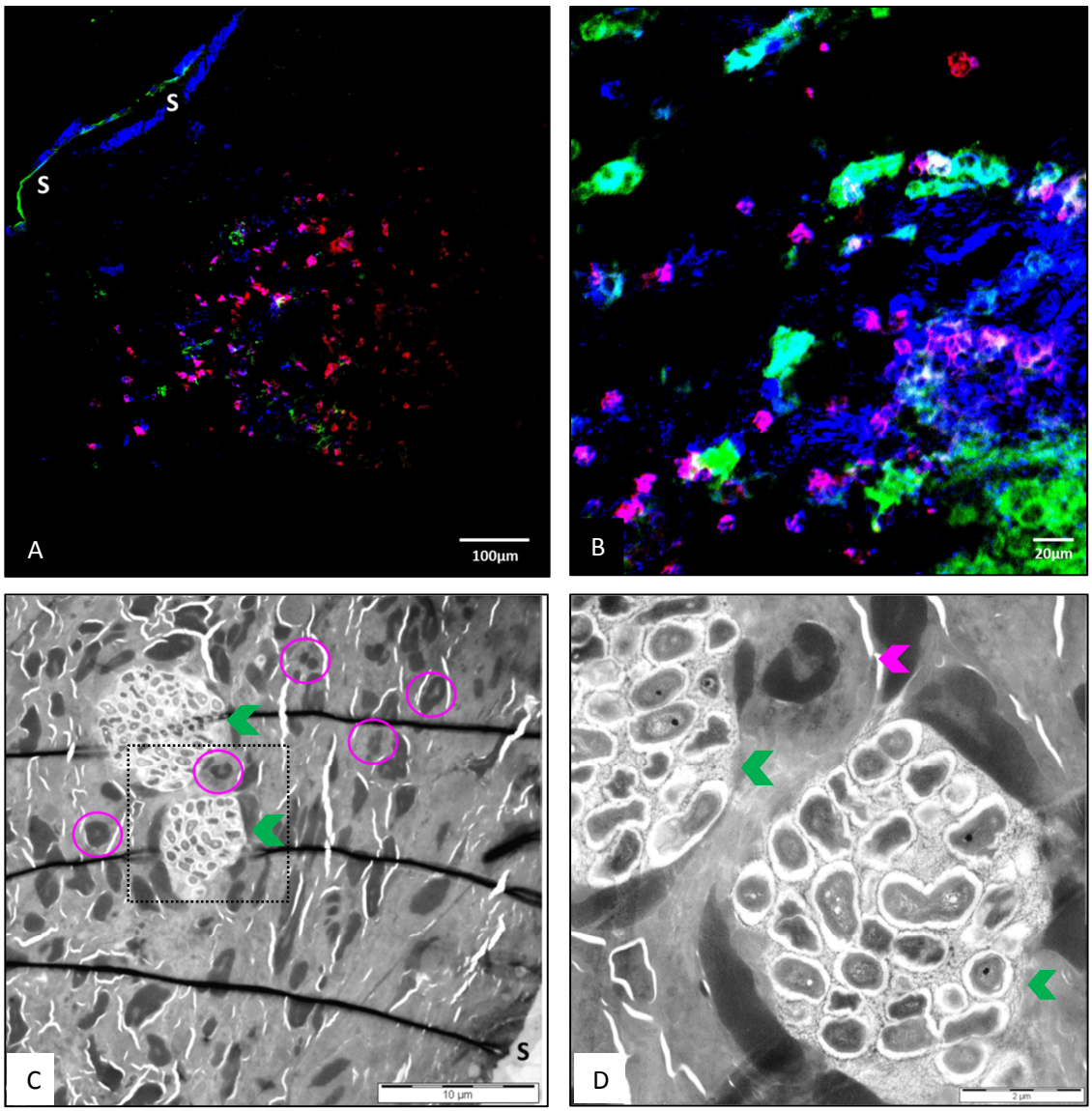

Figure 39: Co-localization of TANs and *P. aeruginosa* in the viable tumor zone
BALB/c WT mice were s.c. injected with CT26 cells and after 10 days of tumor growth i.v. infected with $1x10^6$ *P. aeruginosa*. Tumors were prepped 3 d p.i.. Cryosections were fixed in -20°C acetone and stained for CD11b (blue), Gr-1 (red), and *P. aeruginosa* (green) depicted as merged pictures (A+B). Further tumors were prepared for transmission electron analyses (C). Enlargement of the dotted frame, rotated in D. Tumor-associated neutrophils (pink circle in C or pink arrow in D) and bacterial clusters (green arrows in C and D) were detected directly under the mouse skin (S) in C.

TANs obviously resided also directly under the mouse skin (Figure 39A+C, p.65). There they co-localized with the invaded pathogens, which existed as several clusters in the viable tumor area (Figure 39B, p.65). In more detail, these clusters represented accumulations of 30 to 60 single bacteria embedded within a fibrous biofilm matrix (Figure 39C+D, p.65) as described before [139]. Phagocytosis of such bacterial clusters, which display a multiple size of TANs, was not detected. The bacteria were obviously under severe stress as indicated by the extensive plasma lysis of most of the bacteria. Such biofilms were also detected to similar degrees when *P. aeruginosa* colonized tumors from Rag1$^{-/-}$ mice (Figure 40).

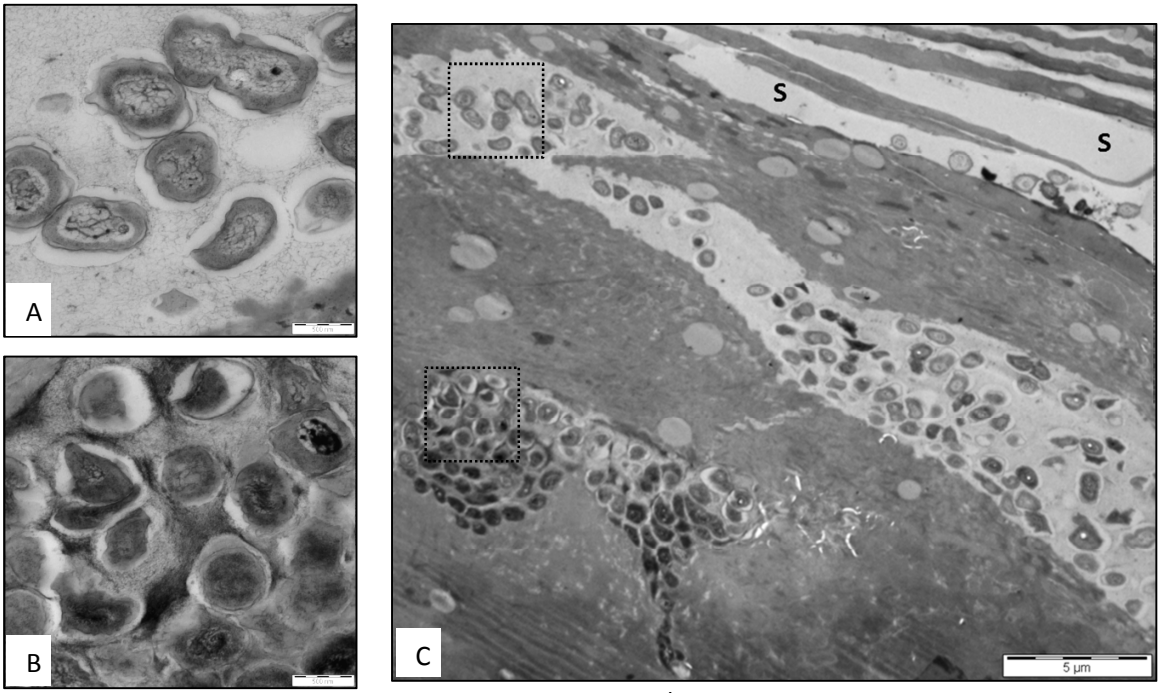

Figure 40: *P. aeruginosa* biofilm formation in tumors on Rag1$^{-/-}$ mice
Rag1$^{-/-}$ mice were s.c. injected with CT26 cells and after 10 days of tumor growth i.v. infected with 9.3x10^5 *P. aeruginosa*. Tumors were prepped 3 d p.i. and prepared for transmission electron analyses. Bacterial clusters were embedded in loose (A) or dense (B) extracellular matrix material, depending on the distance of the clusters to the host skin (S) in C. A+B are enlargements of the dotted areas is C. Scale bars 500 nm (A+B) or 5 µm (C).

All in all *P. aeruginosa* was able to form biofilms inside the tumor tissues and survive the attacks of the pro-inflammatory N1 TANs, in immunocompetent as well as in immunocompromised animals. However, only WT mice were able to clear CT26 tumors after bacterial infection due to specific T cell functions.

4 Discussion

In face of the rising incidence of cancer, the search for therapeutic strategies alternative to such that are presently in routine use is a mandatory enterprise in biomedical research. The employment of pathogenic bacteria for the treatment of solid tumors appears highly promising in this context. Most extensively Salmonella spp. and Clostridia spp. are investigated. However, other so far not explored bacteria might possess therapeutic properties that are more appropriate than such of the microorganisms above. Thus, *P. aeruginosa* was tested in the present work for the treatment of murine solid tumors.

4.1 Tumor size and infection dose are decisive parameters of the model

During tumor development, tumor cells secrete angiogenic factors that enable the establishment of a tumor neovascularization. Since these tumor-associated blood vessels serve as port of entry for the bacteria into the tumor tissue, angiogenesis and the time thereof prior to infection might be very important for tumor colonization. The extent of the tumor neovasculatur system will be reflected in the size of the tumor. Thus, by applying *P. aeruginosa* into mice bearing tumors of different sizes, the optimal tumor size for the day of infection was determined. When tumors were allowed to develop for ten days and accordingly exhibiting a volume of about 100-150 mm^3, they showed a consistent and reliable colonization by *P. aeruginosa*. Tumors of smaller size were inconsistently colonized or even not at all. The vascularization of fast growing tumors is pathological and might be causatively involved in tumor invasion by the bacteria [116]. Thus, sufficient time might be required to develop such blood vessels. On the other hand, the tumor influences the hematopoietic cells. Thus, during early tumor growth, the cytokine storm elicited by the application of the bacteria might be different under such conditions. More investigation will be required to understand this phenomenon. Since this type of therapy is also intended to clear metastases which will be of small size, this is an important question to answer.

Interestingly, the extent of colonization of the tumor tissue was dependent on the size of the bacterial inoculum. This was largely different from what was observed when using Salmonella (Leschner S., unpublished). The optimal infection dose for CT26 tumor-bearing BALB/c mice was determined to be $5x10^6$ *P. aeruginosa*. Mice infected with the highest concentration of bacteria suffered under the infection conditions, probably due to a dramatic cytokine storm and a high colonization of organs like liver and gut. Nevertheless, the colonization by *P. aeruginosa* never reached the levels that were observed with Salmonella and *E. coli*.

Thus, the tumor niche for *P. aeruginosa* might be smaller and dependent on the number of bacteria applied. On the other hand, Pseudomonas is not truly anaerobic. Hence, the various environments within a tumor, especially the anoxic tumor core, might be only to a limited extend suitable for *P. aeruginosa*.

Shortly after application of the bacteria into tumor-bearing mice, the tumors changed their visible phenotype from red to a dark color. Apparently a hemorrhage was taking place. Over the experimental time course, the tumor surface became necrotic and a black crust developed. Previous experiments using *S.* Typhimurium have yielded similar results [116]. The influx of blood is most likely induced by the secretion of pre-stored TNF-α from myeloid cells upon systemic application of the bacteria. The molecule TNF-α is known to be a vasoactive cytokine that might exhibit a particular strong reaction on the pathological endothelia of the tumor and thereby causing increased leakiness of the tumor-associated blood vessels.

4.2 The priming of $CD4^+$- and $CD8^+$ T cells is essential for the anti-tumor effect

When tumor-bearing WT mice were infected with *P. aeruginosa* the tumors did not only change their color, they moreover started to shrink and disappeared within 13 days p.i.. The CT26 tumor cell line is highly immunogenic and previous studies demonstrated that effector T cells of BALB/c WT mice are able to infiltrate tumors in high numbers from day 7 of tumor growth onwards via the circulation [140, 141]. Such anti-tumor effector T cells are probably activated due to an adjuvant effect after i.v. administration of bacteria like Salmonella or *E. coli* [122], which induces the infiltration of tumors by such effector T cells [111]. To test, whether this also holds true for the application of *P. aeruginosa*, WT mice that had cleared the CT26 tumor after infection were re-challenged with CT26 tumor cells and simultaneously with F1A11 fibrosarcoma cells as control. The observed clearance of only CT26 tumors and the concurrent unrestricted growth of F1A11 tumors on the same mouse revealed specificity and immune memory. These two criteria are characteristic for an immune reaction.

The important role of the specific immune system against CT26 tumors after bacterial infection was confirmed when tumor-bearing $Rag1^{-/-}$ mice were treated with *P. aeruginosa.* The infected immunocompromised mice were not able to retard tumor growth at all. Such mice are deficient for $CD4^+$ and $CD8^+$ T cells, which are well known to develop anti-cancer functions [39, 142].

To characterize this reaction in more detail, the impact of differentially primed total T cells, like they should occur during the course of infection of tumor-bearing WT mice was investigated by adoptive transfers. $Rag1^{-/-}$ mice were reconstituted with T cells and at the same time CT26 cells were applied. No effect was detected after the transfer of naïve total T cells as expected. Interestingly, reconstitution of $Rag1^{-/-}$ mice by total T cells isolated from uninfected but tumor-bearing mice resulted in tumor growth retardation. Apparently, already in such mice specific anti-tumor T cells were present although the tumor was still growing. This situation is reminiscent of human cancer patients in which tumor-specific T cells are observed. However they are not able to fight the neoplasia. In addition, the transfer of total T cells from infected mice that had cleared their tumors caused tumor rejection in all the recipient mice.

As a next step it was of interest, whether $CD4^+$- and/or $CD8^+$ effector T cells are responsible for clearance of CT26 tumors. Therefore $CD4^+$- or $CD8^+$ T cells as well as total T cells from mice treated in different ways were adoptively transferred into $Rag1^{-/-}$ mice together with CT26 cells. Whereas the transfer of naïve total T cells did not show any effect again, total T cells isolated from uninfected tumor-bearing WT mice were able to clear CT26 tumors in 75 % of the cases within 21 days. Probably, the final number of effector T cells was still limiting such that the tumors grew in some mice, causing only a retardation of tumor growth in the preceding experiment. However, these total T cells have been isolated out of uninfected tumor-bearing WT mice in which they were not able to induce tumor growth retardation, even though they had obviously encountered tumor antigens and became tumor-antigen specific. Probably, the 12 day old tumor had developed immune-escape mechanisms through which the T cells were not able to influence the tumor development anymore. Since the adoptive T cell transfer into $Rag1^{-/-}$ mice was done simultaneously with the injection of tumor cells, the potentially tumor-antigen specific effector T cells could have targeted the cancer cells before these developed immune-escape mechanisms. To inhibit the function of effector T cells, tumors are supposed to activate several inhibitory checkpoint pathways in the immune cells, like through the expression of the PD-1 ligand or CTLA-4 ligands [143]. Nevertheless, it might explain the efficient induction of anti-tumor immunity when bacteria are applied. The adjuvant properties of such microorganisms are supposed to act on preexisting immune cells of the tumor-bearing host.

None of the isolated $CD4^+$- or $CD8^+$ T cells out of uninfected tumor-bearing WT mice were able to reject CT26 tumors after transfer. Because the cell numbers of transferred cells were similar for total and single T cells, and the sample of total T cells comprised a mixture of the isolated single positive cells, a reduced number of effector T cells within the $CD4^+$- or $CD8^+$ population was unlikely.

It was more likely that a synergy due to $CD4^+$-$CD8^+$ T cell cooperation was responsible for the observed effect. It was demonstrated recently that the cytokine IFN-γ, which is supposed to be essential for the cytotoxic activity of $CD8^+$ T cells [139], was produced by isolated effector $CD4^+$ T cells after seven days of CT26 tumor growth [141]. On the other hand, the CTLs may have experienced licensing, through the activation of APCs by $CD4^+$ Th cells which in turn trigger and activate CD8 T cells [39, 144]. to carry out sufficient cytotoxic anti-tumor functions.

When total T cells from WT mice which had cleared CT26 tumors after infection were transferred into $Rag1^{-/-}$ mice, the animals cleared the tumors within 13 days after transfer. The same was true when only $CD8^+$ T cells from such mice were transferred. Such $CD8^+$ memory T cells might have been able to autonomously expand in numbers after re-encountering the same tumor-antigens and to kill the tumor cells. This feature of CTLs has been demonstrated in previous studies using several mouse models. They showed that effector $CD8^+$ T cells were able to maintain their anti-tumor functions in the absence of $CD4^+$ T cells [145]. And furthermore, that transgenic CT26 tumors which have developed on BALB/c mice were rejected by the CTLs once they had completed their specialization [141]. Interestingly, under such conditions also isolated $CD4^+$ T cells reduced the tumor size significantly from day 8 p.t. onwards, although they were not able to clear the tumors completely. Similarly, in the study mentioned above $CD4^+$ T cells were not able to completely reject newly developed transgenic CT26 tumors [141]. In further studies it was shown that primed $CD4^+$ T cells were indeed able to eliminate cancer cells in $CD8^+$ T cell deficient hosts by for example the secretion of TNF-α [39, 146]. This could be extended to the present study by for instance digestion of tumors and subsequent FACS analyses, or immune histology of tumor cryosections. Additionally, the secretion of enzymes like granzyme-B or perforin by the tumor-specific $CD4^+$ T cells could be tested. Such molecules were described to be employed by immune cells to kill neoplastic cells [142, 147].

4.3 TANs infiltrate tumors with prominent MIP-2 / CXCL-2 gradients

To investigate the tumor microenvironment of CT26 solid tumors, immune histology of paraffin-embedded tumors as well as luminex analyses of tumor lysates were deployed. The analysis of consecutive tumor sections revealed the presence of a large number of tumor-associated neutrophils between the viable and the necrotic tumor zone within the colonized tumor tissue. The attraction of neutrophils to the inflammatory side was possibly influenced by PDGF-bb in combination with the detected cytokines TNF-α and VEGF.

Due to the function of these molecules, the vascular permeability of the tumor-associated blood vessels might have been increased and consequently enabled a strong influx of neutrophils into the tumor microenvironment.

The combined illustration of the chemokine concentrations in blood samples and tumor lysates revealed the presence of only one chemokine gradient in infected mice able to recruit neutrophils into tumors. This was the concentration gradient of MIP-2 / CXCL-2. Malignant- as well as stromal cells of the tumor microenvironment are described to secrete the cytokine [148] and thus might have been responsible for the increased concentration of MIP-2 in the tumor tissue. Thereby, this chemokine could have triggered the extravasation of neutrophils into infected tumors. This would be in accordance with a previous study, which highlighted the importance of MIP-2 for the recruitment of neutrophils into necrotic tumor areas [165]. TANs inside untreated tumors could have been influenced by the neutrophil chemoattractants KC / CXCL-1, MCP-1 / CCL-2, MIP-1α / CCL-3, or Rantes / CCL-5 in addition to infiltrate the tumor tissues. Also these cytokines are reported to be secreted by malignant- as well as stromal cells [22, 51, 149, 150]. Hence these cells could have caused the increased availability of the molecules inside such tumor microenvironments. But even though five chemokine gradients for the possible attraction of neutrophils were detected in untreated tumors, the total number of TANs was decreased compared to colonized tumors. Whether the decreased amount of MIP-2 in uninfected tumors might be responsible for that, could be investigated by applying recombinant MIP-2 into tumor bearing mice in future experiments.

However, also further chemokines like CXCL-5 / ENA-78 (epithelial neutrophil activating peptide-78) or CXCL-12 / SDF-1 (stromal cell-derived factor 1), which were not included in the present study, might have influenced the infiltration of neutrophils into tumors. This was demonstrated in recent studies of our group [48, 69]. Thus this study should be extended to concentrations of CXCL-5 or CXCL-12 inside *P. aeruginosa* infected CT26 tumors. For that, enzyme-linked immunosorbent assays of tumor lysates could be performed. To test furthermore whether tumor-associated neutrophils generally respond to a certain chemokine gradient, the receptor for the chemokine of interest could be blocked on neutrophils prior to infection, or the establishment of the respective cytokine gradient could be manipulated by the application of specific antibodies.

4.4 TANs change their phenotypes to N1 after infection or TNF-α treatment

Since the functional specialization of TANs is supposed to be influenced by the various conditions within the tumor microenvironment, the impact of a systemic infection with the *P. aeruginosa* WT strain PA14 on the phenotype of the TAN population was investigated. Recombinant TNF-α was applied as a control group to distinguish the impact of a common necrotic tumor region from the effects of a necrotic core which might include bacterial colonization. Because the definitions of N1- and N2-phenoytpes are only end-stage descriptions, the present study rather described the changes of single phenotypic markers than determining gross population-phenotypes under the respective conditions in the tumor. Thus, not all markers analyzed had to be up- or downregulated at a time to indicate a certain phenotypic switch.

First of all, the total number of TANs per gram tumor tissue was compared between PBS-, PA14-, and TNF-α-treated tumor-bearing BALB/c -WT or -Rag1$^{-/-}$ mice. Here, the number of TANs was generally increased after PA14- or TNF-α injection. Additionally, a phenotypic switch of the whole TAN population to a stronger tumor-suppressive N1 phenotype was demonstrated after *P. aeruginosa* infection and to a less extent after TNF-α treatment. This was characterized by individual numbers of increased percentages of TANs expressing certain pro-inflammatory markers. Thus, the responses of TANs seemed to be not specific for bacterial PAMPs like LPS or flagellin, rather than induced by a general boost of pro-inflammatory molecules within the tumor microenvironment.

In infected tumor-bearing mice, the N1-inducing cytokine IFN-β was strongly secreted by the host cells. Hence, the detected phenotypic switches after infection, especially the general up-regulations of Icam, Fas and active caspase 3 in a high number of TANs, could have been induced by IFN-β. This would be in accordance with a new study from our lab, in which we revealed the partial dependency of Icam, Fas, and active caspase 3 expression by TANs on IFN-β in another tumor model [75]. Thus, in the present study the increased secretion of IFN-β seemed to be dependent on the bacterial stimulus, since the induced extrinsic inflammatory effects by the application of recombinant TNF-α did not trigger an endogenous IFN-β-response in the host.

On the other hand, the concentration of the six neutrophil polarizing cytokines analyzed, especially of G-CSF and MCP-1 / CCL-2, were decreased after infection. G-CSF and MCP-1 have been reported to influence the lifetime of neutrophils [151, 152]. Therefore, a decreased concentration of such cytokines might have favored a prolonged lifespan of TANs inside the tumors, and thereby increased the chances for phenotypic switches back to a tumor-suppressive N1 phenotype.

Since the corresponding luminex analyses and the *in vivo*-imaging of IFN-β reporter mice were performed on tumors from WT mice only, similar contributions of the cytokines on neutrophil infiltration and phenotypes within $Rag1^{-/-}$ mice can solely be assumed.

The percentage of TANs with a tumorigenic N2 phenotype was generally higher in PBS-treated control tumors with broadened hypoxic islands compared to tumors with few hypoxic areas but large necrotic regions like after injection of *P. aeruginosa* or recombinant TNF-α. Therefore, it might be possible that the sustained development of tumor-supporting N2 TANs was favored by the increased hypoxic conditions inside PBS-treated tumors of WT- and $Rag1^{-/-}$ mice to promote the ongoing tumor growth. The activation of the transcription factor HIF-1α is described to be necessarily induced in cells surviving under hypoxic conditions and to trigger tumor-supportive N2 functions in $CD11b^{+}$ $Gr1^{+}$ cells in addition [30]. HIF-1α is for example supposed to decrease the production of ROS in TANs or to favor the prolongation of the lifetime of such cells [153, 154]. Future experiments could analyze ROS production in tumor-bearing WT- or $Rag1^{-/-}$ mice by first applying luminol (5-amino-2,3-dihydro-1,4-phthalazine-dione) into the mice to visualize the concentration of ROS produced by immune cells using live *in vivo* imaging [155, 156]. In a second step, consecutive tumor sections could be stained for neutrophils, H&E, hypoxia, and ROS to determine the exact localization of ROS-producing TANs. For the latter, a polyclonal rabbit-anti-ROS1 antibody (Novus Biologicals, USA) or several other antibodies detecting protein- or lipid oxidations [157] may be used. In tumors of infected or TNF-α-treated WT- and $Rag1^{-/-}$ mice, the area of hypoxic tumor zones was dramatically decreased. As a consequence, the concentration of HIF-1α inside TANs and further cells within the tumor microenvironment might have been reduced. A recent study demonstrated an increased tumor rejection rate in such tumor-bearing mice, whose BMDCs were deficient for HIF-1α [30]. To show an impact of HIF-1α on the functional phenotypes of TANs in our model, tumor-bearing BALB/c mice deficient for HIF-1α might be tested.

All in all, the observed phenotypic switches from N2 to N1 TANs inside tumors of mice injected with *P. aeruginosa* or recombinant TNF-α might have been induced either by a reduction of hypoxia, or by an increased availability of certain pro-inflammatory molecules in such tumor microenvironments. In addition, components of the necrotic cells could have been involved. However, the availability of these pro-inflammatory triggers strongly affected the production of the N1-inducing cytokine IFN-β only in infected tumor-bearing mice. Based on these observations, it is supposed that endogenous IFN-β alone is not responsible for the phenotypic switches from tumor-supportive N2 to tumor-suppressive N1 TANs in the present study.

4.5 TANs might induce *P. aeruginosa* biofilm formation in oxic tumor areas

In tumors of PBS-treated mice (data not shown) as well as in infected tumors, tumor-infiltrated neutrophils resided between hypoxic islands and the necrotic tumor core. Under such hypoxic to anoxic conditions, the lifespan of neutrophils was described to be increased [156], because the cells are able to adapt their metabolism to the low oxygen concentrations. Also for that they stabilize the transcription factor HIF-1α, which induces a metabolic switch from oxidative phosphorylation to glycolysis [157]. Thus, TANs are supposed to be very resistant and functional under low oxygen levels [158]. In respect to our solid tumor model, the localization of TANs in hypoxic areas close to the necrotic tumor center obviously represented the most favorable niche for such cells.

Especially in the context of their assumed anti-tumor functions [40, 47, 158], the additional detection of TANs within the zone of viable tumor cells is reasonable. Since TANs are pro-inflammatory phagocytic cells, their localization close to *P. aeruginosa* was expected. Likewise, the appearance of bacterial clusters embedded in biofilm material inside tumors from WT mice was published by our group recently [139]. Nevertheless, the previous study suggested a connection between functions of the adaptive immune system and *in vivo* biofilm formation by the *P. aeruginosa* WT strain PA14 [124]. However, the present study demonstrated that PA14 *in vivo* biofilm formation was independent of the presence of the adaptive immune system. A huge amount of such bacterial matrix material was detected around PA14 clusters in the viable zone of tumors on immunocompromised $Rag1^{-/-}$ mice. Therefore the occurrence of T- or B cells is apparently not crucial for the development of PA14 biofilms in the present model. As the evidence for biofilm production is derived from electron microscopical analysis, the biofilms formed by PA14 in tumors of $Rag1^{-/-}$ mice might have simply been missed in the previous study.

Since neutrophils were co-localized with bacterial clusters inside the tumors from WT- and $Rag1^{-/-}$ animals, it is proposed that the bacteria produced the energy-costly extracellular biofilm material to protect themselves from antimicrobial- and phagocytic functions of TANs. The direct effect of neutrophils on *P. aeruginosa in vivo* biofilm formation could not be tested, since WT mice did not survive the infection after neutrophil depletion (results not shown). Future investigations using different histological techniques might figure out, if the increased concentration of oxygen in the viable tumor zone influences the antimicrobial activity of TANs, and whether such cells show a rather N1 phenotype compared to TANs within the hypoxic tumor area.

4.6 Concluding remarks and future investigations

Immunocompetent WT mice bearing CT26 tumors were i.v. infected with the *P. aeruginosa* WT strain PA14. This activated tumor specific effector $CD4^+$- and $CD8^+$ T cells. The CTLs were able (i) to reject tumors when present in sufficient numbers, and (ii) to generate a functional and tumor-specific T cell memory able to suppress the development of new CT26 tumors. The present study demonstrated furthermore, that tumor-suppressive N1 phenotypes of tumor-associated neutrophils were successfully induced in tumor-bearing mice by the i.v. infection with *P. aeruginosa*. The strongest phenotypic switch of the TAN population was detected in $Rag1^{-/-}$ mice three days p.i. Nonetheless, such tumor-bearing mice were not able to reject tumors in contrast to infected WT animals due to their immune deficiency.

The ability of TANs to adapt to highly diverse conditions and to fulfill tumor-suppressing functions are new promising tools for cancer immunotherapies. The actual literature already describes possibilities of applications of N1 TANs in tumor therapy based on their reduced secretion of arginase and a consequently reduced suppression of T cells within tumor microenvironments [75], and their increased production of ROS, by which N1 TANs might be able to kill tumor cells directly [159]. Thus, bacteria-mediated tumor therapy might represent a promising strategy to control the functional specialization of TANs inside tumor microenvironments and to induce phenotype switches from N2 to N1. Since the type I interferon IFN-β that was believed to be responsible for the N1 phenotype was not exclusively in charge of these phenotypic switches in the present study, further investigations should aim at describing additional cytokines or conditions within tumor microenvironments which induce tumor-suppressive N1 TANs.

Our solid tumor model would enable such future investigations as well as experiments to detect additional pro-inflammatory triggers which favor the development of N1 TANs. Besides that, further molecules important for the recruitment of neutrophils into tumors, signaling pathways inside TANs leading to the induction of pro-inflammatory phenotypes, additional anti-tumor mechanisms of N1 TANs, as well as possible interaction partners of the cells might be characterized *in vivo*. Moreover, screenings for intervention strategies against the development of tumor-suppressive microenvironments are issues which might be addressed. The use of syngeneic mouse lines will allow analyses in defined immunocompromised hosts and the characterization of important effector cells and molecules under standardized conditions.

5 Abstract

In the present work, first parameters important for the optimal colonization of tumors by *Pseudomonas aeruginosa* were established. The optimal tumor volume and the concentration of the bacterial inoculum for the infection of tumor-bearing BALB/c wild-type (WT) mice was determined. Apparently, CT26 tumors need to develop for ten days to guarantee a qualified colonization of the tumor tissue. Moreover, the infection dose of $5x10^6$ *P. aeruginosa* was suitable for intravenous (i.v.) infections of tumor-bearing mice, resulting in a high and reproducible colonization of the subcutaneous tumor. The use of these newly determined parameters resulted in minimal burden for the mice, which allowed further experimentation due to animal survival of infection and tumor clearance.

Since the i.v. application of the bacteria lead to tumor clearance in WT mice, the quality of differentially primed $CD4^+$- and $CD8^+$ T cells to specifically act against tumor cells was investigated by adoptive transfer experiments in syngeneic $Rag1^{-/-}$ animals. Interestingly, T cells isolated from uninfected tumor-bearing WT mice achieved the complete rejection of new tumors, when a combination of $CD4^+$ + $CD8^+$ T cells was injected into the recipient mice. This demonstrated that also uninfected tumor-bearing mice contain tumor-antigen specific T cells, which are nevertheless not able to reject such tumors. The adjuvant effect of the bacteria that activates the tumor-specific T cells seemed to be necessary to enable tumor clearance in WT animals. On the other hand, when T cells were isolated out of WT mice which had cleared CT26 tumors after infection with *P. aeruginosa*, the application of $CD8^+$ T cells alone prevented the development of tumors on modified Rag1 mice. By that, the development of a T cell memory and functional specificity was revealed.

The impact of the bacterial infection on functional specializations of tumor-associated neutrophils (TANs) in the tumor microenvironment was investigated. To this end, the expression of the extracellular phenotypic markers Icam, Fas, and CD62L, as well as the production of the intracellular markers TNF-α and active caspase 3 was determined. The analyses revealed phenotype switches of the respective TAN population from N2 to N1 after the i.v. injection of *P. aeruginosa* into tumor-bearing WT- as well as $Rag1^{-/-}$ mice. The most and maximal significant changes of the percental number of TANs expressing a certain phenotypic marker were observed three days post infection of tumor-bearing $Rag1^{-/-}$ mice. By the application of *P. aeruginosa* into tumor-bearing mice, tumor-supportive N2 TANs were obviously forced to switch to tumor-suppressing N1 TANs. Now, defined functions of N1 TANs can be investigated in future experiments and their onset in the present model probably induced by the bacteria-mediated tumor therapy.

6 Zusammenfassung

Eine Intension der Arbeit war es wichtige Parameter für die optimale Kolonisierung von Tumoren durch *Pseudomonas aeruginosa* herauszufinden. Dazu wurde das optimale Tumorvolumen und die effizienteste Konzentration des bakteriellen Inokulums am Tag der Infektion von tumortragenden BALB/c Wildtyp (WT) -Mäusen etabliert. Offensichtlich müssen sich syngene CT26 Tumore über zehn Tage entwickeln, um eine qualifizierte Kolonisierung des Tumorgewebes durch die Bakterien zu garantieren. Darüber hinaus war eine Infektionsdosis von $5x10^6$ *P. aeruginosa* für intravenöse (i.v.) Infektionen von tumortragenden Mäusen optimal, da sie in einer hohen und reproduzierbaren Kolonisierung der subkutanen Tumore resultierte. Die Anwendung der neu bestimmten Parameter resultierte darüber hinaus in einer minimalen Belastung für die Tiere, was ihr Überleben nach der Infektion und die komplette Eradizierung des Tumors ermöglichte.

Da die i.v. Anwendung der Bakterien in einer Beseitigung der Tumore in WT-Mäusen resultierte, wurden $CD4^+$- und $CD8^+$ T-Zellen aus derartigen Mäusen, durch adoptive Transferexperimente in syngene $Rag1^{-/-}$ Mäuse untersucht. Interessanterweise ermöglichten T-Zellen, die aus uninfizierten CT26 tumortragenden WT-Mäusen isoliert wurden, eine komplette Abstoßung neuer CT26 Tumore, wenn eine Kombination aus solchen $CD4^+$- + $CD8^+$ T-Zellen in die Rezipienten-Mäuse injiziert wurde. Dadurch wurde gezeigt, dass auch uninfizierte tumortragende Mäuse Tumorantigen-spezifische T-Zellen besitzen, die allerdings nicht dazu fähig sind bereits ausgebildete Tumore zu beseitigen. Der adjuvante Effekt der applizierten Bakterien erscheint für eine solche Beseitigung von Tumoren in WT-Mäusen notwendig zu sein. Allerdings, wenn T-Zellen aus solchen WT-Mäusen isoliert wurden, welche die Tumore nach der Infektion mit *P. aeruginosa* beseitigt hatten, war die Anwendung von ausschließlich $CD8^+$ T-Zellen ausreichend, um die Entwicklung von Tumoren in den modifizierten Rag1-Mäusen zu verhindern. Dadurch konnte das Bestehen von Gedächtnis-T-Zellen und deren funktionelle Spezifität bestätigt werden.

Ebenfalls wurde der Einfluss der bakteriellen Infektion auf die funktionelle Spezialisierung von Tumor-assoziierten Neutrophilen (TANs) im Tumormikromilieu untersucht. Dazu wurde die Expression der extrazellulären Phänotypisierungsmarker Icam, Fas und CD62L, sowie die Produktion der Zytokine TNF-α und aktive Caspase 3, die als intrazelluläre Phänotypisierungsmarker analysiert wurden, bestimmt. Die Analysen zeigten einen Phänotyp-Wechsel der jeweiligen TAN-Population von N2 zu N1 nach der i.v. Injektion von *P. aeruginosa* in tumortragenden WT- als auch $Rag1^{-/-}$-Mäusen an.

Die meisten und maximal signifikanten Veränderungen der prozentualen Anzahl an TANs, die einen bestimmten Phänotyp-Marker exprimierten, wurden drei Tage nach der Infektion von tumortragenden $Rag1^{-/-}$ Mäusen festgestellt. Aufgrund der Verwendung von *P. aeruginosa* in tumortragenden Mäusen wurden Tumor-unterstützende N2 TANs offensichtlich dazu gebracht sich in Tumor-hemmende N1 TANs umzuwandeln. Folglich können bestimmte Funktionen von N1 TANs in zukünftigen Experimenten untersucht und ihre Aktivierung mittels der Bakterien-vermittelten Tumortherapie induziert werden, ein möglicher Vorzug dieser Therapie.

7 References

1. World Health Organization. *Noncommunicable diseases*. 01.2015, cited 06.08.2015; Available from: http://www.who.int/mediacentre/factsheets/fs355/en/.
2. World Health Organization. *The top 10 causes of death*. 05.2014, cited 06.08.2015; Available from: http://www.who.int/mediacentre/factsheets/fs310/en/index1.html.
3. Robert Koch-Institut. *Krebs gesamt*. 25.03.2015, cited 06.08.2015; Available from: http://www.krebsdaten.de/Krebs/DE/Content/Krebsarten/Krebs_gesamt/krebs_gesamt_node.html.
4. The World Bank Group. *Country income groups (World Bank classification)*. 07.2011, cited 06.08.2015; Available from: http://chartsbin.com/view/2438.
5. Robert Koch-Institut. *Krebsarten*. 13.12.2013, cited 06.08.2015; Available from: http://www.krebsdaten.de/Krebs/DE/Content/Krebsarten/krebsarten_node.html.
6. Renan, M.J., *How many mutations are required for tumorigenesis? Implications from human cancer data.* Mol Carcinog, 1993. 7(3): p. 139-46.
7. Hanahan, D. and R.A. Weinberg, *Hallmarks of cancer: the next generation.* Cell, 2011. 144(5): p. 646-74.
8. World Health Organization. *Cancer*. 02.2015, cited 07.08.2015; Available from: http://www.who.int/mediacentre/factsheets/fs297/en/.
9. Karakashev, S.V. and M.J. Reginato, *Progress toward overcoming hypoxia-induced resistance to solid tumor therapy.* Cancer Manag Res, 2015. 7: p. 253-64.
10. Tellier, C., D. Desmet, L. Petit, L. Finet, C. Graux, M. Raes, O. Feron, and C. Michiels, *Cycling hypoxia induces a specific amplified inflammatory phenotype in endothelial cells and enhances tumor-promoting inflammation in vivo.* Neoplasia, 2015. 17(1): p. 66-78.
11. Schlie, K., J.E. Spowart, L.R. Hughson, K.N. Townsend, and J.J. Lum, *When Cells Suffocate: Autophagy in Cancer and Immune Cells under Low Oxygen.* Int J Cell Biol, 2011. DOI 10.1155/2011/470597.
12. Powis, G. and L. Kirkpatrick, *Hypoxia inducible factor-1α as a cancer drug target.* Molecular Cancer Therapeutics, 2004. 3: p. 647-654.
13. Jones, R.G. and C.B. Thompson, *Tumor suppressors and cell metabolism: a recipe for cancer growth.* Genes Dev, 2009. 23(5): p. 537-48.
14. Carmeliet, P. and R.K. Jain, *Angiogenesis in cancer and other diseases.* Nature, 2000. 407(6801): p. 249-57.
15. Hanahan, D. and J. Folkman, *Patterns and emerging mechanisms of the angiogenic switch during tumorigenesis.* Cell, 1996. 86(3): p. 353-64.
16. Naumov, G.N., J. Folkman, O. Straume, and L.A. Akslen, *Tumor-vascular interactions and tumor dormancy.* APMIS, 2008. 116: p. 569-585.
17. Bellone, M. and A. Calcinotto, *Ways to enhance lymphocyte trafficking into tumors and fitness of tumor infiltrating lymphocytes.* Front Oncol, 2013. DOI 10.3389/fonc.2013.00231.

18. Nozawa, H., C. Chiu, and D. Hanahan, *Infiltrating neutrophils mediate the initial angiogenic switch in a mouse model of multistage carcinogenesis.* Proc Natl Acad Sci U S A, 2006. 103(33): p. 12493-8.

19. Medina-Echeverz, J., F. Aranda, and P. Berraondo, *Myeloid-derived cells are key targets of tumor immunotherapy.* Oncoimmunology, 2014. 3(4): e28398.

20. Joyce, J.A. and J.W. Pollard, *Microenvironmental regulation of metastasis.* Nat Rev Cancer, 2009. 9(4): p. 239-52.

21. Vesely, M.D., M.H. Kershaw, R.D. Schreiber, and M.J. Smyth, *Natural innate and adaptive immunity to cancer.* Annu Rev Immunol, 2011. 29: p. 235-71.

22. Fridlender, Z.G., J. Sun, S. Kim, V. Kapoor, G. Cheng, L. Ling, G.S. Worthen, and S.M. Albelda, *Polarization of tumor-associated neutrophil phenotype by TGF-beta: "N1" versus "N2" TAN.* Cancer Cell, 2009. 16(3): p. 183-94.

23. Brandau, S., K. Moses, and S. Lang, *The kinship of neutrophils and granulocytic myeloid-derived suppressor cells in cancer: Cousins, siblings or twins?* Seminars in Cancer Biology, 2013. 23: p. 171-182.

24. Peranzoni, E., S. Zilio, I. Marigo, L. Dolcetti, P. Zanovello, S. Mandruzzato, and V. Bronte, *Myeloid-derived suppressor cell heterogeneity and subset definition.* Curr Opin Immunol, 2010. 22(2): p. 238-44.

25. Vatner, R.E. and S.C. Formenti, *Myeloid-derived cells in tumors: effects of radiation.* Semin Radiat Oncol, 2015. 25(1): p. 18-27.

26. Youn, J.I., M. Collazo, I.N. Shalova, S.K. Biswas, and D.I. Gabrilovich, *Characterization of the nature of granulocytic myeloid-derived suppressor cells in tumor-bearing mice.* J Leukoc Biol, 2012. 91(1): p. 167-81.

27. Mantovani, A., *Macrophages, Neutrophils, and Cancer: A Double Edged Sword.* New Journal of Science, 2014. 2014: p. 1-14.

28. Virtuoso, L.P., J.L. Harden, P. Sotomayor, W.J. Sigurdson, F. Yoshimura, N.K. Egilmez, B. Minev, and M.O. Kilinc, *Characterization of iNOS(+) Neutrophil-like ring cell in tumor-bearing mice.* J Transl Med, 2012. DOI 10.1186/1479-5876-10-152.

29. Elpek, K.G., V. Cremasco, H. Shen, C.J. Harvey, K.W. Wucherpfennig, D.R. Goldstein, P.A. Monach, and S.J. Turley, *The tumor microenvironment shapes lineage, transcriptional, and functional diversity of infiltrating myeloid cells.* Cancer Immunol Res, 2014. 2(7): p. 655-67.

30. Corzo, C.A., T. Condamine, L. Lu, M.J. Cotter, J.I. Youn, P. Cheng, H.I. Cho, E. Celis, D.G. Quiceno, T. Padhya, et al., *HIF-1alpha regulates function and differentiation of myeloid-derived suppressor cells in the tumor microenvironment.* J Exp Med, 2010. 207(11): p. 2439-53.

31. Movahedi, K., D. Laoui, C. Gysemans, M. Baeten, G. Stange, J. Van den Bossche, M. Mack, D. Pipeleers, P. In't Veld, P. De Baetselier, et al., *Different tumor microenvironments contain functionally distinct subsets of macrophages derived from Ly6C(high) monocytes.* Cancer Res, 2010. 70(14): p. 5728-39.

32. Sagiv, J.Y., J. Michaeli, S. Assi, I. Mishalian, H. Kisos, L. Levy, P. Damti, D. Lumbroso, L. Polyansky, R.V. Sionov, et al., *Phenotypic diversity and plasticity in circulating neutrophil subpopulations in cancer.* Cell Rep, 2015. 10(4): p. 562-73.

33. Liu, C.Y., Y.M. Wang, C.L. Wang, P.H. Feng, H.W. Ko, Y.H. Liu, Y.C. Wu, Y. Chu, F.T. Chung, C.H. Kuo, et al., *Population alterations of L-arginase- and inducible nitric oxide synthase-expressed CD11b+/CD14(-)/CD15+/CD33+ myeloid-derived suppressor cells and CD8+ T lymphocytes in patients with advanced-stage non-small cell lung cancer.* J Cancer Res Clin Oncol, 2010. 136(1): p. 35-45.

34. Sippel, T.R., J. White, K. Nag, V. Tsvankin, M. Klaassen, B.K. Kleinschmidt-DeMasters, and A. Waziri, *Neutrophil degranulation and immunosuppression in patients with GBM: restoration of cellular immune function by targeting arginase I.* Clin Cancer Res, 2011. 17(22): p. 6992-7002.

35. Pillay, J., T. Tak, V.M. Kamp, and L. Koenderman, *Immune suppression by neutrophils and granulocytic myeloid-derived suppressor cells: similarities and differences.* Cell Mol Life Sci, 2013. 70(20): p. 3813-27.

36. Murdoch, C., M. Muthana, S.B. Coffelt, and C.E. Lewis, *The role of myeloid cells in the promotion of tumour angiogenesis.* Nat Rev Cancer, 2008. 8(8): p. 618-31.

37. Ostrand-Rosenberg, S., *Immune surveillance: a balance between protumor and antitumor immunity.* Curr Opin Genet Dev, 2008. 18(1): p. 11-8.

38. Ralainirina, N., A. Poli, T. Michel, L. Poos, E. Andres, F. Hentges, and J. Zimmer, *Control of NK cell functions by CD4+CD25+ regulatory T cells.* J Leukoc Biol, 2007. 81(1): p. 144-53.

39. Janeway, C., P. Travers, M. Walport, and M. Shlomchik, *Immunobiology: the immune system in health and disease*. 6th ed. 2005, Garland Science Publishing, New York and London.

40. Fridlender, Z.G. and S.M. Albelda, *Tumor-associated neutrophils: friend or foe?* Carcinogenesis, 2012. 33(5): p. 949-55.

41. Nathan, C., *Neutrophils and immunity: challenges and opportunities.* Nat Rev Immunol, 2006. 6(3): p. 173-82.

42. Senovilla, L., E. Vacchelli, J. Galon, S. Adjemian, A. Eggermont, W.H. Fridman, C. Sautes-Fridman, Y. Ma, E. Tartour, L. Zitvogel, et al., *Trial watch: Prognostic and predictive value of the immune infiltrate in cancer.* Oncoimmunology, 2012. 1(8): p. 1323-1343.

43. Sheshachalam, A., N. Srivastava, T. Mitchell, P. Lacy, and G. Eitzen, *Granule protein processing and regulated secretion in neutrophils.* Front Immunol, 2014. DOI 10.3389/fimmu.2014.00448.

44. Perobelli, S.M., R.G. Galvani, T. Goncalves-Silva, C.R. Xavier, A. Nobrega, and A. Bonomo, *Plasticity of neutrophils reveals modulatory capacity.* Braz J Med Biol Res, 2015. 10.1590/1414-431X20154524: p. 1-11.

45. von Kockritz-Blickwede, M. and V. Nizet, *Innate immunity turned inside-out: antimicrobial defense by phagocyte extracellular traps.* J Mol Med (Berl), 2009. 87(8): p. 775-83.

46. Sims, G.P., D.C. Rowe, S.T. Rietdijk, R. Herbst, and A.J. Coyle, *HMGB1 and RAGE in inflammation and cancer.* Annu Rev Immunol, 2010. 28: p. 367-88.

47. Mishalian, I., R. Bayuh, L. Levy, L. Zolotarov, J. Michaeli, and Z.G. Fridlender, *Tumor-associated neutrophils (TAN) develop pro-tumorigenic properties during tumor progression.* Cancer Immunol Immunother, 2013. 62(11): p. 1745-56.

48. Jablonska, J., C.F. Wu, L. Andzinski, S. Leschner, and S. Weiss, *CXCR2-mediated tumor-associated neutrophil recruitment is regulated by IFN-beta.* Int J Cancer, 2014. 134(6): p. 1346-58.

49. Futosi, K., S. Fodor, and A. Mocsai, *Neutrophil cell surface receptors and their intracellular signal transduction pathways.* Int Immunopharmacol, 2013. 17(3): p. 638-50.

50. Sparmann, A. and D. Bar-Sagi, *Ras-induced interleukin-8 expression plays a critical role in tumor growth and angiogenesis.* Cancer Cell, 2004. 6(5): p. 447-58.

51. Piccard, H., R.J. Muschel, and G. Opdenakker, *On the dual roles and polarized phenotypes of neutrophils in tumor development and progression.* Critical Reviews in Oncology/Hematology, 2012. 82: p. 296-309.

52. Jain, R.K. and N.S. Forbes, *Can engineered bacteria help control cancer?* Proc Natl Acad Sci U S A, 2001. 98(26): p. 14748-50.

53. Gabig, T.G., S.I. Bearman, and B.M. Babior, *Effects of oxygen tension and pH on the respiratory burst of human neutrophils.* Blood, 1979. 53(6): p. 1133-9.

54. Campbell, E.L. and S.P. Colgan, *Neutrophils and inflammatory metabolism in antimicrobial functions of the mucosa.* J Leukoc Biol, 2015. DOI 10.1189/jlb.3MR1114-556R.

55. Dresch, C., Y. Najean, and J. Bauchet, *Kinetic studies of 51Cr and DF32P labelled granulocytes.* Br J Haematol, 1975. 29(1): p. 67-80.

56. Pillay, J., I. den Braber, N. Vrisekoop, L.M. Kwast, R.J. de Boer, J.A. Borghans, K. Tesselaar, and L. Koenderman, *In vivo labeling with 2H2O reveals a human neutrophil lifespan of 5.4 days.* Blood, 2010. 116(4): p. 625-7.

57. Tofts, P.S., T. Chevassut, M. Cutajar, N.G. Dowell, and A.M. Peters, *Doubts concerning the recently reported human neutrophil lifespan of 5.4 days.* Blood, 2011. 117(22): p. 6050-2.

58. Tecchio, C., A. Micheletti, and M.A. Cassatella, *Neutrophil-derived cytokines: facts beyond expression.* Front Immunol, 2014. DOI 10.3389/fimmu.2014.00508.

59. Uddin, M., G. Seumois, L.C. Lau, P. Rytila, D.E. Davies, and R. Djukanovic, *Enhancement of neutrophil function by the bronchial epithelium stimulated by epidermal growth factor.* Eur Respir J, 2008. 31(4): p. 714-24.

60. Kobayashi, Y., *The role of chemokines in neutrophil biology.* Front Biosci, 2008. 13: p. 2400-7.

61. Kansas, G.S., *Selectins and their ligands: current concepts and controversies.* Blood, 1996. 88(9): p. 3259-87.

62. Lee, P.Y., J.X. Wang, E. Parisini, C.C. Dascher, and P.A. Nigrovic, *Ly6 family proteins in neutrophil biology.* J Leukoc Biol, 2013. 94(4): p. 585-94.

63. Mishalian, I., R. Bayuh, E. Eruslanov, J. Michaeli, L. Levy, L. Zolotarov, S. Singhal, S.M. Albelda, Z. Granot, and Z.G. Fridlender, *Neutrophils recruit regulatory T-cells into tumors via secretion of CCL17--a new mechanism of impaired antitumor immunity.* Int J Cancer, 2014. 135(5): p. 1178-86.

64. Gabrilovich, D.I., S. Ostrand-Rosenberg, and V. Bronte, *Coordinated regulation of myeloid cells by tumors.* Nat Rev Immunol, 2012: p. 159-175.

65. Cortez-Retamozo, V., M. Etzrodt, A. Newton, P.J. Rauch, A. Chudnovskiy, C. Berger, R.J. Ryan, Y. Iwamoto, B. Marinelli, R. Gorbatov, et al., *Origins of tumor-associated macrophages and neutrophils.* Proc Natl Acad Sci U S A, 2012. 109(7): p. 2491-6.

66. Esen, N. *Research Grant Program Winning Abstract*. 2009, cited 12.08.2015; Available from: https://www.bdbiosciences.com/research/grant/winners/.

67. Rumble, J.M., A.K. Huber, G. Krishnamoorthy, A. Srinivasan, D.A. Giles, X. Zhang, L. Wang, and B.M. Segal, *Neutrophil-related factors as biomarkers in EAE and MS.* J Exp Med, 2015. 212(1): p. 23-35.

68. Kolaczkowska, E. and P. Kubes, *Neutrophil recruitment and function in health and inflammation.* Nat Rev Immunol, 2013. 13(3): p. 159-75.

69. Jablonska, J., S. Leschner, K. Westphal, S. Lienenklaus, and S. Weiss, *Neutrophils responsive to endogenous IFN-beta regulate tumor angiogenesis and growth in a mouse tumor model.* J Clin Invest, 2010. 120(4): p. 1151-64.

70. Van Overmeire, E., D. Laoui, J. Keirsse, J.A. Van Ginderachter, and A. Sarukhan, *Mechanisms driving macrophage diversity and specialization in distinct tumor microenvironments and parallelisms with other tissues.* Front Immunol, 2014. DOI 10.3389/fimmu.2014.00127.

71. Andzinski, L., C.F. Wu, S. Lienenklaus, A. Kroger, S. Weiss, and J. Jablonska, *Delayed apoptosis of tumor associated neutrophils in the absence of endogenous IFN-beta.* Int J Cancer, 2015. 136(3): p. 572-83.

72. Shimizu, M., A. Fontana, Y. Takeda, T. Yoshimoto, A. Tsubura, and A. Matsuzawa, *Fas/Apo-1 (CD95)-mediated apoptosis of neutrophils with Fas ligand (CD95L)-expressing tumors is crucial for induction of inflammation by neutrophilic polymorphonuclear leukocytes associated with antitumor immunity.* Cell Immunol, 2001. 207(1): p. 41-8.

73. Liles, W.C., P.A. Kiener, J.A. Ledbetter, A. Aruffo, and S.J. Klebanoff, *Differential expression of Fas (CD95) and Fas ligand on normal human phagocytes: implications for the regulation of apoptosis in neutrophils.* J Exp Med, 1996. 184(2): p. 429-40.

74. Strasser, A., P.J. Jost, and S. Nagata, *The many roles of FAS receptor signaling in the immune system.* Immunity, 2009. 30(2): p. 180-92.

75. Andzinski, L., N. Kasnitz, S. Stahnke, C.F. Wu, M. Gereke, M. Von Köckritz-Blickwede, B. Schilling, S. Branau, S. Weiss, and J. Jablonska, *Type I IFNs induce anti-tumor polarization of tumor associated neutrophils in mice and human.* International Journal of Cancer, 2015. Manuscript ID: IJC-15-1245.R2.

76. Carswell, E.A., L.J. Old, R.L. Kassel, S. Green, N. Fiore, and B. Williamson, *An endotoxin-induced serum factor that causes necrosis of tumors.* Proc Natl Acad Sci U S A, 1975. 72(9): p. 3666-70.

77. Watanabe, N., Y. Niitsu, H. Umeno, H. Kuriyama, H. Neda, N. Yamauchi, M. Maeda, and I. Urushizaki, *Toxic effect of tumor necrosis factor on tumor vasculature in mice.* Cancer Res, 1988. 48(8): p. 2179-83.

78. Pillay, J., V.M. Kamp, E. Van Hoffen, T. Visser, T. Tak, J.-W. Lammers, L.H. Ulfman, L.P. Leenen, P. Pickkers, and L. Koenderman, *A subset of neutrophils in human systemic inflammation inhibits T cell responses through Mac-1.* The Journal of Clinical Investigation, 2012. 22(1): p. 327-336.

79. Andzinski, L., *Influence of IFN-beta on the life span and apoptosis of tumor infiltrating neutrophil granulocytes*, in *Molecular Immunology*, Technical University Braunschweig, 2014.

80. Lebedeva, T., M.L. Dustin, and Y. Sykulev, *ICAM-1 co-stimulates target cells to facilitate antigen presentation.* Curr Opin Immunol, 2005. 17(3): p. 251-8.

81. Gaglia, J.L., E.A. Greenfield, A. Mattoo, A.H. Sharpe, G.J. Freeman, and V.K. Kuchroo, *Intercellular adhesion molecule 1 is critical for activation of CD28-deficient T cells.* J Immunol, 2000. 165(11): p. 6091-8.

82. Schreiber, R.D., L.J. Old, and M.J. Smyth, *Cancer immunoediting: integrating immunity's roles in cancer suppression and promotion.* Science, 2011. 331: p. 1565-1570.

83. Coffelt, S.B., K. Kersten, C.W. Doornebal, J. Weiden, K. Vrijland, C.S. Hau, N.J. Verstegen, M. Ciampricotti, L.J. Hawinkels, J. Jonkers, et al., *IL-17-producing gammadelta T cells and neutrophils conspire to promote breast cancer metastasis.* Nature, 2015. 522(7556): p. 345-8.

84. Houghton, A.M., D.M. Rzymkiewicz, H. Ji, A.D. Gregory, E.E. Egea, H.E. Metz, D.B. Stolz, S.R. Land, L.A. Marconcini, C.R. Kliment, et al., *Neutrophil elastase-mediated degradation of IRS-1 accelerates lung tumor growth.* Nat Med, 2010. 16(2): p. 219-23.

85. Wislez, M., N. Rabbe, J. Marchal, B. Milleron, B. Crestani, C. Mayaud, M. Antoine, P. Soler, and J. Cadranel, *Hepatocyte growth factor production by neutrophils infiltrating bronchioloalveolar subtype pulmonary adenocarcinoma: role in tumor progression and death.* Cancer Res, 2003. 63(6): p. 1405-12.

86. Morton, J., B. Coles, K. Wright, A. Gallimore, J.D. Morrow, E.S. Terry, P.B. Anning, B.P. Morgan, V. Dioszeghy, H. Kuhn, et al., *Circulating neutrophils maintain physiological blood pressure by suppressing bacteria and IFNgamma-dependent iNOS expression in the vasculature of healthy mice.* Blood, 2008. 111(10): p. 5187-94.

87. Puga, I., M. Cols, C.M. Barra, B. He, L. Cassis, M. Gentile, L. Comerma, A. Chorny, M. Shan, W. Xu, et al., *B cell-helper neutrophils stimulate the diversification and production of immunoglobulin in the marginal zone of the spleen.* Nat Immunol, 2012. 13(2): p. 170-80.

88. Swain, S.L., K.K. McKinstry, and T.M. Strutt, *Expanding roles for CD4(+) T cells in immunity to viruses.* Nat Rev Immunol, 2012. 12(2): p. 136-48.

89. Harlin, H., Y. Meng, A.C. Peterson, Y. Zha, M. Tretiakova, C. Slingluff, M. McKee, and T.F. Gajewski, *Chemokine expression in melanoma metastases associated with CD8+ T-cell recruitment.* Cancer Res, 2009. 69(7): p. 3077-85.

90. Staveley-O'Carroll, K., E. Sotomayor, J. Montgomery, I. Borrello, L. Hwang, S. Fein, D. Pardoll, and H. Levitsky, *Induction of antigen-specific T cell anergy: An early event in the course of tumor progression.* Proc Natl Acad Sci U S A, 1998. 95(3): p. 1178-83.

91. Vinay, D.S., E.P. Ryan, G. Pawelec, W.H. Talib, J. Stagg, E. Elkord, T. Lichtor, W.K. Decker, R.L. Whelan, H.M. Kumara, et al., *Immune evasion in cancer: Mechanistic basis and therapeutic strategies.* Semin Cancer Biol, 2015. DOI 10.1016/j.semcancer.2015.03.004.

92. Gajewski, T.F., H. Schreiber, and Y.X. Fu, *Innate and adaptive immune cells in the tumor microenvironment.* Nat Immunol, 2013. 14(10): p. 1014-22.

93. Pasche, B., *Role of transforming growth factor beta in cancer.* J Cell Physiol, 2001. 186(2): p. 153-68.

94. Dudley, M.E., J.R. Wunderlich, T.E. Shelton, J. Even, and S.A. Rosenberg, *Generation of tumor-infiltrating lymphocyte cultures for use in adoptive transfer therapy for melanoma patients.* J Immunother, 2003. 26(4): p. 332-42.

95. Andersen, M.H., *The specific targeting of immune regulation: T-cell responses against Indoleamine 2,3-dioxygenase.* Cancer Immunol Immunother, 2012. 61(8): p. 1289-97.

96. Manuel, E.R., J. Chen, M. D'Apuzzo, M.G. Lampa, T.I. Kaltcheva, C.B. Thompson, T. Ludwig, V. Chung, and D.J. Diamond, *Salmonella-Based Therapy Targeting Indoleamine 2,3-Dioxygenase Coupled with Enzymatic Depletion of Tumor Hyaluronan Induces Complete Regression of Aggressive Pancreatic Tumors.* Cancer Immunol Res, 2015. DOI 10.1158/2326-6066.CIR-14-0214.

97. Foster, A.E., G. Dotti, A. Lu, M. Khalil, M.K. Brenner, H.E. Heslop, C.M. Rooney, and C.M. Bollard, *Antitumor activity of EBV-specific T lymphocytes transduced with a dominant negative TGF-beta receptor.* J Immunother, 2008. 31(5): p. 500-5.

98. Pardoll, D.M., *The blockade of immune checkpoints in cancer immunotherapy.* Nat Rev Cancer, 2012. 12(4): p. 252-64.

99. Wolchok, J., *How recent advances in immunotherapy are changing the standard of care for patients with metastatic melanoma.* Ann Oncol, 2012. 23 : p. 15-21.

100. Hodi, F.S., S.J. O'Day, D.F. McDermott, R.W. Weber, J.A. Sosman, J.B. Haanen, R. Gonzalez, C. Robert, D. Schadendorf, J.C. Hassel, et al., *Improved survival with ipilimumab in patients with metastatic melanoma.* N Engl J Med, 2010. 363(8): p. 711-23.

101. Drake, C.G. and E.S. Antonarakis, *Current status of immunological approaches for the treatment of prostate cancer.* Curr Opin Urol, 2012. 22(3): p. 197-202.

102. Reck, M., I. Bondarenko, A. Luft, P. Serwatowski, F. Barlesi, R. Chacko, M. Sebastian, H. Lu, J.M. Cuillerot, and T.J. Lynch, *Ipilimumab in combination with paclitaxel and carboplatin as first-line therapy in extensive-disease-small-cell lung cancer: results from a randomized, double-blind, multicenter phase 2 trial.* Ann Oncol, 2013. 24(1): p. 75-83.

103. Yang, J.C., M. Hughes, U. Kammula, R. Royal, R.M. Sherry, S.L. Topalian, K.B. Suri, C. Levy, T. Allen, S. Mavroukakis, et al., *Ipilimumab (anti-CTLA4 antibody) causes regression of metastatic renal cell cancer associated with enteritis and hypophysitis.* J Immunother, 2007. 30(8): p. 825-30.

104. Fousek, K. and N. Ahmed, *The Evolution of T-cell Therapies for Solid Malignancies.* Clin Cancer Res, 2015. 21(15): p. 3384-92.

105. Topalian, S.L., F.S. Hodi, J.R. Brahmer, S.N. Gettinger, D.C. Smith, D.F. McDermott, J.D. Powderly, R.D. Carvajal, J.A. Sosman, M.B. Atkins, et al., *Safety, activity, and immune correlates of anti-PD-1 antibody in cancer.* N Engl J Med, 2012. 366(26): p. 2443-54.

106. Van Egmond, M. and J.E. Bakema, *Neutrophils as effector cells for antibody-based immunotherapy of cancer.* Seminars in Cancer Biology, 2013. 23: p. 190-199.

107. Bakema, J.E., S.H. Ganzevles, D.M. Fluitsma, M.W. Schilham, R.H. Beelen, T. Valerius, S. Lohse, M.J. Glennie, J.P. Medema, and M. van Egmond, *Targeting FcalphaRI on polymorphonuclear cells induces tumor cell killing through autophagy.* J Immunol, 2011. 187(2): p. 726-32.

108. Guettinger, Y., K. Barbin, M. Peipp, J. Bruenke, M. Dechant, H. Horner, D. Thierschmidt, T. Valerius, R. Repp, G.H. Fey, et al., *A recombinant bispecific single-chain fragment variable specific for HLA class II and Fc alpha RI (CD89) recruits polymorphonuclear neutrophils for efficient lysis of malignant B lymphoid cells.* J Immunol, 2010. 184(3): p. 1210-7.

109. June, C.H., *Adoptive T cell therapy for cancer in the clinic.* J Clin Invest, 2007. 117(6): p. 1466-76.

110. Hodge, J.W., J. Higgins, and J. Schlom, *Harnessing the unique local immunostimulatory properties of modified vaccinia Ankara (MVA) virus to generate superior tumor-specific immune responses and antitumor activity in a diversified prime and boost vaccine regimen.* Vaccine, 2009. 27(33): p. 4475-82.

111. Stern, C., N. Kasnitz, D. Kocijancic, S. Trittel, P. Riese, C.A. Guzman, S. Leschner, and S. Weiss, *Induction of CD4 and CD8 anti-tumor effector T cell responses by bacteria mediated tumor therapy.* Int J Cancer, 2015. DOI 10.1002/ijc.29567.

112. Frahm, M., S. Felgner, D. Kocijancic, M. Rohde, M. Hensel, R. Curtiss, 3rd, M. Erhardt, and S. Weiss, *Efficiency of conditionally attenuated Salmonella enterica serovar Typhimurium in bacterium-mediated tumor therapy.* MBio, 2015. DOI 10.1128/mBio.00254-15.

113. Donskov, F., *Immunomonitoring and prognostic relevance of neutrophils in clinical trials.* Semin Cancer Biol, 2013. 23(3): p. 200-7.

114. Coley, W.B., *The treatment of malignant tumors by repeated inoculation of erysipelas.* Clin Orthop Relat Res., 1991. 262: p. 3-11.

115. Wood, L.M. and Y. Paterson, *Attenuated Listeria monocytogenes: a powerful and versatile vector for the future of tumor immunotherapy.* Front Cell Infect Microbiol, 2014. DOI 10.3389/fcimb.2014.00051.

116. Leschner, S., K. Westphal, N. Dietrich, N. Viegas, J. Jablonska, M. Lyszkiewicz, S. Lienenklaus, W. Falk, N. Gekara, H. Loessner, et al., *Tumor invasion of Salmonella enterica serovar Typhimurium is accompanied by strong hemorrhage promoted by TNF-alpha.* PLoS One, 2009. 4(8): e6692.

117. Kim, S.H., F. Castro, Y. Paterson, and C. Gravekamp, *High efficacy of a Listeria-based vaccine against metastatic breast cancer reveals a dual mode of action.* Cancer Res, 2009. 69(14): p. 5860-6.

118. Herr, H.W., D.M. Schwalb, Z.F. Zhang, P.C. Sogani, W.R. Fair, W.F. Whitmore, Jr., and H.F. Oettgen, *Intravesical bacillus Calmette-Guerin therapy prevents tumor progression and death from superficial bladder cancer: ten-year follow-up of a prospective randomized trial.* J Clin Oncol, 1995. 13(6): p. 1404-8.

119. Staedtke, V., R. Bai, W. Sun, J. Huang, K.K. Kibler, B.M. Tyler, G.L. Gallia, K. Kinzler, B. Vogelstein, S. Zhou, et al., *Clostridium novyi-NT can cause regression of orthotopically implanted glioblastomas in rats.* Oncotarget, 2015. 6(8): p. 5536-5546.

120. Felgner, S., D. Kocijancic, M. Frahm, and S. Weiss, *Bacteria in Cancer Therapy - Renaissance of an old Concept*, 2015. Unpublished manuscript.

121. Chong, D.L.W. and S. Sriskandan, *Pro-Inflammatory Mechanisms in Sepsis.* Contrib Microbiol, 2011. 17: p. 86-107.

122. Kocijancic, D., *Therapy of Solid Tumors using Recombinant Probiotic E. coli*, in *Molecular Immunology*, Leibniz University Hannover, 2015.

123. Epaulard, O., B. Toussaint, L. Quenee, M. Derouazi, N. Bosco, C. Villiers, R. Le Berre, B. Guery, D. Filopon, L. Crombez, et al., *Anti-tumor immunotherapy via antigen delivery from a live attenuated genetically engineered Pseudomonas aeruginosa type III secretion system-based vector.* Mol Ther, 2006. 14(5): p. 656-61.

124. Komor, U., *An animal model for biofilm formation by Pseudomonas aeruginosa*, in *Molecular Immunology*, Leibniz University Hannover, 2012.

125. Bjarnsholt, T., T. Tolker-Nielsen, N. Hoiby, and M. Givskov, *Interference of Pseudomonas aeruginosa signalling and biofilm formation for infection control.* Expert Rev Mol Med, 2010. 12: e11.

126. Rasamiravaka, T., Q. Labtani, P. Duez, and M. El Jaziri, *The formation of biofilms by Pseudomonas aeruginosa: a review of the natural and synthetic compounds interfering with control mechanisms.* Biomed Res Int, 2015. DOI 10.1155/2015/759348.

127. Cohen, T.S. and A. Prince, *Cystic fibrosis: a mucosal immunodeficiency syndrome.* Nat Med, 2012. 18(4): p. 509-19.

128. Avogadri, F., D. Mittal, F. Saccheri, M. Sarrafiore, M. Ciocca, P. Larghi, R. Orecchia, and M. Rescigno, *Intra-tumoral Salmonella typhimurium induces a systemic anti-tumor immune response that is directed by low-dose radiation to treat distal disease.* Eur J Immunol, 2008. 38(7): p. 1937-47.

129. Pawar, V., K. Crull, U. Komor, N. Kasnitz, M. Frahm, D. Kocijancic, K. Westphal, S. Leschner, K. Wolf, H. Loessner, et al., *Murine solid tumours as a novel model to study bacterial biofilm formation in vivo.* J Intern Med, 2014. 276(2): p. 130-9.

130. Gregory, A.D. and A.M. Houghton, *Tumor-associated neutrophils: new targets for cancer therapy.* Cancer Res, 2011. 71(7): p. 2411-6.

131. Caruso, R.A., R. Bellocco, M. Pagano, G. Bertoli, L. Rigoli, and C. Inferrera, *Prognostic value of intratumoral neutrophils in advanced gastric carcinoma in a high-risk area in northern Italy.* Mod Pathol, 2002. 15(8): p. 831-7.

132. Schmidt, H., S. Suciu, C.J. Punt, M. Gore, W. Kruit, P. Patel, D. Lienard, H. von der Maase, A.M. Eggermont, U. Keilholz, et al., *Pretreatment levels of peripheral neutrophils and leukocytes as independent predictors of overall survival in patients with American Joint Committee on Cancer Stage IV Melanoma: results of the EORTC 18951 Biochemotherapy Trial.* J Clin Oncol, 2007. 25(12): p. 1562-9.

133. Atai, N.A., M. Bansal, C. Lo, J. Bosman, W. Tigchelaar, K.S. Bosch, A. Jonker, P.C. De Witt Hamer, D. Troost, C.A. McCulloch, et al., *Osteopontin is up-regulated and associated with neutrophil and macrophage infiltration in glioblastoma.* Immunology, 2011. 132(1): p. 39-48.

134. Bellocq, A., M. Antoine, A. Flahault, C. Philippe, B. Crestani, J.F. Bernaudin, C. Mayaud, B. Milleron, L. Baud, and J. Cadranel, *Neutrophil alveolitis in bronchioloalveolar carcinoma: induction by tumor-derived interleukin-8 and relation to clinical outcome.* Am J Pathol, 1998. 152(1): p. 83-92.

135. Sun, R., J. Luo, L. Dong, Y. Shu, C. Luo, S. Wang, J. Qin, G. Zhang, and Z. Feng, *Neutrophils with protumor potential could efficiently suppress tumor growth after cytokine priming and in presence of normal NK cells.* Oncotarget, 2014. 5(24): p. 12621-12634.

136. Houghton, A.M., *The paradox of tumor-associated neutrophils: Fueling tumor growth with cytotoxic substances.* Cell Cycle, 2014. 9(9): p. 1732-1737.

137. Lienenklaus, S., M. Cornitescu, N. Zietara, M. Lyszkiewicz, N. Gekara, J. Jablonska, F. Edenhofer, K. Rajewsky, D. Bruder, M. Hafner, et al., *Novel reporter mouse reveals constitutive and inflammatory expression of IFN-beta in vivo.* J Immunol, 2009. 183(5): p. 3229-36.

138. Pawar, V., U. Komor, N. Kasnitz, P. Bielecki, M.C. Pils, B. Gocht, A. Moter, M. Rohde, S. Weiss, and S. Haussler, *In Vivo Efficacy of Antimicrobials against Biofilm-Producing Pseudomonas aeruginosa.* Antimicrob Agents Chemother, 2015. 59(8): p. 4974-81.

139. Komor, U., P. Bielecki, H. Loessner, M. Rohde, K. Wolf, K. Westphal, S. Weiss, and S. Haussler, *Biofilm formation by Pseudomonas aeruginosa in solid murine tumors - a novel model system.* Microbes Infect, 2012. 14(11): p. 951-8.

140. Lechner, M.G., S.S. Karimi, K. Barry-Holson, T.E. Angell, K.A. Murphy, C.H. Church, J.R. Ohlfest, P. Hu, and A.L. Epstein, *Immunogenicity of murine solid tumor models as a defining feature of in vivo behavior and response to immunotherapy.* J Immunother, 2013. 36(9): p. 477-89.

141. Klein, L., L. Trautman, S. Psarras, S. Schnell, A. Sierman, R. Liblau, H. Von Boehmer, and K. Khazaie, *Visualizing the course of antigen-specific CD8 and CD4 T cell responses to a growing tumor.* Eur J Immunol, 2003. 33: p. 806-814.

142. Haabeth, O.A., A.A. Tveita, M. Fauskanger, F. Schjesvold, K.B. Lorvik, P.O. Hofgaard, H. Omholt, L.A. Munthe, Z. Dembic, A. Corthay, et al., *How Do CD4(+) T Cells Detect and Eliminate Tumor Cells That Either Lack or Express MHC Class II Molecules?* Front Immunol, 2014. DOI 10.3389/fimmu.2014.00174.

143. Slaney, C.Y., M.H. Kershaw, and P.K. Darcy, *Trafficking of T cells into tumors.* Cancer Res, 2014. 74(24): p. 7168-74.

144. Zhang, S., H. Zhang, and J. Zhao, *The role of CD4 T cell help for CD8 CTL activation.* Biochem Biophys Res Commun, 2009. 384(4): p. 405-8.

145. Hanson, H.L., D.L. Donermeyer, H. Ikeda, J.M. White, V. Shankaran, L.J. Old, H. Shiku, R.D. Schreiber, and P.M. Allen, *Eradication of established tumors by CD8+ T cell adoptive immunotherapy.* Immunity, 2000. 13(2): p. 265-76.

146. Fujiwara, H., M. Fukuzawa, T. Yoshioka, H. Nakajima, and T. Hamaoka, *The role of tumor-specific Lyt-1+2- T cells in eradicating tumor cells in vivo. I. Lyt-1+2- T cells do not necessarily require recruitment of host's cytotoxic T cell precursors for implementation of in vivo immunity.* J Immunol, 1984. 133(3): p. 1671-6.

147. Quezada, S.A., T.R. Simpson, K.S. Peggs, T. Merghoub, J. Vider, X. Fan, R. Blasberg, H. Yagita, P. Muranski, P.A. Antony, et al., *Tumor-reactive CD4(+) T cells develop cytotoxic activity and eradicate large established melanoma after transfer into lymphopenic hosts.* J Exp Med, 2010. 207(3): p. 637-50.

148. Owen, J.L., M.F. Criscitiello, S. Libreros, R. Garcia-Areas, K. Guthrie, M. Torroella-Kouri, and V. Iragavarapu-Charyulu, *Expression of the inflammatory chemokines CCL2, CCL5 and CXCL2 and the receptors CCR1-3 and CXCR2 in T lymphocytes from mammary tumor-bearing mice.* Cell Immunol, 2011. 270(2): p. 172-82.

149. Acharyya, S., T. Oskarsson, S. Vanharanta, S. Malladi, J. Kim, P.G. Morris, K. Manova-Todorova, M. Leversha, N. Hogg, V.E. Seshan, et al., *A CXCL1 paracrine network links cancer chemoresistance and metastasis.* Cell, 2012. 150(1): p. 165-78.

150. Yoshimura, T., O.M. Howard, T. Ito, M. Kuwabara, A. Matsukawa, K. Chen, Y. Liu, M. Liu, J.J. Oppenheim, and J.M. Wang, *Monocyte chemoattractant protein-1/CCL2 produced by stromal cells promotes lung metastasis of 4T1 murine breast cancer cells.* PLoS One, 2013. 8(3): e58791.

151. Mayadas, T.N., X. Cullere, and C.A. Lowell, *The multifaceted functions of neutrophils.* Annu Rev Pathol, 2014. 9: p. 181-218.

152. Reichel, C.A., M. Rehberg, M. Lerchenberger, N. Berberich, P. Bihari, A.G. Khandoga, S. Zahler, and F. Krombach, *Ccl2 and Ccl3 mediate neutrophil recruitment via induction of protein synthesis and generation of lipid mediators.* Arterioscler Thromb Vasc Biol, 2009. 29(11): p. 1787-93.

153. Walmsley, S.R., C. Print, N. Farahi, C. Peyssonnaux, R.S. Johnson, T. Cramer, A. Sobolewski, A.M. Condliffe, A.S. Cowburn, N. Johnson, et al., *Hypoxia-induced neutrophil survival is mediated by HIF-1alpha-dependent NF-kappaB activity.* J Exp Med, 2005. 201(1): p. 105-15.

154. McGovern, N.N., A.S. Cowburn, L. Porter, S.R. Walmsley, C. Summers, A.A. Thompson, S. Anwar, L.C. Willcocks, M.K. Whyte, A.M. Condliffe, et al., *Hypoxia selectively inhibits respiratory burst activity and killing of Staphylococcus aureus in human neutrophils.* J Immunol, 2011. 186(1): p. 453-63.

155. Gross, S., S.T. Gammon, B.L. Moss, D. Rauch, J. Harding, J.W. Heinecke, L. Ratner, and D. Piwnica-Worms, *Bioluminescence imaging of myeloperoxidase activity in vivo.* Nat Med, 2009. 15(4): p. 455-61.

156. Liu, W.F., M. Ma, K.M. Bratlie, T.T. Dang, R. Langer, and D.G. Anderson, *Real-time in vivo detection of biomaterial-induced reactive oxygen species.* Biomaterials, 2011. 32(7): p. 1796-801.

157. Liou, G.Y. and P. Storz, *Detecting reactive oxygen species by immunohistochemistry.* Methods Mol Biol, 2015. 1292: p. 97-104.

158. Hicks, A.M., G. Riedlinger, M.C. Willingham, M.A. Alexander-Miller, C. Von Kap-Herr, M.J. Pettenati, A.M. Sanders, H.M. Weir, W. Du, J. Kim, et al., *Transferable anticancer innate immunity in spontaneous regression/complete resistance mice.* Proc Natl Acad Sci U S A, 2006. 103(20): p. 7753-8.

159. Granot, Z., E. Henke, E.A. Comen, T.A. King, L. Norton, and R. Benezra, *Tumor entrained neutrophils inhibit seeding in the premetastatic lung.* Cancer Cell, 2011. 20(3): p. 300-14.

8 Acknowledgement

First I want to thank my advisor and boss Dr. Siegfried Weiß. On the one hand he let me work as independently as I wanted to, but on the other hand he always kept an eye on the project development and optimal results. I had the possibility to learn many techniques like flow cytometry or confocal laser scanning microscopy, and to perform different kinds of animal experiments. When I applied for his project, I started as a microbiologist. Now I will finish my PhD study as an immunologist! Thank you for that and the yuccas Siggi!!

I thank Prof. Dr. Susanne Häußler for involving me in her group especially during internal meetings or conferences. Additionally, she and Prof. Dr. Peter Valentin-Weigand supported me in thesis committees and gave me conductive advices. Thanks to both of you!!

I am very grateful that Prof. Dr. Manfred Rohde became my mentor at the HZI. He always made time for me and my questions, especially concerning *P. aeruginosa* biofilm formation. And now he will make time again for my thesis review. Thank you Manfred!!

Likewise I am very thankful that Prof. Dr. Stefan Dübel and Prof. Dr. Martin Korte instantly accepted my request and became the second referee and third examiner for my thesis review and oral defence. I thank both of you for your time and criticism!!

During my time at the Molis, I had a lot of support from many people! Thank you all for the kind introductions within my first year, the comforting words necessary at some time points during my second year, and the home-feeling atmosphere at the end of my PhD time!!

Special thanks go to Anne Lorenz, Regina Lesch and Susanne zur Lage. You helped me a lot during my experiments. You had always time, as quickly or long as I needed you! Thank you very much!!

I am very happy to had the chance to cooperate with Prof. Dr. Susanne Häußler, Prof. Dr. Manfred Rohde, Dr. Marina Pils, Prof. Dr. Christine Falk, and their teams. Thank you all for your effort and the fruitful discussions!!

I thank the Helmholtz Graduate School for Infection Research for their advising and together with the Federal Ministry of Education and Research for the financial support for this project (12/0713), and the Helmholtz Centre for Infection Research for the provision of instruments, my lab- and my beautiful office place!!

A million thanks go to my future husband Christopher Kösterke for his unrestricted support!!